Disruption of the intracellular trafficking of ganglioside GM_1 in a genetically accurate model of the neurodegenerative storage disease juvenile neuronal ceroid-lipofuscinosis

Dissertation
zur Erlangung des Doktorgrades der Naturwissenschaften

vorgelegt beim Fachbereich Biowissenschaften
der Johann Wolfgang Goethe -Universität
in Frankfurt am Main

von
Aleksandra Somogyi
aus Zamość (Polen)

Frankfurt am Main (2016)
(D 30)[1]

[1] (D30: D=Dissertation 30=Bibliothekskennzeichen)

vom Fachbereich Biowissenschaften
der Johann Wolfgang Goethe - Universität als Dissertation angenommen.

Dekanin: Frau Prof. Dr. Meike Piepenbring

Gutachter : Herr Professor Dr. Walter Volknandt
Herr Professor Dr. Paul W. Dierkes

Datum der Disputation : 08.07.2016

I. TABLE OF CONTENTS

II. LIST OF ABBREVIATIONS

APP	amyloid precursor protein
ATPsubC	subunit C of mitochondrial ATPase
a. u.	arbitrary units
Btn1p	Battenin1 protein
Cb	cerebellar
CERT	ceramide transfer protein
CI-M6PR	cation-independent mannose-6-phosphate receptor
Cln3	ceroid-lipofuscinosis, neuronal 3
CNS	central nervous system
CTxB	cholera toxin subunit B
DHCer	dihydroceramide
ELISA	Enzyme-linked immunosorbent assay
FITC	fluorescein isothiocyanate
GalCer	galactosylceramide
GluCer	glucosylceramide
Glb1	β-galactosidase
GSL	glycosphingolipid
HPLC	high performance liquid chromatography
HPTLC	high-performance thin layer chromatography
LacCer	lactosylceramide
Lamp1	lysosome-associated membrane protein 1
LBPA	lysobisphosphatidic acid
LDL	low density lipoprotein
M6P	mannose-6-phosphate
MAM	mitochondria-associated ER-membrane
MβCD	methyl-β-cyclodextrin
MBEC	mouse brain epithelial cells
MTT	3-(4,5-Dimethylthiazol-2-yl)-2,5-diphenyl-tetrazolium bromide
Neu1	neuraminidase 1
PM	plasma membrane
PPCA	protective protein cathepsin A

PPD	palmitoyl-protein Δ-9 desaturase
RFP	red fluorescent protein
Sap	saposin, sphingolipid activator protein
SBDS	Schwachmann-Bodian-Diamond Syndrome
SERCA	sarcoplasmic reticulum Ca^{2+}-ATPase
TCA	trichloroacetic acid
TGN	trans-Golgi network
TLC	thin-layer chromatography
WGA	wheat germ agglutinin

III. SUMMARY

Juvenile neuronal ceroid-lipofuscinosis (JNCL) is a rare lysosomal storage disease in children with lethal outcome and no therapy. The origin of JNCL has been traced to autosomal recessive mutations in the *CLN3* gene, and ~85% of the JNCL patients harbor a 1.02 kb deletion that removes the exons 7 and 8 and the surrounding intronic DNA (*CLN3*$^{\Delta ex7/8}$). So far, structure, function and localization of the CLN3 protein remain elusive. However, there is strong evidence that CLN3 modulates a process or condition that is essential in many cellular pathways. Lipid metabolism and antero-/retrograde transport, two mechanisms CLN3 was previously implicated in, fulfill these requirements. Notably, also a bioactive group of glycosphingolipids referred to as gangliosides is tightly interrelated with these functions. Furthermore, a-series gangliosides have been shown to be involved in the development and sustenance of the brain, where they are essential for neurite outgrowth and cell survival. Defects in ganglioside metabolism were shown to play a crucial role in many lysosomal storage disorders. However, the contribution of gangliosides to NCL pathology is largely unknown.

The present study analyzed central enzymes and metabolites of the a-series ganglioside pathway in a JNCL cell model. The core finding was, thereby, the reduced amount of the neuroprotective ganglioside GM_1 in homozygous Cb*Cln3*$^{\Delta ex7/8}$ cells. This was caused by the enhanced action of the GM_1-degrading multimeric enzyme complex and in particular, by the upregulation of protein levels and increased enzyme activity of β-galactosidase (Glb1). Improved binding of Glb1 to substrate-carrying membranes was provided by an increase in LBPA levels. In combination with other smaller alterations in the ganglioside pattern, a shift towards less complex gangliosides became present. The resulting loss of neuroprotection may be the reason for the multifocal pathology in homozygous Cb*Cln3*$^{\Delta ex7/8}$ cells.

The second part of the present study investigated the cellular mechanisms behind the altered ganglioside profile with regard to the potential role of CLN3. Here, the anterograde transport of GM_1 to the plasma membrane presented a positive correlation with the amount of full-length CLN3. In case of the truncated protein this correlation was missing, resulting in reduced PM staining with CTxB-FITC. However, transfection of full-length CLN3 in these cells restored the CTxB-FITC intensity. Based on the neuroprotective role

of GM_1, the corresponding increase in GM_1 levels may be the cause for the restoration effects observed in previous studies using full-length CLN3. Hence, administration of GM_1 was expected to improve cell viability of homozygous Cb*Cln3*$^{\Delta ex7/8}$ cells and beyond that to rescue potentially some disease phenotypes. However, no effect could be observed. The reason for this may be reduced caveolar uptake and the mislocalization of ganglioside GM_1 to the trans-Golgi network (TGN) and redirection towards degradative compartments. Both are in line with the idea of an impaired endocytic flux in CLN3 deficiency. The observed localization of CLN3 in the TGN suggests a potential role for CLN3 in the lipid sorting machinery, subsequently altering membrane composition and its regulatory functions. The resulting imbalance may affect many of the cellular processes impaired in JNCL.

IV. INTRODUCTION

1. Neuronal ceroid-lipofuscinosis disordes (NCL)

Neuronal ceroid-lipofuscinosis disorders (NCLs) are a group of inherited, neurodegenerative, lysosomal storage diseases with a world-wide incidence of 1.2 per 100,000 live births. In the USA and Scandinavian countries they accumulate up to 1 per 12,500 live births (1, 2). NCLs share certain histopathological features and affect the central nervous system (CNS) of the patients drastically. The main similarity is the accumulation of distinctive abnormal storage material in cellular organelles, particularly lysosomes. Via histochemical and ultrastructural analysis in the twentieth century, it became possible to separate NCLs from other diseases (3, 4), like Tay-Sachs disease, in which the storage material is composed of GM_2 ganglioside. The prevalent storage material is referred to as ceroid lipofuscin and consists predominantly of proteins, but lipids and traces of metallic ions are also stored in autofluorescent inclusion bodies. Staining with periodic acid-Schiff (PAS) and/or Sudan black-B allowed classification of the ultrastructural appearance of the storage material into three major subtypes. Lipopigments consisting predominantly of subunit C of the mitochondrial ATP synthase revealed composed curvilinear and fingerprint patterns and were typical for the juvenile variant of NCL. Solely curvilinear patterns were seen in late infantile NCL, and granular osmiophilic deposits (GROD) containing saposin A and D were detected mainly in infantile NCL (5).

Common pathological phenotypes of NCLs are progressive loss of vision, myoclonic seizures, decline of cognitive and pyramidal/extrapyramidal motor functions and finally premature demise and early death. At the histological level, microglial activation is seen in areas of greatest neuronal loss, whereas astrocyte activation appears prominently in areas, where neuronal loss is less evident (6).

NCLs can be roughly distinguished by temporal onset and ethnological descent of the patient, but due to incidence of retracted disease course in case of less severe mutations, this correlation is fault-prone. Hence, contemporary classification is based on the genetic

background. Twelve genes are known causing independent variants of NCL, but their functions are not totally understood yet.

CLN1, or Santavuori-Haltia disease, is an infantile NCL caused by a deficiency of the soluble lysosomal enzyme palmitoyl-protein thioesterase 1 (PPT1). PPT1 cleaves the palmitate moiety from cysteine residues of S-palmitoylated proteins which can be found in the myelin sheath (7, 8). CLN2, or Janský-Bielschowsky disease, appears at the age of two to four years (classical late infantile NCL) and is caused by a deficiency of the lysosomal serine protease tripeptidyl peptidase (TPP1) (9, 10). Similar to CLN2, the gene of the Finnish variant of late infantile NCL, CLN5, encodes for a soluble lysosomal protein interacting with the lysosomal targeting mannose-6-phosphate (M6P) receptors (11–13). Four patients with clinical features identical to those seen in CLN3-deficient patients were previously described as CLN9 variant, but now reclassified as CLN5 (14). The affected protein may be a regulator of dihydroceramide synthase and functionally related to CLN8 (15). CLN8 contains the TRAM-Lag1p-CLN8 (TLC) domain, common for ceramide synthases (16). The disease course of CLN8 is split to Finnish families with Northern epilepsy (EPMR) and Turkish patients with a more typical NCL phenotype. The Costa Rican/Turkish/Indian variants of LINCL are known as CLN6 (17–19). CLN7 was assigned to the major facilitator protein superfamily (MFS), but its substrate specificity remains to be elucidated (20). The adult-onset NCL, CLN4/DNAJC5 or dominant Type A Kufs disease, is not well-understood yet, but a putative correlation exists with patients deficient in CLN13/cathepsin F developing recessive Type B Kufs disease (21). CLN10, a congenital variant of the disorder, is based on a deficiency in cathepsin D, a soluble lysosomal aspartic protease. The group of NCLs was completed by means of latest sequencing technology that allowed to identify disease genes in single families (CLN11/GRN, CLN12/AP13A2 and CLN14/KCTD7) (22). Additional NCL-related phenotypes are seen in mice with deficiencies of chloride channel proteins (CLC-3, CLC-7) (23, 24). A comprehensive overview has been published in a textbook by Mole et al. (25).

Target of the present study is CLN3 protein encoded by the *Cln3* gene that causes Batten disease, a juvenile form of NCL.

2. Juvenile neuronal ceroid-lipofuscinosis (JNCL)

Juvenile neuronal ceroid-lipofuscinosis (JNCL), Batten or Spielmeyer-Vogt-Sjögren disease (OMM #204200), is the most common inherited pediatric neurodegenerative disease and counts 0.2-7 per 100000 live births per year (2, 26, 27). The highest frequencies are reported in Scandinavian countries, but there are also cases noted from Brazil, Argentina, Canada and the USA (all out of the European genetic lineage), India and Japan. The inheritance is autosomal recessive. As heterozygous carriers with one wild type allele seem to be healthy, little is known about their phenotype. They are usually identified in correlation with diseased family members, only.

The first symptoms are typically reported within the age of four to eight years. Usually, the disease process starts with deterioration of the visual perception and subtle psychological disturbances. Decline of vision progresses to blindness, caused by macular and retinal degeneration with pigment aggregations and optic atrophy when the patient reaches adolescence. In the early second decade, severe dementia occurs together with epileptic seizures of generalized, complex-partial or myoclonic type. The electroencephalogram is abnormal, but without diagnostic or specific features. The disease course culminates in Parkinson-like disability with rigidity, hypokinesia, stooped posture and shuffling gait. Compulsive speaking appears in the mid-second decade and progressively worsens to severe dysarthria. Psychiatric disturbances result in social, thought and attention problems, psychosomatic complaints, aggressive behavior and are accompanied by sleep impairments like settling difficulties, nightmares and nocturnal awakenings. In the late second or early third decade the patients reach a non-ambulatory state followed by death usually within a year.

At the tissue level, low signal intensity in thalami and high signal intensity in periventricular white matter were detected by MRI and patients suffer from cerebral and cerebellar atrophy. Both are already observable in the late first decade, followed by significant decrease in the gray matter volume in the dorsomedial thalami and in the white matter volume in the corona radiata. A loss of melanin in the substantia nigra was reported by Rakheja *et al*. (28). Furthermore, typical for Batten disease are vacuolated lymphocytes in peripheral blood, that possess the curvilinear and fingerprint-like ultrastructural findings mentioned above (29, 30). Besides these, biopsied chorionic

tissue revealed a lamellar appearance of inclusion bodies, pointing to the assumption that the described epiphenomenon is changing during development of the organism. In skeletal muscle fibers, no inclusion bodies could be detected (31).

Although multiple cellular processes, *e.g.* lysosomal acidification, lysosomal arginine import, membrane fusion, vesicular transport, cytoskeletal organization, autophagy, apoptosis and proteolipid modification, were shown to be affected by *CLN3* mutations, the structure, function and localization of the CLN3 protein remain disputed (32).

3. CLN3

3.1 The *Cln3* gene

The gene underlying juvenile neuronal ceroid-lipofuscinosis was first described in 1995 by the International Batten Disease Consortium (33). It is located at chromosome 16p12.1 and has an open reading frame of 1314 base pairs, subdivided in 15 exons and 14 introns (34). All exon/intron-changings are reported to conform to the GT/AG-rule and regulating elements comprised potential binding sites for the transcription factors AP-1, AP-2, SP1 as well as two motifs for the erythroid-specific transcription factor GATA-1. Mitchison *et al*. (34) and other investigators (5, 35) reported several splicing variants of CLN3 at the 5'-end, but no attempts have been made so far to elucidate their biological function.

Chattopadhyay and Pearce (36) performed a microarray based approach and showed continuous *Cln3* mRNA expression in many different tissues. Notably, not the central nervous system, but gastrointestinal, glandular and secretory tissues showed the highest levels.

3.2 Structural characteristics of CLN3 protein

The glycoprotein CLN3, also called Battenin, is a putative hydrophobic membrane protein with 438 amino acids and an estimated molecular weight of 43 kDa before modifications (37). The molecular weight of glycosylated CLN3 varies depending on cell type (38) and tissue (39). Since discovery of the gene in 1995 and disclosure of the corresponding amino

acid sequence, many predictions were made to unravel the protein's topology. In 1999 Golabek *et al*. (38) demonstrated that CLN3 is an integral membrane protein.

Five to twelve transmembrane domains were subject of debate, resulting from different approaches to find characteristic structures or folding possibilities, but no successful crystallization could be performed yet to prove one of them. *In vivo* studies by Kyttälä *et al*. (40) described six transmembrane helices with cytoplasmic N and C-termini, supported by the computational sequence analysis of Nugent *et al.* (41). The latest topology model by Ratajczak *et al*. shows one large cytoplasmic loop and three luminal loops in this structure, where the third may contain an amphipathic helix partially embedded in the membrane (42) (Figure 1). Most disease causing mutations are located within this helix and the transmembrane domains flanking the second luminal loop; the common 1.02 kb deletion described in section 3.3 leads to excision of a highly conserved domain within the second luminal loop. In 1999 Michalewski *et al*. described the absence of the regular lysosomal sorting motif M6P (43). Two alternative lysosomal targeting motifs, a dileucine motif ($Leu_{253}Ile_{254}$) in the C-terminal cytoplasmic domain combined with an upstream acidic patch and another unconventional $MetX_9Gly$ motif, where X can be any amino acid except Pro or Asp, were reported later (40, 44). Several posttranslational modifications were suggested for CLN3. N-glycosylation is described at asparagine residues 71 and 85 (45) and potentially 310 (46). Six putative cytoplasmic phosphorylation sites are reported in this model (41), located at Ser and Thr residues spread over the whole sequence and amino acids on position 7, 125 and 232 are candidates for the protein kinases A and G and casein kinase II (43). Considering that lipid modifications are essential for many membrane proteins with neuronal functions, a putative N-myristoylation site was predicted at the N-terminus of CLN3 (47) and the CaaX box at the C-terminus is modified by farnesylation (48).

Furthermore, a binding site for galactosylceramide is reported for the CLN3 protein, consisting of a helix-turn-helix Motif $Val_{291}TyrPheAlaGlu_{295}$ (49) and two aromatic binding residues Tyr_{284} and Phe_{287}. This topic is discussed in detail below (section VII.3.1).

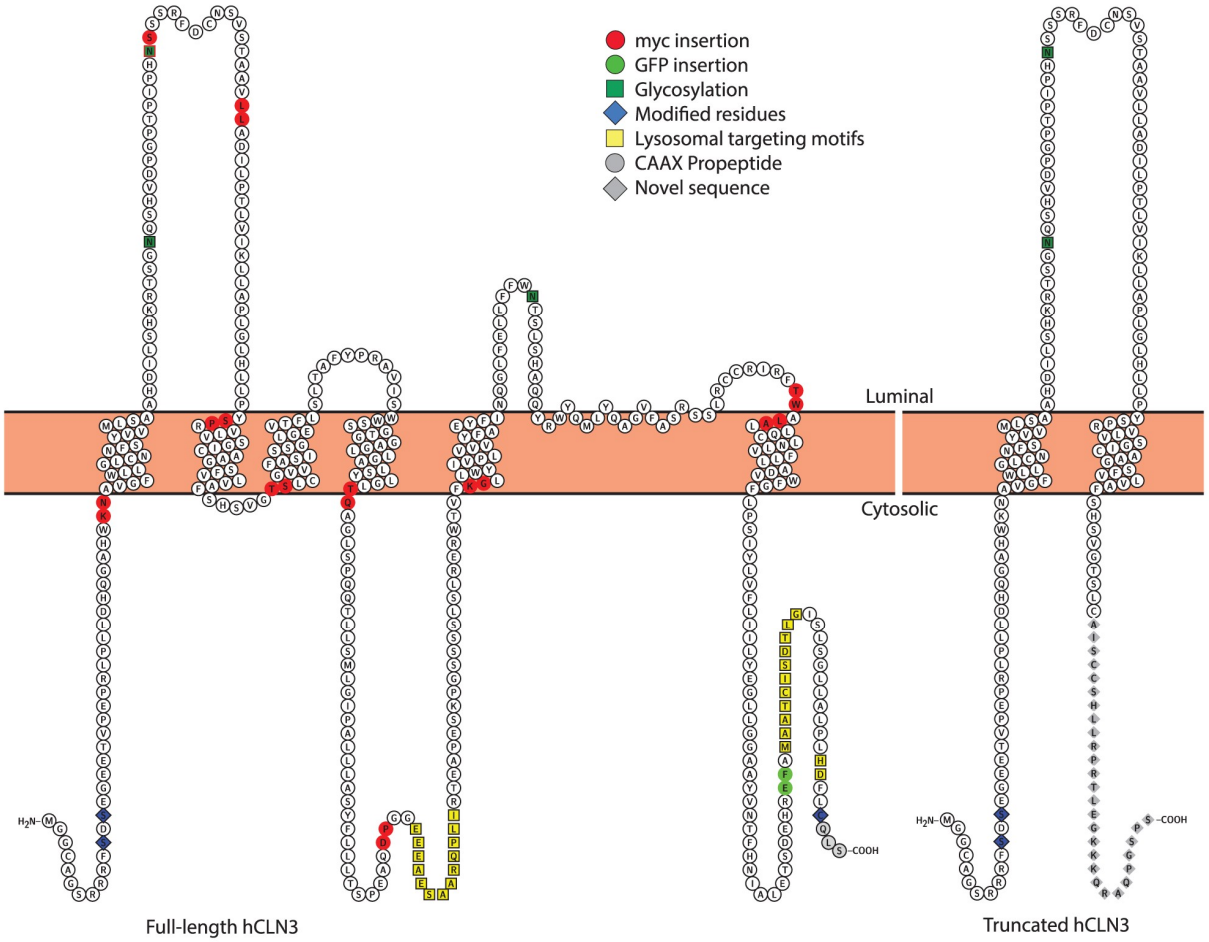

Figure 1. Membrane topology model of human CLN3. Adapted from Ratajczak *et al.*, 2014 (42).

3.3 Gene defects in JNCL

Until today 13 polymorphisms and 65 distinct mutations causing JNCL have been found; these are listed on UCL with their respective reference, location and length (50).

In 74% of the cases, JNCL results from a homozygous mutation in the *Cln3* gene causing a 1.02 kb deletion, which eliminates exons seven and eight and the surrounding intronic DNA. This results in a frameshift after the 153rd amino acid, 28 nonsense amino acids and a premature stop codon after the 182nd amino acid (Figure 1). Järvelä *et al*. (51) calculated for the resulting putative protein a molecular weight of 24 kDa in an overexpression study with CHO cells by using a construct resembling the 1.02 kb deletion mutation.

Different phenotypes may be associate with mutations other than the 1.02 kb deletion (52). For example, 22% of the patients are compound heterozygous for this and one of the

other rare mutation (53). They present a protracted disease and show less severe symptoms. Prior to genetic analysis, many of these patients were assigned to adult onset NCLs. Furthermore, the $Glu_{295}Lys$ mutation of CLN3 is reported to end in apoptosis, assuming an anti-apoptotic function of the galactosylceramide binding site. Whole CLN3 deletion has never been associated with a case of JNCL (54).

3.4 Models of JNCL

Among eukaryotic species, CLN3 is a highly conserved gene (55, 56). Homologues were detected in many model organisms including yeast, mouse, dog, sheep, *Drosophila melanogaster* and *Caenorhabditis elegans,* but no equivalent gene was detected in plants, bacteria or archaea. In general, this extent of conservation is an evidence for fundamental cellular functions, indispensable for survival of the organism. The most frequently examined homologues of CLN3 are the murine CLN3 protein, manipulated in four mouse models of JNCL, and the Btn1 protein in yeast.

3.4.1 Yeast models

Unicellular lower eukaryote models of JNCL have been created in the budding yeast *Saccharomyces cerevisiae* (*S. cerevisiae*) and the fission yeast *Saccharomyces pombe* (*S. pombe*) (57, 58). Lysosomal phenotypes were studied by investigating their yeast equivalent, the vacuole. Both models displayed alterations in the vacuolar pH in the absence of Btn1p, although the observations were contradictory (52, 57). Additionally, decreased lysosomal import of arginine has been shown in the *S. cerevisiae* model (59), potentially resulting in a limited nitric oxide synthesis (60). Studies in *S. pombe* added affected polarization of sterol-rich membrane domains and polarized cell growth (61) to the list of alterations, as well as changes in the vacuolar size and dynamics (58). Preservation of functional domains throughout eukaryotic evolution was shown by restoration of the phenotypes in Btn1p deficient cells through expression of human CLN3 (57, 58).

3.4.2 The Cln3$^{-/-}$ knock-out mouse models

First, two Cln3$^{-/-}$ null mutant mice have been established by replacing either exons 1-6 (*Cln3*$^{\Delta ex1-6}$) (62) or exons 7 and 8 (*Cln3*$^{\Delta ex7/8/neo}$) (63) of the *Cln3* gene with a neo selection cassette. Visual failure, accumulation of storage material and neuronal loss are present in both models, but they do not result in a severe neurologic disease (62–65). However, it remains disputed if these two mouse models are real null mutants since they were found to express *Cln3* transcripts and may retain part of their functionality (52).

In contrast, no transcript was detected in the recently generated *Cln3*$^{lacZ/lacZ}$ knock-in reporter mouse, where exons 1-8 have been replaced with the β-galactosidase gene lacZ behind the endogenous *Cln3* promotor (66). These mice show autofluorescent storage material, lysosomal enzyme elevation and neurologic deficits, including impaired motor function. Additionally, the reporter function provides the unique ability to track CLN3 expression temporally and spatially and thereby overcomes the difficulty in generating good CLN3 antibodies (25).

3.4.3 The Cln3$^{\Delta ex7/8/\Delta ex7/8}$ *knock-in mouse and cell model*

It remains disputed if the truncated protein resulting from the common 1.02 kb deletion retains a residual function. In order to create a genetically accurate mouse model, an identical deletion has been recreated by excision of exons 7 and 8 using the Cre-loxP system. *Cln3*$^{\Delta ex7/8/\Delta ex7/8}$ mice exhibit autofluorescent storage material, retinal degeneration and the neurologic disease is more severe when compared to Cln3$^{-/-}$ knock-out mice, including astrogliosis, motor deficits and premature death (35).

Since JNCL symptoms are prevailing in the CNS, cerebellar granule neuron precursor cells from *Cln3*$^{\Delta ex7/8/\Delta ex7/8}$ mice (hereinafter referred to as Cb*Cln3*$^{\Delta ex7/8}$ cells) were immortalized via transfection with a retroviral vector, bearing a temperature-sensitive tsA58 SV40 large T antigen, and cultured as a neuronal cell model. Lysosomal storage material appeared after 'aging' the cells seven days under confluent growth (67), but defective endocytosis, abnormally elongated mitochondria, decreased ATP levels and affected maturation of autophagic vesicles have been found to be earlier phenotypes. Cultured Cb*Cln3*$^{\Delta ex7/8}$ cells showed a three- to ten-fold reduction of mRNA levels of *Cln3*$^{\Delta ex7/8/\Delta ex7/8}$,

indicating that not all mutant CLN3 protein was removed by nonsense-mediated decay. Additionally, mutant splice variants of the protein were reported in this mouse model, including a variant deleted for exons 5, 7 and 8 that results in a protein with intact N- and C-termini, but internal deletion and an internal substitution of 29 amino acids (35, 52). This construct was described to restore the vacuolar/lysosomal enlargement phenotype in *Saccharomyces cerevisiae* and human fibroblasts described in 3.4.1.

3.5 Localization and intracellular trafficking of CLN3 protein

The low endogenous expression levels of CLN3 in mammalian cells result in difficulties to determine its intracellular localization. Many studies were carried out by overexpressing the CLN3 protein and often a fluorescence- or FLAG-tag was attached to facilitate the detection (38–40, 68–70). Using this approach, CLN3 has been shown to be located in many intracellular compartments with the highest abundance in lysosomes. However, both methods, overexpression and tagging, harbor the risk of mislocalization of the protein. For example, the high colocalization with lysosomes could be caused by degradation processes resulting from the cell's effort to downregulate the surplus of CLN3 or from tags masking unknown modification and targeting sites (69). To avoid this uncertainty, development of antibodies against CLN3 was initiated in order to study the native protein. Unfortunately, so far no monoclonal antibody against the full length protein could be generated and many studies on native proteins were vigorously disputed, because of contested binding of the used antibodies. In 2003, the first specific antibodies against the N-terminal amino acids 5-19 and the sequence of amino acids 225-280 were developed by Ezaki *et al.* (39). The N-terminal anti-CLN3 antibody used in the present study is identically prepared as the first one (obtained from S. Cotman, Molecular Neurogenetics Unit and Center for Human Genetic Research, Massachusetts General Hospital, Boston, Massachusetts, USA). By using the antibodies from Ezaki *et al*. in hepatic macrophages, Kupffer cells, CLN3 was shown to colocalize with acid phosphatase, a lysosomal protein activated by lysosomal fusion with endosomes and the late endosome marker lysobisphosphatic acid (LBPA), which is mediating the fusion of intraluminal vesicles within multivesicular bodies. However, usage of other cell models still resulted in a diversity of localizations reported for CLN3 protein and not all tissues expressing *Cln3*

mRNA (36, 71) produced the protein. The reason for this may be posttranslational regulation and demonstrates the importance of a preconceived choice concerning the appropriate cell line for localization and trafficking studies. So far, the majority of those studies were performed in non-neuronal cell lines, e.g. JNCL patient fibroblasts. The few studies using neuronal cell lines favor trafficking of CLN3 through the endoplasmic reticulum (ER) and Golgi apparatus to its main localization in lysosomal/endosomal vesicles (37, 40, 49, 70, 72) and within/adjacent to synaptic vesicles (40, 45, 73). Approximately 10% of CLN3 protein was reported to be present at the plasma membrane (PM) (45, 49, 74) and in lipid raft preparations (75). Alternatively, CLN3 may also traffic between the Golgi apparatus or trans-Golgi network and the PM, from where internalization could occur via the endocytic system. A recent overview about the putative intracellular trafficking is given by Cotman and Staropoli. (54).

Location of CLN3 within the Golgi and trans-Golgi network has been reported earlier in overexpression studies (68, 69, 76) and studies on Btn1p, the yeast orthologue of CLN3, showed a steady-state localization in the Golgi apparatus, where it colocalized with the UDP-galactose transporter Gms1p (77–79). The tubular Golgi structure was disrupted and fragmented and the expression level of Btn1p influenced number, localization and distribution of Golgi structures. In line with this, an extensive colocalization study detecting the endogenous CLN3 protein in human and rat neurons as well as human fibroblasts, confirmed localization of wild type CLN3 within the Golgi and TGN, where it colocalized with GRASP65, a structural protein involved in staple-formation, TGN-38, a marker of Golgi and early endosomes, β-1,4-galactosyl transferase, an integral Golgi protein transferring galactose to proteins or glucosylceramide (GluCer) (49). Colocalization with several endosomal proteins (RhoB, Rab11 and Rab4: small GTPases from early sorting, slow and dynamic recycling endosomes, respectively) and PM proteins (the neuromodulin GAP43; TNF-R1: a protein recycled between the PM and Golgi and participating in neurotoxic processes; alkaline phosphatase; Caveolin-1 and galactosylceramide (GalCer): a molecule resident on the cell surface and inside the Golgi) was also detected. No colocalization for wild type CLN3 was detected for the lysosomal proteins cathepsin D and Lamp1, nor for Rab7 (late endosomes and lysosomes) and EEA1 (early sorting endosomes). Vesicles positive for CLN3 were classified as dynamic and highly mobile.

In contrast, the mutant CLN3 protein was examined only in human fibroblasts harboring the common 1.02 kb mutation and not in neurons. The protein was reported to colocalize with lysosomal proteins cathepsin D and Lamp1, Golgi proteins GRASP65, TGN38 and Rab7 from late endosomes (49). As described before the regular tubular Golgi-structure was shown to be fragmented in these cells and displayed a rather perinuclear localization and colocalization with GalCer was detected solely in the fragmented Golgi and was absent from the PM. This phenotype is already known from Alzheimer disease, Creutzfeld-Jakob disease and prion protein disease and results from caspase-mediated cleavage of GRASP65 (49, 80–82). The mutant protein was not found to colocalize with Rab4, Rab11, GAP43, alkaline phosphatase or Caveolin-1, suggesting an impairment of the trafficking of CLN3 in the post-TGN-pathway. Suitably, Kyttälä *et al*. (40) reported CLN3 to reach early endosomes independently from both sorting motifs and the combination of dileucine motif and acidic patch is similar to a motif found in insulin-regulated aminopeptidase, functioning as an anchor to retain the protein in slow endosomal recycling compartments (83).

3.6 Putative functions and interaction partners of CLN3

Many theories about the innate function of CLN3 have been put forth, based on colocalization studies, computer predictions and immunoprecipitations. CLN3 was suggested to play a role in lysosomal acidification, arginine import, vesicle fusion and size, vesicular transport, a cytoskeleton linked function, autophagy, apoptosis and proteolipid modification. Although the exact cellular mechanisms are still unknown, it may be possible that the truncated CLN3$^{\Delta ex7/8}$ protein retains some of these functions (58, 72, 84) as supported by a study showing that worsening of phenotypes occurred after knock-down of human CLN3 with siRNA in JNCL patient cells (52).

3.6.1 Lysosomal function and pH homeostasis

A study by Pearce and Sherman in a *S. cerevisiae* strain with deleted Btn1p presented the vacuolar pH to be decreased during early growth phase. In contrast, deleted Btn1p in *S. pombe* results in an elevation of the pH and additive enlargement of the vacuole (58). This

is in line with the elevation of lysosomal pH in JNCL patient fibroblasts and a weaker lysosomal staining with LT-Red in a cerebellar cell model of JNCL (67, 85). The underlying cause may be a deregulation of the chloride channels ClC-3, ClC-4 and ClC-5 that was shown to result in an elevated endosomal pH and subsequently in a disease analogue to JNCL (23). Consequences of this pH elevation are less mature cathepsin D, altered processing of amyloid precursor protein (APP), impaired release of proteins bearing the M6P targeting signal and thereby disturbed metabolism of numerous proteins essential for cell functions (38, 86, 87). These effects aggravate by an additional trafficking defect of the cation-independent M6P receptor (CI-M6PR). After siRNA-mediated knock-down of CLN3, the exit of CI-M6PR from the TGN is reduced by 50% (88). Suitably, an increase of M6P-modified lysosomal enzymes was described by Sleat *et al*. (89), which could represent a compensatory effort of the cell to overcome the sorting defect (88). This process may involve the stress-response protein SBDS, that leads to Schwachmann-Bodian-Diamond Syndrome and was shown to interact with the C-terminus of CLN3 (79).

Therefore it is likely that CLN3 regulates vacuolar/lysosomal homeostasis indirectly by acting in the TGN as suggested previously by Gachet *et al.* (58).

3.6.2 Links to membrane trafficking

As the lysosomal changes can be implicated by disrupted delivery of their required enzymes, several studies were performed with regard to the whole vesicle trafficking system. Korade *et al*. (90) and Pike *et al*. (91) proposed a role for CLN3 in influencing membrane protein trafficking, regulation of neurotransmission and receptor trafficking, due to the implication that CLN3 may reside on specific membrane microdomains, which serve as centers for the assembly of signaling molecules. Hence, it was suggested that JNCL may represent a breakdown of lipid raft recycling from endosomes to cell membranes, impairing neuronal signaling and synaptic transmission (92). Suitably, Luiro *et al.* (93) described a delayed uptake of low density lipoprotein (LDL) in JNCL cells. In endocytosis experiments, LDL was incorporated only by EEA1 positive early endosomes and colocalized earliest two hours later with the lysosomal marker LBPA. Also Kyttälä *et al.* (40) reported for epithelial polarized cells, an involvement of CLN3 in lysosomal

transport, endocytosis and basolateral sorting. This was supported by the interaction between CLN3 and the protein causing the Finnish variant of LINCL, CLN5, that interacts itself with TPP1/CLN2 and might play a role in endosome-to-Golgi retrograde trafficking (94).

A sequence analysis of CLN3 showed a distant similarity with the equilibrative nucleoside transporter family SLC29 (95). This resemblance is based on two dileucine motifs in the hydrophilic N-terminal region prior to the first transmembrane domain. A similar structure was found in several proteins sorting polypeptides towards the TGN, endosomes or the PM. In line with these suggestions, Järvelä *et al*. (51) proposed CLN3 to be active in early endosomes by participating in their putative function as donor compartments for synaptic vesicles. This was supported by Luiro *et al*. (73) who showed that CLN3 is colocalizing with a beads-on-a string structure in neurites, and Järvelä *et al*. (51) suggested the ability of wild type and mutant CLN3 to move along the axon towards the neuronal plate. An explanation for this pattern would be a directed transport to the synapses. In fact, CLN3 was implicated in anterograde transport of microdomain-associated proteins and sphingolipids as GalCer and ganglioside GM_1 from the TGN to the PM in mouse brain endothelial cells (MBEC) (49, 76).

The influence of CLN3 on different trafficking routes within the cell may be explained by a functional linkage to the cytoskeleton. In fact, Getty *et al.* (96) found CLN3 to interact with non-muscle myosin II-B and Uusi-Rauva *et al.* (97) showed interaction between CLN3 and β-fodrin, Na^+K^+-ATPase and GRP78/BiP. Furthermore, Luiro *et al*. (93) reported an interaction of CLN3 with Hook1, which interacts by itself with Rab7, Rab9 and Rab11 in COS-1 cells. Additionally, Hook1 interacts with Ankyrin G, an adaptor protein for the spectrin-actin-cytoskeleton and with Vps18, a component of the HOPS complex (homotypic fusion and protein sorting). As interaction sites of CLN3, the cytoplasmic domains 1-33 and 232-280 were presented (93). CLN3 overexpression resulted in aggregation of Hook1, indicating a common binding site for both proteins. This site could play a role in the linkage of cytoskeletal elements and endosomes or other vesicles, explaining the colocalization of CLN3 with both networks. In accordance to this, the Hook1 homologue in Drosophila is involved in transport regulation of endocytosed ligands to the late endosomes. This function is mediated via maturation and/or stabilization of the

multivesicular bodies and fusion of endosomal membranes. Furthermore, mutations in Hook1 lead to a decrease in the number of late endosomes and premature degradation of endocytosed proteins (98). Also Cao *et al*. (99) showed a disability in membrane fusion events in Cb*Cln3*$^{\Delta ex7/8}$ cells. They described the inclusion bodies as immature autophagosomes incapable to fuse with lysosomes. Wild type Cb*Cln3*$^{+}$ cells displayed a gradual degradation of cellular organelles in different types of autophagic vacuoles (AV15, AV20) and finally lysosomes, where subcellular components were already unidentifiable. In contrast, both AV fractions and lysosomal fraction in cells from *Cln3*$^{\Delta ex7/8}$ liver presented the typical 'fingerprint profile'. Interestingly, accumulation of the subunit C of mitochondrial ATPase (ATPsubC) was also shown in liver cells from 12 month old wild type mice, assuming that this phenotype is not strictly NCL specific (99). A recent study of Chang *et al.* (100) supported the idea of fusion disability between autophagosomes and lysosomes and showed a reduction of accumulated LC3-II positive vesicles in mutant cerebellar cells after treatment with lithium. This treatment relocated the acidic vesicles in a rather perinuclear region, but it remained unclear which signaling pathway lithium is using to generate these effects. One option is the increased intracellular uptake of soluble N-ethylmaleimide-sensitive-factor attachment receptor (SNARE) complexes via lithium-mediated down-regulation of complexin 2 (101). Suitably, Btn1 overexpression was shown to reduce the assembly between Sed5 and other SNAREs, for example the SNARE recognition molecule Ykt6 that is required in phagophore formation is 1.4-fold upregulated in Cb*Cln3*$^{\Delta ex7/8}$ cells (54, 78, 102). Its homologue, synaptobrevin, was shown to be involved in removal of late autophagosomal compartments (103), a process defective in JNCL and leading to the observed accumulation of storage material.

3.6.3 Lipid metabolism

Many of the proteins affected in JNCL are proteolipids and therefore dependent on an intact membrane composition. Hence, the defects described above may be also caused by alterations in the integrity of the lipid metabolism in JNCL model systems. Already in 1996, a 33% reduction of fatty acid oxidation was claimed in CLN3 deficient patient fibroblasts (104) and an earlier version of the computer prediction software PFAM showed low level homology between the N-terminus of CLN3 and fatty acid desaturases

(105). Rakheja *et al.* (28) proposed CLN3 to be a novel palmitoyl-protein Δ-9 desaturase (PPD). Although they could not demonstrate that CLN3 directly desaturases the palmitoyl groups and the decreased activity was only shown in brain and pancreas of CLN3 deficient mice, CLN3 may influence different proteins by regulating their palmitoylation status (78, 106). For example, Chang *et al*. suggested an interaction of Calsenilin with the C-terminal amino acids 385-438 of CLN3 (107). Calsenilin is known to be palmitoylated and to interact with the presenilin proteins PSEN1 and PSEN2, which regulate APP processing and are shown to be mutated in Alzheimer disease (108, 109). Furthermore, Calsenilin induces Ca^{2+}-toxicity through modulation of neuronal sensitivity in a pro-apoptotic manner (110). Higher Ca^{2+}-concentrations decreased the interaction with CLN3 supporting the notion of an antiapoptotic role of CLN3 (see also VII.3.1.2).

Several other studies lead to the assumption that CLN3 could influence properties of membrane proteins located in the same microdomains independently from a PPD-function. Hobert and Dawson (111) assumed that CLN3 plays a role in biosynthesis of the lipid raft component bis(monoacylglycerol)phosphate (BMP), what can be indirectly due to changes in the lysosomal pH (28). Seigel *et al*. (64) reported high concentrations of dolichol-pyrophosphoryl-oligosaccharides in the brains of JNCL patients and assumed that synthesis of the glycosylation metabolite $Glc_3Man_9GlcNAc_2$-PP-dolichol was unaffected, but catabolic by-products were stored in lysosomes due to inefficient degradation. An increase in phosphodolichol was also described by Pullarkat *et al*. (112) and Hall *et al*. (113) in NCLs, Alzheimer, GM_1-Gangliosidosis and aged tissues and recently, phospholipid levels and their distribution were shown to be altered in Btn1p-deficient *S. cerevisiae* (114). Furthermore, Persaud-Sawin *et al*. (49) reported increased ceramide levels in CLN3-deficient brains and cells that could be restored by overexpression of the wild type protein as described in detail in 3.1.1. The current version of PFAM lists CLN3 as a member of the major facilitator superfamily (MFS) clan, suggesting a possible role as a transporter with yet unknown substrate specificity (115). Although most MFS transporters are predicted to contain 12 transmembrane domains, a homodimer of CLN3 as described by Storch *et al.* may lead to similar functionality (45, 54).

In summary, the actual function of CLN3 remains elusive, but there is strong evidence that it modulates a process or condition that is essential in many cellular pathways (116) and that is related to lipid metabolism.

4. Membrane lipid rafts

The regulation of many cellular processes in eukaryotic cells is achieved by compartmentalization of cellular membranes to organizing centers for molecules carrying out a particular function. These specialized membrane lipid microdomains, referred to as membrane rafts, serve as platforms for the assembly of signaling complexes, control neurotransmission, endocytosis and membrane protein trafficking, and regulate intrinsic membrane properties as fluidity and curvature (117). It is heavily debated, if the occurrence of these domains is caused by conditions arising from the detection method. However, theoretical considerations and experimental data from artificial membranes suggest their generation as an impact of physico-chemical properties of their components (118). The efficient composition of rafts is tightly regulated and their high enrichment in sphingolipids and cholesterol appears essential for lateral phase segregation (117, 119).

5. Glycosphingolipid metabolism

5.1 (Glyco-)sphingolipid biosynthesis

5.1.1 De novo biosynthetic pathway

The first steps of glycosphingolipid (GSL) *de novo* synthesis take place at the cytoplasmic site of the ER and lead to the formation of ceramide (120). From there, ceramide is translocated to the lumenal site, where it is galactosylated by a ceramide galactosyltransferase in order to form GalCer. GalCer is then transferred to the lumenal site of the Golgi apparatus (121, 122). A part of GalCer can be sialylated there to the gala-series ganglioside GM_4 which localizes with myelin as a rare ganglioside of the human brain (123–125).

Alternatively, ceramide is transferred from the ER to the cytosolic site of the *cis*-Golgi by the aid of the ceramide transfer protein (CERT), where either sphingomyelin is formed or ceramide is glucosylated by glucosyl-transferase forming glucosylceramide (GluCer) (126–129). GluCer is then flipped to the lumenal Golgi site. Presumably this action is carried out by a multidrug transporter (130). Further processing of GluCer leads to the formation of gangliosides as shown in Figure 2. The complexity of ganglioside headgroups is achieved by a gradient distribution of glycosyl-transferases and possibly by the formation of multiglycosyl-transferase complexes for each ganglioside (131–134).

5.1.2 Degradative process

The degradation of GSLs takes place in the endocytic-endosome-lysosome pathway and is carried out by (exo)glycohydrolases (120). Glycohydrolases are soluble enzymes that require the formation of multivesicular bodies by invagination of membranes to gain access to their substrates. Furthermore, acidic pH and the presence of sphingolipid activator proteins (saposins) are necessary for their function (123).

First, all multi-sialogangliosides are desialylated to the a-series gangliosides GM_1 and GM_2, which are resistant to lysosomal sialidase, and lactosylceramide (LacCer; from GM_3) (120). The turnover of GM_1 to GM_2 is then accomplished by the enzyme β-galactosidase in the presence of the GM_2 activator protein (GM_2-AP) or saposin B (Sap-B) (135). GM_2-AP is also required in the degradation of GM_2 to GM_3 by β-hexosaminidase (136). In some cell types/animals a special GM_1 and GM_2 sialidase is then transforming these gangliosides to their asialo-derivatives GA_1 and GA_2, that are then further degraded to LacCer (137–140). Alternatively, endoglycoceramidases were reported to hydrolyze the *O*-glycosidic linkage between ceramide and the oligosaccharide chain of various GSLs, but they are not likely to be present in mammals (141).

5.1.3 Ganglioside/Glycosphingolipid turnover

Salvage processes are indispensable to remodel the membrane GSL composition in response to focal stimuli. This is underlined by the fact that approximately 80% of

sphingosine undergoes metabolic recycling and large parts of GSLs are directly recycled without processing (120, 142). Both, sialyltransferases and sialidases were shown to exist on the PM and reciprocally interconvert GSLs in order to adapt in a highly dynamic manner to the current requirements of the cell. Yohe *et al.* described a myelin-associated sialidase and cultured rat cerebellar granule cells were capable to process exogenously added GM_3, GD_{1a} and GD_{1b} while endocytosis and lysosomal function were suppressed (143–145). Furthermore, GM_1 levels in cultured hippocampal neurons were reported to be regulated by a ganglioside-specific PM-associated sialidase. This regulation is essential for axonal growth and regeneration after axotomy (146).

5.2 Sphingolipids

The hydrophobic core structure of sphingolipids consists of ceramide, a sphingoid base in amid linkage to a fatty acid of 18-20 carbon atoms at the C2 position. The headgroup is attached to C1 and responsible for the classification into phospho- and glycosphingolids (GSLs) (147). Both classes of sphingolipids are particularly abundant in the central nervous system. Due to their amphiphilic nature sphingolipids localize within membranes, but they are able to interact with other proteins and lipids in cis- (laterally) and trans-mode (extracellular matrix or other cells) (148). Phosphosphingolipids play a central role in survival and growth. Their primary representatives are sphingomyelin in animals and inositol phosphoceramide (IPC) in plants and fungi (147). Sphingomyelin is particularly abundant in the myelin sheath and therefore considered as insulator of nerve fibers.

5.3 Glycosphingolipids

Glycosphingolipids (GSLs) show a broad structural heterogeneity in their headgroups. These structures are built from a variety of monosaccharides linked by various types of glycosidic bonds and are proposed to determine the function of the respective GSL (147). GSLs are detected in many subcellular compartments *en route* to their intracellular destinations, but localize mainly to the outer leaflet of the PM (120). They play an important role in immuno-modulation, receptor activity, cell-cell interactions, cell

adhesion, neural differentiation and development, functional recovery of damaged nervous system and tumor growth (122 and references within). In contrast to phosphosphingolipids, GSLs are dispensable for normal growth and survival of animal cells in culture, but mice with disrupted glucosylceramide synthase are embryonically lethal, proposing a role for GSLs in the development on organism level (149–151). Furthermore, GSLs are involved in membrane trafficking events. Depletion of all sphingolipids by knock-out of serine palmitoyltransferase was shown to inhibit caveolar endocytosis and *vice versa* (152, 153). Likewise, reduction of GSL levels by the glucosylceramide synthesis inhibitors 1-phenyl-2-decanoylamino-3-morpholino-1-propanol (PDMP) and DL-threo-1-phenyl-2-palmitoylamino-3-morpholino-1-propanol (PPMP) led to accumulation of autophagic vesicles (154, 155). These reports show contradictory effects on the autophpagy markers Beclin-1, ATG5 and mTOR, raising the question whether the increased number of autophagic vesicles is caused by blockage of the maturation process, by an upregulation of autophagy in general, or if it differs depending on the cell type. The mechanism describing how GSLs influence membrane trafficking events is also heavily disputed. Colocalization with cytoskeletal elements was shown by Sakakibara *et al.* (156) and Gillard *et al.* (157–159) and GSLs were implicated in determining the localization of membrane bound enzymes as the APP-processing γ- and β-secretases (160). Additionally, GSLs may influence fusion/fission events by modulating the physic-chemical membrane properties. The surface area occupied by their oligosaccharide chain is very large and imparts therefore a strong curvature to the membrane (118).

5.3.1 GSLs as part of the cell's sorting machinery

As modulators of the membrane structure, GSLs were suggested to be indispensable parts of the Golgi sorting machinery (147). GSL containing membranes are 30% thicker than membranes of unsaturated phospholipids. The efficacy of this feature in sorting was shown by David *et al.* in 1998 (161). Under normal conditions, exocytic vSNAREs are necessary for secretion in yeast. This requirement could be bypassed by elongation of the long-chain fatty acids of some secreted proteins. As the membrane thickness increases gradually towards the *trans*-Golgi, its membrane composition converges to the typical

membrane raft segregation of the PM. Therefore, GPI-anchored proteins and GSLs were shown to associate in detergent resistant complexes already in the Golgi when transport to the TGN was blocked by monensin (162). The exact mechanism how the gradual segregation within the Golgi is achieved and maintained remains a matter of dispute, but the exclusion of sphingolipids and cholesterol from coat protein 1 (COPI)-positive vesicles contributes to this process (163). The tendency of sphingolipids to trigger phase separation by generating rigid bilayers may result in adjacent areas of higher membrane curvature that are prone to bud from the Golgi cisternae. Such a sorting machinery would be self-organizing eliminating the need of active transport. For example, lipids with longer and more saturated chains are preferentially transported to LE instead of recycling endosomes (164).

A similar lipid-based sorting was shown for apical and basolateral membranes or axons and dendrites (165–167). Besides discrete tyrosine- or dileucine based motifs that often resemble endocytosis or lysosomal/endosomal targeting signals basolateral sorting was shown to be mediated via N-glycans of sorted glycoproteins (168, 169). These oligosaccharides may interact with the headgroups of certain GSLs in order to direct their trafficking. As a consequence, apical sorting may be realized in a passive manner by retention of the remaining proteins.

5.4 Gangliosides

Gangliosides are GSLs highly involved in the development and maintenance of the brain. They are required for neurite outgrowth and long-term axonal stability via axon-myelin interactions (172, 173 and references within). Gangliosides also contribute to the regulation of Ca^{2+} homeostasis. They carry one or more sialic acid residues, such as N-acetylneuraminic acid (Neu5Ac), N-glycolylneuraminic acid (Neu5Gc) or 5,9-diacetyl-neuraminic acid (Neu5Ac9Ac). The negative charge of this residues results in interaction with calcium ions that are critical for neuronal responses (172). During brain development both, the levels of gangliosides and their degree of sialylation increase (173, 174). In the adult brain 75% of the sialic acid content is bound to gangliosides (171) and they constitute 10-12% of the total lipid content (20-25% of the outer layer) of neuronal

membranes (120). Besides the complexity of their oligosaccharide chain, also the type of fatty acid attached to the sphingoid base of gangliosides changes during development. While stearic acid (C18) is the main fatty acid in most tissues, CNS gangliosides contain often arachidic acid (C20). During development the ratio of C20/C18-sphingosine changes dramatically as shown for ganglioside GD_{1a} in the cerebellum of rats. Sonnino *et al*. measured a 16-fold increase between 8-days and 2-years of age (175).

The main gangliosides of adult human brain are GM_1, GD_{1a}, GD_{1b} and GT_{1b} (97%) in this order of occurrence (174). They share the same neutral glycan core, but vary in their number of sialic acids (171). GM_1 concentrates in white matter tracts, GD_{1a} shows a similar pattern in the gray matter and GD_{1b} and GT_{1b} are present in the whole brain (176). However, mutations in biosynthetic enzymes eliminating the normal complement of a- and b-series (see Figure 2) lead only to weak phenotypes, implicating that the presence of complex 0- or a-series gangliosides alone is sufficient for the stabilization of the axon-myelin interaction (173 and references within). In contrast, mutations in the *B4galnt1* gene in mice, resulting in a lack of complex gangliosides (only GM_3 and GD_3), lead to enlarged and disorganized paranodal loops that occasionally fail to form axon-glial junctions (177). This results in the loss of the regenerative capacity of the nervous system (178). Additional elimination of the *St8sia1* gene (*B4galnt1/St8sia1*-double null mice generate only GM_3) causes nerve degeneration and progressive motor, behavioral and sensory deficits (179, 180). Finally, a mutation in the gene encoding the GM_3 synthase leads to a severe infantile neurodegenerative disorder with progressive brain atrophy, epilepsy and chorea (181). Although defects in ganglioside metabolism have been shown to play a crucial role in other lysosomal storage disorders, their contribution to NCL pathology is largely unknown.

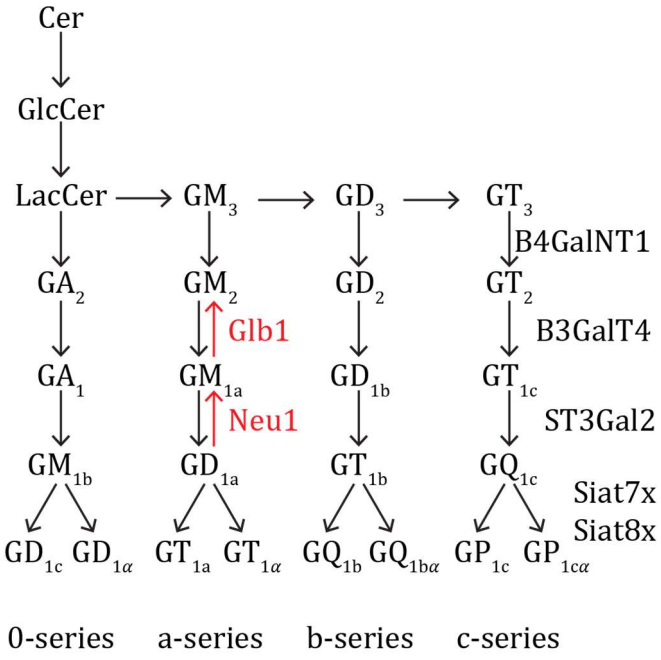

Figure 2. Scheme of ganglioside biosynthesis.

5.5 Ganglioside GM_1

Monosialotetrahexosylganglioside (GM_1) is the most thoroughly investigated member of the a-series gangliosides. It carries a single sialic acid residue linked to the inner galactose molecule and acts as the binding site for subunit B of cholera toxin (CTxB), co-receptor for serotonin, GABA and glutamate and seed for Aβ fibrillation (reviewed in 182–184). GM_1 has been proposed to play a critical role in neurogenesis, particularly in process extension, arborization, and possibly also synaptogenesis (185). While the total amount of gangliosides increases approximately three-fold during the development of the central nervous system, that of GM_1 and GD_{1a} increases 12- to 15-fold during the same period (186). Both, GM_1 and GD_{1a} were shown to be essential in neurons during the myelination process (177). In cerebellar granule cells GM_1 associates with the neural cell adhesion molecule TAG-1 that was shown to be required for the correct localization of the K^+-channels Kv1.1 and Kv1.2 in juxtapranodes (187, 188). Suitably, lack of GM_1 in GM_2/GD_2 synthase null mice results in the disruption of paranodal junctions (177). Furthermore, the extracellular matrix molecule laminin-1 leads to the formation of large GM_1 clusters in the cell membrane that activate the nerve growth factor (NGF) receptor TrkA in the absence of neurotrophins and induce neurite outgrowth via Lyn, Akt and MAPK (189). GM_1 is also thought to modulate the binding properties of cell adhesion molecules, such as NCAM and N-cadherin, concomitant with an increased nuclear Ca^{2+} efflux during neuronal differentiation (190). Both effects were shown to be blocked in living cerebellar cells after administration of CTxB. Besides its putative functions on the PM, GM_1 was also reported to act on intracellular membranes, for example by stimulating autophagy (154). The neuroprotective role of GM_1 was reviewed by Mocchetti (2005) (191) and will be detailed in section VII.4.1.

6. Scope of the Study

Defects in ganglioside metabolism play a crucial role in many lysosomal storage disorders; however, the contribution of gangliosides to NCL pathology is largely unknown. Particularly, a-series gangliosides have been shown to be involved in the development and sustenance of the brain, where they are essential for neurite outgrowth and cell survival (192). The present study focuses on the analysis of central enzymes and metabolites of the a-series ganglioside pathway in a JNCL cell model.

The specific aims of this study are:

- A detailed overview of the differences in the a-series ganglioside pattern between homozygous Cb*Cln3*$^{+}$ and Cb*Cln3*$^{\Delta ex7/8}$ cells.
- Characterization of the enzymes and metabolites responsible for these alterations.
- Identification of cellular mechanisms leading to the observed changes.
- Investigation of a potential role of CLN3 protein in ganglioside metabolism.

V. MATERIALS AND METHODS

Chemicals, equipment and software used in the present study are listed in the Appendix.

1. Cell culture

1.1 General media and other solutions

Dulbecco's Modified Eagle Medium (DMEM) containing 4.5 g/l glucose, 110 mg/l sodium pyruvate and L-glutamate (Gibco®) supplemented with 10% (v/v) FBS (Sigma-Aldrich®), 100 µg/ml Penicillin/Streptomycin (Invitrogen™), 24 mM potassium-chloride and 200 µg/ml Geneticin G418 (Invitrogen™) and filtered through a 0.22 µm bottle top filter (neoLab®) was used for culturing the Cb cells. Washings were carried out with 1x phosphate buffered saline (PBS) containing 137 mM sodium chloride, 10 mM phosphate and 2.7 mM potassium-chloride at pH 7.4 (Invitrogen™). For sample preparation before fixation, complete PBS (CPBS) was used containing 0.9 mM Ca2+ and 0.9 mM Mg2+, pH 7.4 to maintain the integrity of cell adherence.

1.2 Model organism/cell lines

Cell lines used for this study were obtained from Dr. S. Cotman (Molecular Neurogenetics Unit and Center for Human Genetic Research, Massachusetts General Hospital, Boston, Massachusetts, USA). In particular, the experiments were carried out on conditionally immortalized cerebellar (Cb) granule neuronal precursor cells, derived from P4 *Cln3*$^{+/+}$ (clones 7c1-2 and 7c1-3) and homozygous *Cln3*$^{\Delta ex7/8/\Delta ex7/8}$ (clones 6a3-2 and 4c1-3) CD1 mice (67). The *Cln3*$^{\Delta ex7/8}$ mutation present in these cells corresponds to the 1.02 kb deletion of human JNCL patients. Handling and maintenance of these cells occured in the same manner as described by Fossale et al. (67).

Hereafter, the general terms 'Cb*Cln3*$^{+}$' and 'Cb*Cln3*$^{\Delta ex7/8'}$ will refer to the 7c1- 2 clone of the *Cln3*$^{+/+}$ cell line and the 6a3-2 clone of the homozygous *Cln3*$^{\Delta ex7/8/\Delta ex7/8}$ cell line, respectively. Usage of the other clones in particular cases will be pointed out.

1.3 Cell culture growth

Both cell lines were kept at 33°C with 5% CO_2 atmosphere. They were maintained in 0.01% poly-ornithine coated 75 cm^2 Sarstedt cell culture bottles and passaged shortly before reaching 95% confluence.

All work with living cells was conducted under a Herasafe™ KSP Class II Biological Safety Cabinet. Prior to application, DMEM and PBS were warmed up to 33°C in a water bath. Cell culture medium was removed by aspiration and after washing with 10 ml PBS, the cells were detached from the bottle surface by rinsing with 2 ml Trypsin-EDTA (Invitrogen™) and 5 min incubation at 33°C. To reach a 100% cell suspension, the appropriate amount of growth medium was added to the cells. Finally, Cb cells were passaged in fresh medium at the required density.

Cb cells grown for additional seven days after reaching confluency are considered 'aged'. In contrast to non-aged homozygous $CbCln3^{\Delta ex7/8/\Delta ex7/8}$ cells, 'aged' $CbCln3^{\Delta ex7/8/\Delta ex7/8}$ cells aggregate lysosomal storage material (67).

1.4 Cryopreservation of the cells

Cells from both strains between the passage numbers 3 and 7 were frozen down in order to preserve them for long-term storage. First, freezing medium was prepared containing 70% DMEM, 20% FBS and 10% of the cryoprotective agent DMSO. Cells were trypsinized and resuspended in ice-cold PBS. $1x10^6$ cells per tube were aliquoted, centrifuged at 4°C and 1500 x g for 5 minutes, resuspended in 1 ml of freezing medium and transferred into Cryo Pure tubes (Sarstedt). Finally, aliquots were frozen for 24 hours at -80°C and then translocated into the liquid nitrogen tank.

1.5 Reactivating cells from cryopreserved stock

For any experiments, cells from both strains were used only between passage number 3 and 20. For this purpose, a fresh batch of cells had to be revived from aliquots frozen in the gas phase of liquid nitrogen tank every 6 weeks. A 1.6 ml Cryo Pure tube (Sarstedt)

for every cell line was thawed quickly. The cells were suspended thoroughly in 1 ml growth medium and transferred to a 15 ml falcon tube with 4 ml fresh medium. Then the tubes were centrifuged at 1125 x g for 5 min and the DMSO-containing supernatant drained.

The pellet was resuspended in 4-5 ml DMEM and transferred into a 25 cm^2 cell culture bottle. When the cells reached 90-95% confluency, they were passaged into a 75 cm^2 bottle and maintained as usual.

1.6 Removal of cholesterol with methyl-β-cyclodextrin

Proliferating Cb*Cln3*$^{+}$ and Cb*Cln3*$^{\Delta ex7/8}$ cells were seeded in 12 well plates to a surface area density of 20-30%, grown up to 60% density and half of the cell culture medium was exchanged to DMEM with or without 10 µg/ml methyl-β-cyclodextrin (MβCD). After 10 min of incubation at 33°C, cells were fixed and stained as described in section 4.1.

1.7 Transfection

3.5x10^4 proliferating Cb*Cln3*$^{+}$ and Cb*Cln3*$^{\Delta ex7/8}$ cells were seeded in 12 well plates, grown to 60% density and transfected with CLN3-myc or red fluorescent protein (RFP), respectively. Thereby 1 µg of DNA was added to 100 µl JetPRIME buffer, vortexed for 10 seconds and spinned down. Afterwards, 2 µl of JetPRIME reagent were added to the DNA solution, vortexed again for 10 seconds and spinned down. After 10 minutes at room temperature to enable complexes formation, 100 µl of the solution was added to each well and kept for 24 hours at 33°C. One sample per genotype and immunofluorescence staining was not transfected (controls) in order to distinguish transfected from non-transfected cells.

2. Biochemistry

2.1 Dot blot

Proliferating Cb*Cln3*$^{+}$ and Cb*Cln3*$^{\Delta ex7/8}$ cells were seeded in 6 well plates to a surface area density of 20-30%, grown up to 80% density, and lysed with CellLytic M cell lysis reagent (Sigma, C2978) containing Protease Inhibitor Cocktail (Sigma, P8340). Triplicate dots from three different passages (P8, P10, and P12) were applied on nitrocellulose membranes, and the membranes were blocked with 5% milk powder in PBS. CTxB-HRP (Invitrogen, C34780) was used to detect GM_1 and the ECL reaction imaged using Intas ChemoStar (Intas, Göttingen, Germany). Intensity analysis was performed with ImageJ after background correction. Thereby mean background value was subtracted from all intensity values and all values normalized to the mean signal intensity value of Cb*Cln3*$^{+}$ cells. Statistical significance was determined performing unpaired Student's t-test.

2.2 Precipitation with trichloroacetic acid (TCA)

In order to obtain a higher concentration of total cell lysates, TCA was added to the sample to a final 10% solution and kept 30 minutes on ice. After 30 minutes of centrifugation at 13000 rpm and 4°C, the supernatant was drained and the pellet dried thoroughly. The resulting concentrate was resuspended in LDS loading buffer.

2.3 Immunoblot

Proteins of total cell lysates of Cb*Cln3*$^{+}$ and Cb*Cln3*$^{\Delta ex7/8}$ cells were separated on 4-12% Bis-Tris SDS-PAGE and transferred to PVDF. Membranes were blocked for 2 h with either 5% milk- or 5% BSA-0.05% Tween-TBS and probed with anti-β-gal (1:1000, Abcam, ab156766), anti-caveolin-1 (1:500, Santa Cruz, SC-894), anti-Lamp1 (1:1000, Sigma, L1418), anti-Neu1 (1:200, Sigma, AV44286), anti-PPCA (1:200, Sigma, SAB4502268) and anti-β-actin (1:5000, Sigma, A1978) primary antibodies, incubated with peroxidase-conjugated goat-anti-mouse IgG (1:30 000, Jackson IR, 115-035-003) and developed with ECL solution (50 mM Tris-HCl, pH 8.5, 1.25 mM Luminol, 0.2 mM coumaric acid). Intas ChemoStar was used for detection and LabImage 1D (Kapelan, Bio-Imaging Solutions) and Fiji/ImageJ v1.47b for further analysis.

3. Fluorimetric quantifications

The fluorimetric quantifications described below were performed by Anton Petcherski (Goethe University, Frankfurt am Main).

3.1 CTxB-FITC flow cytometry

$4x10^5$ proliferating Cb*Cln3*$^+$ and Cb*Cln3*$^{\Delta ex7/8}$ cells were seeded per well in 6 well plates. After 24 h, cells were trypsinized and resuspended into ice-cold PBS buffer containing 20 mM HEPES. Subsequently, cells were either permeabilized with 11 µg/ml digitonin (for intracellular labeling), or left unpermeabilized (for cell surface labeling), and incubated with 1 µg/ml CTxB-FITC. Labeled cells and unlabeled autofluorescence controls were measured with a BD FACSAria flow cytometer (10,000 events per sample). WinMDI 2.9 software was used to compute geometrical mean. Means were corrected for autofluorescence and subsequently normalized pairwise to the wild-type sample to adjust for staining and treatment variations. Due to the higher susceptibility of living cells to minimal deviations in the staining procedure, paired t-test was used to test for statistical significance.

3.2 CTxB-FITC fluorometry

$1.0x10^5$ proliferating Cb*Cln3*$^+$ and Cb*Cln3*$^{\Delta ex7/8}$ cells per well were seeded in 24 well plates. After 24 h in culture, the cells were washed twice with CPBS and fixed with 4% PFA in CPBS. Cells were either left unpermeabilized (surface staining) or permeabilized (total staining) with 20 µg/ml digitonin and labeled with CTxB-FITC (1 µg/ml). Fluorescence signal was measured with a PerkinElmer Victor X3 plate reader with each treatment group represented at least as triplicate. Arithmetic mean signals were corrected for autofluorescence. Unpaired Student's t-test was used to test for statistical significance.

3.3 Measurement of β-Galactosidase activity

Non-aged and aged Cb*Cln3*$^+$ and Cb*Cln3*$^{\Delta ex7/8}$ cells were seeded onto 15 mm glass coverslips at a density of 50,000 cells per well in 12 well plates and allowed to attach

overnight. Subsequently, cells were fixed and processed using a senescence β-galactosidase staining kit (Cell Signaling) according to the manufacturer's guidelines. In order to stain lysosomal β-galactosidase, the pH of the staining solution was adjusted to 4.5. The following day, the samples were washed three times with PBS and mounted onto 1 mm object slides (neoLab®) using Mowiol mounting medium. Images were recorded on a Zeiss Axioskop 50 upright microscope equipped with a 10x and a 63x Zeiss Plan Neofluar objective and a Moticam 1SP CMOS camera. Positive β-galactosidase signal was identified and quantified using Cellprofiler (version 2.0.11710) module UnmixColors. Statistical significance was tested using unpaired Student's t-test.

3.4 *MTT assay*

Non-aged Cb*Cln3*$^{+}$ and Cb*Cln3*$^{\Delta ex7/8}$ cells were seeded into 96 well plates at a density of 10,000 cells per well in 100 µl. After 24 hours DMSO (Sigma) or ganglioside GM_1 salt (Avanti Polar Lipids) diluted in DMSO were added to the cells in 10 µl to the final concentration. The treatments were performed in four replicates and the DMSO concentration was kept below 0.1% at all times. After 22 hours, 22 µl of 3-(4,5-Dimethylthiazol-2-yl)-2,5-diphenyl-tetrazolium bromide (MTT) solution (5 mg/ml) were added to the cell culture media and incubated for 2 hours. Subsequently, wells were briefly analyzed for the formation of formazan crystals and 100 µl of MTT solubilization solution (5 mg/ml sodium dodecylsulfate, 50% dimethylformamide in 0.05 N HCl) were added to the wells. After overnight incubation, the complete solubilization of the crystals was confirmed and absorption at λ 540 nm was measured with a PerkinElmer Victor X3 plate reader. Statistical significance between treatments was assessed by one-way ANOVA.

4. Microscopy

4.1 Immunofluorescence

Proliferating Cb*Cln3*$^{+}$ and Cb*Cln3*$^{\Delta ex7/8}$ cells grown to 60% confluency were washed three times briefly with CPBS, fixed with 4% para-formaldehyde and subsequently permeabilized with 20 µg/ml digitonin for 10 min. Autofluorescence caused by free aldehydes was quenched for 10 min with 50 mM glycine and unspecific antibody-binding

Table 1. Primary and secondary antibodies and dyes used for (immuno)labelings

dyes			
dye	**epitope/ligand**	**supplier**	**concentration**
AlexaFluor®647-conjugated WGA	GlcNAc and NeuAc containing proteins	Molecular Probes®, W32466	2 µg/ml
CTxB-FITC	GM_1 ganglioside	Invitrogen, C-22841	2 µg/ml
DAPI	DNA	Sigma, D9542	10 ng/ml
Filipin III	cholesterol	Sigma, F4767	125 µg/ml
Lysotracker® Red DND-99	acidic organelles	Molecular Probes®, L-7528	500 mM

primary antibodies			
epitope/ligand	**host**	**supplier**	**concentrations**
Glb1	mouse	Abcam, ab156766	1:100
caveolin-1	rabbit	Santa Cruz, SC-894	2:25
CLN3	rabbit	S. Cotman, 'C9681'*	1:100
DyLight™ 549-labeled CLN3	rabbit	S. Cotman, 'C9681'*	1:50
GM_1	rabbit	Calbiochem, 345757	1:100
GM_2	rabbit	Calbiochem, 345759	1:100
GD_{1a}	mouse	Millipore, MAB5606	1:100, 1:500
Giantin	rabbit	Sigma, SAB2100948	1:50
gm130	rabbit	Sigma, G7295	1:100
HRas	rabbit	Abcam, ab32417	1:50
LC3B	rabbit	Abcam, ab51520	1:50
LBPA	mouse	echelon, Z-PLBPA	1:500
Myc	mouse	Cell Signaling, 9B11	1:1000
neuraminidase 1	rabbit	Sigma, AV44286	1:100
NRas	goat	Abcam, ab77392	1:50
PPCA	rabbit	Sigma, SAB4502268	1:50
Rab7	rabbit	Cell Signaling, 9367	1:50
TGN46	rabbit	Abcam, ab50595	1:100

secondary antibodies				
epitope	**host**	**label**	**supplier**	**concentration**
rabbit	donkey	AlexaFluor® 647	Molecular Probes®, A31573	1:500
rabbit	donkey	AlexaFluor® 488	Molecular Probes®, A21206	1:500
mouse	donkey	AlexaFluor® 546	Molecular Probes®, A10036	1:500
mouse	donkey	AlexaFluor® 647	Molecular Probes®, A31571	1:500
goat	donkey	DyLight™ 649	Dianova, 705-495-147	1:500

* custom antibody established by Cotman laboratory to identical epitope (amino acids 5-19) as that reported in Ezaki et al (2003) (39)

blocked with 5% BSA for 30 min. (Immuno)labeling was performed using the antibodies and dyes listed in Table 1. Incubation with DAPI (Sigma, D9542) was performed for 5 min with a 10 ng/ml dilution. All solutions were prepared in sterile filtered PBS, pH 7.4 (Invitrogen, 10010-056). Finally, coverslips were mounted onto 1 mm object slides (neoLab®) using Mowiol mounting medium.

4.1.1 Samples stained with filipin

After fixation, cells were washed 20 times with PBS and subsequently quenched for 10 min with 50 mM glycine to avoid autofluorescence caused by free aldehydes. Samples were stained/permeabilized for two hours with 125 µg/ml filipin in blocking buffer (5% BSA-PBS) to prevent unspecific antibody-binding or only 5% BSA-PBS (controls). After 20 washings with 0.5% BSA-PBS, cells were immunostained as described above, washed further five times with 0.5% BSA-PBS and two times with PBS only. Finally, coverslips were mounted onto 1 mm object slides (neoLab®) using Mowiol mounting medium.

4.2 CTxB-FITC pulse-chase

Non-aged Cb*Cln3*$^{+}$ and Cb*Cln3*$^{\Delta ex7/8}$ cells were seeded onto 15 mm glass coverslips at a density of 50,000 cells per well in 12 well plates and allowed to attach overnight. The cells were then given a 5 min pulse of CTxB-FITC, and after a chase time of 0, 5, 15 or 30 min fixed with 4% PFA in PBS. For better identification of the perinuclear signal, CTxB-FITC signal intensity was normalized. Cells positive for perinuclear CTxB-FITC accumulation were counted from four individual experiments using CellCounter plugin for Fiji/ImageJ v1.47b. Immunofluorescence labelings were performed as described above using anti-LBPA, anti-TGN46, anti-gm130, anti-β-gal, anti-CLN3 and anti-WGA-647. This work was performed in collaboration with Anton Petcherski (Goethe University, Frankfurt am Main).

4.3 Confocal microscopy

Confocal microscopy images were obtained with a Leica TCS SP5 confocal laser scanning microscope equipped with a HCX PL APO ×63/1.4 NA objective. To avoid emission crosstalk all channels were recorded sequentially with appropriate excitation and emission wavelengths.

4.4 Wide field microscopy

Wide field microscopy images were obtained either with a Zeiss Axiovert 200M wide field fluorescence microscope with a Zeiss Plan Apochromat equipped with 63x/1.4 NA objective and Micro-Manager 1.4 software, or with a Zeiss Axioskop 2 mot plus wide field fluorescence microscope equipped with a Zeiss Neofluar 40x objective and Zeiss Axiovision 4.6 software.

4.5 Förster resonance energy transfer (FRET)

For measurement of the FRET efficacy of endogenous GM_1 and CLN3 levels, immunofluorescence samples were prepared as described above. As FRET pairs CTxB-FITC and a DyLight™549-labeled anti-CLN3 antibody or an AlexaFluor®546-labeled anti-Neu1 antibody and transfected CLN3-GFP were used. Fluorescence images were acquired at 495 nm (for FITC, GFP) and 556 ± 20 nm (for DyLight™549, AlexaFluor®546) by using dual-view optics. Analysis and calculation of FRET efficacy were performed automatically using the ImageJ plugin pixFRET. Thereby spectral bleed-through (SBT) models were calculated using the best-fitting model.

5. *In silico*/statistical analysis and image processing

All values are means ± s.e.m besides the measurements of CTxB-FITC that where shown as mean ± SD to emphasize the small variation. Mean values are considered as significantly different if $p\text{-value}<0.05$.

5.1 Automatic signal intensity analysis

Cell area of individual cells was detected and measured by normalization of the CTxB-FITC or WGA signal using CellProfiler (version 2.0.11710). Mean signal intensity of each image was measured and summarized to the mean ± SEM of each sample. Outliers were removed using Grubb's test and unpaired Student's t-test was applied to determine statistical significance.

5.2 Analysis of gene expression data

The analysis of the expression of genes connected to GM_1 metabolism is based on previously generated expression data by Cao *et al.* (193). The alteration in the expression between Cb*Cln3*$^{+}$ and Cb*Cln3*$^{\Delta ex7/8}$ cells was calculated and the obtained values were plotted as a network using Cytoscape software (version 3.02). The direction and magnitude of the alteration where thereby color coded (green = decrease, red = increase) and statistical significance was depicted in the size of the nodes. This analysis was performed by Anton Petcherski (Goethe University, Frankfurt am Main).

5.3 Colocalization analysis

For each fluorescence image (single slices), a background intensity was calculated using a median filter of 32x32 pixels and subtracted from the original image (194). Otsu algorithm was used to compute intensity thresholds, and tresholded images were used to compute Mander's colocalization coefficients M1 and M2 for each channel pair. M1 describes the fraction of signal A overlapping with that of B, and M2 the fraction of signal B overlapping with that of A.

$$M1 = \frac{fraction\ of\ A\ colocalizing\ with\ B}{total\ A}, \qquad M2 = \frac{fraction\ of\ B\ colocalizing\ with\ A}{total\ B}$$

Outliers were removed using Grubb's test and unpaired Student's t-test was applied to determine statistical significance if sample values were normally distributed. If normal distribution was not given Kruskal-Wallis ANOVA was applied to determine statistical

significance.

For the colocalization between Glb1 and PPCA Pearson's colocalization coefficient was calculated instead of Mander's because here the main focus lay on the integrity of the multimeric complex.

For the colocalization figures, additional z-stacks of 10 slices were imaged from the samples used for analysis and deconvoluted using Huygens software version 14.xx (SVI, Hilversum, the Netherlands).

5.4 Analysis of LBPA/GM_1 vesicles

Individual cells in fluorescence micrographs were identified and segmented with the aid of nuclear (DAPI) and cell membrane (CTxB-FITC, anti-GM_1) stainings. Fraction of cell area covered by LBPA, mean signal intensity per vesicle area, mean vesicle area, number of GM_1/LBPA vesicles per cell and cell area and absolute/relative distance of GM_1/LBPA vesicles to the nucleus were determined using CellProfiler (version 2.0.11710) modules MeasureImageIntensity, MeasureImageArea and MeasureObjectSizeShape. Statistical analysis was performed with OriginPro 9. Outliers were removed using Grubb's test. Unpaired Student's t-test was applied to determine statistical significance, if sample values were normally distributed. If normal distribution was not given, Kruskal-Wallis ANOVA was applied to determine statistical significance.

5.5 Correlation analysis

Individual cells in fluorescence micrographs were identified and segmented with the aid of nuclear (DAPI) and cell membrane (WGA-647) stainings, and the mean signal intensities of CTxB-FITC and anti-CLN3 antibody determined using CellProfiler (version 2.0.11710) module MeasureObjectIntensity. Value pairs of five individual experiments were plotted separately for Cb*Cln3*$^{+}$ and Cb*Cln3*$^{\Delta ex7/8}$ cells and Pearson correlation coefficient calculated, and regression models for both cell types were compared and tested for statistical difference using the 'Fit Comparison of Data' module in OriginPro 9.

VI. RESULTS

1. Altered ganglioside profile

Each cell type exhibits a specific ganglioside pattern that varies with its developmental stage or due to pathological conditions. Three typical gangliosides of cerebellar granule cells, GM_1, GM_2 and GD_{1a}, were therefore analyzed in detail in the present study (195).

1.1 Ganglioside GM_1 levels are reduced in homozygous *Cln3*$^{\Delta ex7/8}$ cerebellar cells.

The binding of ganglioside GM_1 by CTxB is frequently used to detect membrane lipid rafts. In the present study, CTxB-FITC was used to visualize the amount of GM_1 in Cb*Cln3*$^{+}$ and Cb*Cln3*$^{\Delta ex7/8}$ cells. To confirm its applicability, Figure 3 shows the similarity between the staining patterns of CTxB-FITC and a polyclonal antibody against GM_1 in single slices of confocal microscopy images. Although the signal intensity of CTxB-FITC was higher towards the cell periphery, the structures stained by both methods remained the same, encompassing the plasma membrane, intracellular vesicles and the Golgi network.

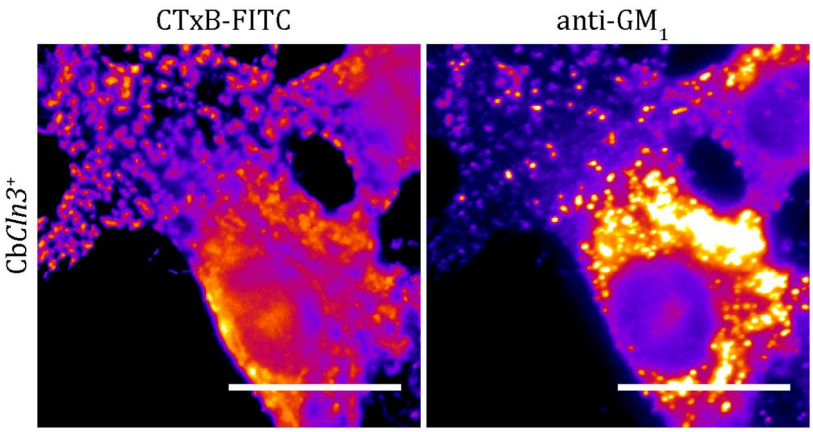

Figure 3. Staining pattern of anti-GM_{1a} antibody.
Confocal microscopy images (single slices) of *Cln3*$^{+}$ cells labeled with CTxB-FITC and a polyclonal anti-GM_{1a} antibody. Scale bar 25 µm.

Quantification of 3D confocal microscopy images of CTxB-FITC-labeled cells reveals a clear reduction of the CTxB-FITC signal intensity on membranes of Cb*Cln3*$^{\Delta ex7/8}$ cells in comparison to Cb*Cln3*$^{+}$ cells (Figure 4A). This decrease is comparable to the reduction observed in cells immunolabeled with anti-GM_1 (data not shown). To specify the origin of the reduced CTxB binding, either non-permeabilized Cb*Cln3*$^{+}$ and Cb*Cln3*$^{\Delta ex7/8}$ cells (PM staining) or cells permeabilized with digitonin (total membrane staining) were stained with CTxB-FITC, and the signal intensity was quantified by a fluorimetric approach (Figure 4C) and by flow cytometry (Figure 4B). As determined by fluorimetric analysis,

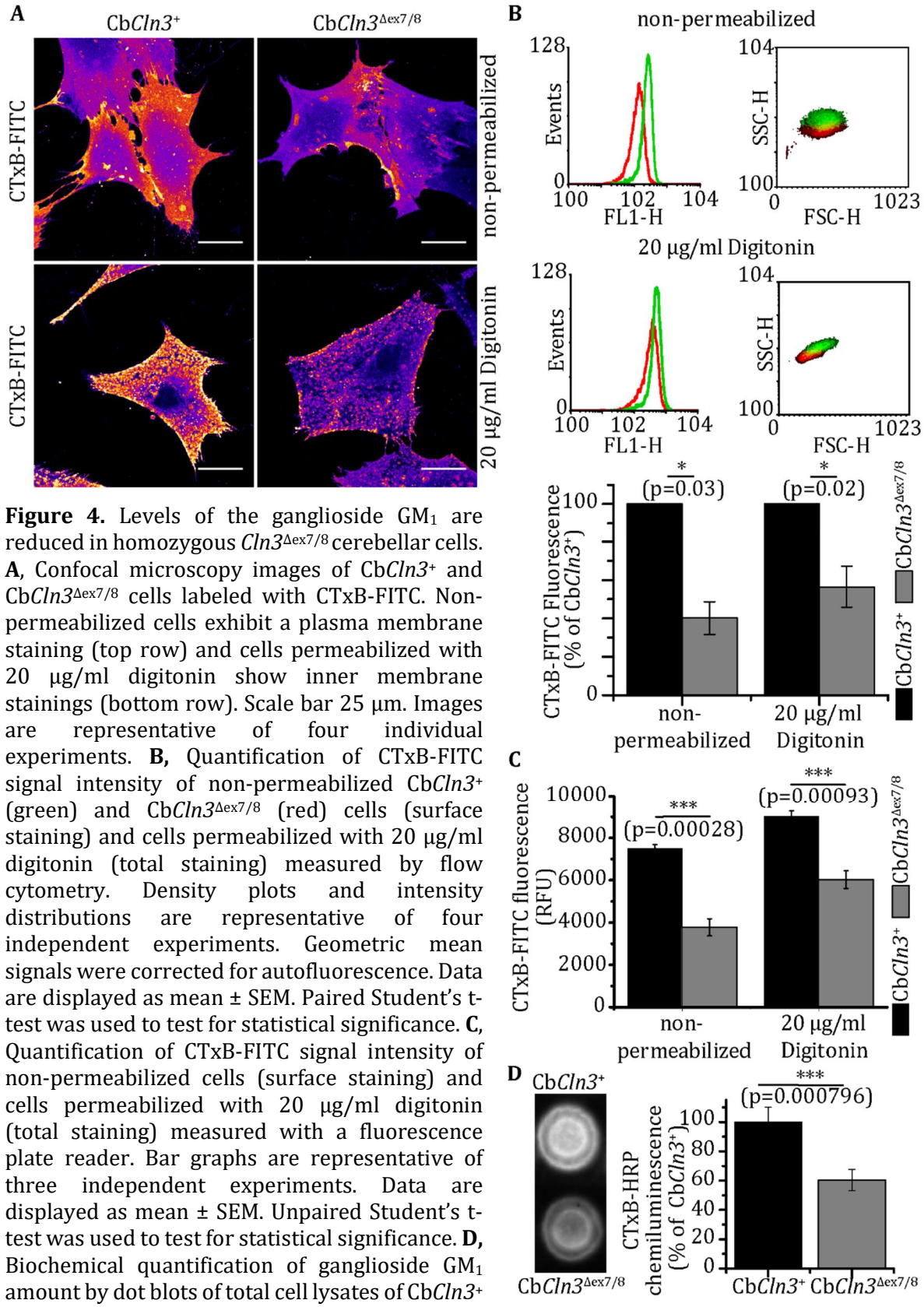

Figure 4. Levels of the ganglioside GM_1 are reduced in homozygous *Cln3*$^{\Delta ex7/8}$ cerebellar cells. **A**, Confocal microscopy images of Cb*Cln3*$^{+}$ and Cb*Cln3*$^{\Delta ex7/8}$ cells labeled with CTxB-FITC. Non-permeabilized cells exhibit a plasma membrane staining (top row) and cells permeabilized with 20 µg/ml digitonin show inner membrane stainings (bottom row). Scale bar 25 µm. Images are representative of four individual experiments. **B,** Quantification of CTxB-FITC signal intensity of non-permeabilized Cb*Cln3*$^{+}$ (green) and Cb*Cln3*$^{\Delta ex7/8}$ (red) cells (surface staining) and cells permeabilized with 20 µg/ml digitonin (total staining) measured by flow cytometry. Density plots and intensity distributions are representative of four independent experiments. Geometric mean signals were corrected for autofluorescence. Data are displayed as mean ± SEM. Paired Student's t-test was used to test for statistical significance. **C**, Quantification of CTxB-FITC signal intensity of non-permeabilized cells (surface staining) and cells permeabilized with 20 µg/ml digitonin (total staining) measured with a fluorescence plate reader. Bar graphs are representative of three independent experiments. Data are displayed as mean ± SEM. Unpaired Student's t-test was used to test for statistical significance. **D,** Biochemical quantification of ganglioside GM_1 amount by dot blots of total cell lysates of Cb*Cln3*$^{+}$ and Cb*Cln3*$^{\Delta ex7/8}$ cells incubated with CTxB-HRP. Data are the mean ± SEM of three experiments. Unpaired Student's t-test was used to test for statistical significance.

the staining intensity in permeabilized Cb*Cln3*$^{\Delta ex7/8}$ cells was reduced by 33.2 ± 3.2% and by 49.7 ± 3.8% in non-permeabilized cells, when compared to Cb*Cln3*$^{+}$ cells. This observation was supported by flow cytometry analysis on living cells showing a CTxB-FITC signal intensity reduction of 44.0± 5.8% in permeabilized and 59.6 ± 4.9% in non-permeabilized Cb*Cln3*$^{\Delta ex7/8}$ cells in comparison to equally treated Cb*Cln3*$^{+}$ cells. To evaluate the possible contribution of a non-linear fluorophore response due to differences in GM_1 distribution, a dot blot analysis was performed on total lysates of Cb*Cln3*$^{+}$ and Cb*Cln3*$^{\Delta ex7/8}$ cells. Cb*Cln3*$^{\Delta ex7/8}$ cell lysates showed a 40 ± 1.7% reduction of CTxB-HRP signal over Cb*Cln3*$^{+}$ cells (Figure 4D).

To prove that the phenotype described above is not caused by a clonal variation, a preliminary experiment was performed measuring the CTxB-FITC and anti-GM_1 signal intensities in the 7c1-3 clone of Cb*Cln3*$^{+}$ cells and the 4c1-3 clone of homozygous Cb*Cln3*$^{\Delta ex7/8}$ cells (data not shown). Consistent with the experiments described above, the 4c1-3 Cb*Cln3*$^{\Delta ex7/8}$ cell clone showed a CTxB-FITC signal intensity of 66.7 ± 1.8% compared to the 7c1-3 Cb*Cln3*$^{+}$ cell clone. 4c1-3 Cb*Cln3*$^{\Delta ex7/8}$ cells immunolabeled with the anti-GM_1 antibody also displayed a reduced signal intensity of 92.6 ± 2.4% in comparison to the 7c1-3 Cb*Cln3*$^{+}$ cell clone, although the reduction here was smaller than for the CTxB-FITC staining. Furthermore, cells were aged by confluent growth for 7 days in order to detect whether further changes appear when the Cb*Cln3*$^{\Delta ex7/8}$ cells start to accumulate lysosomal storage material. However, aging did not intensify the discrepancy in the GM_1 amount between Cb*Cln3*$^{+}$ and Cb*Cln3*$^{\Delta ex7/8}$ cells (Figure 5).

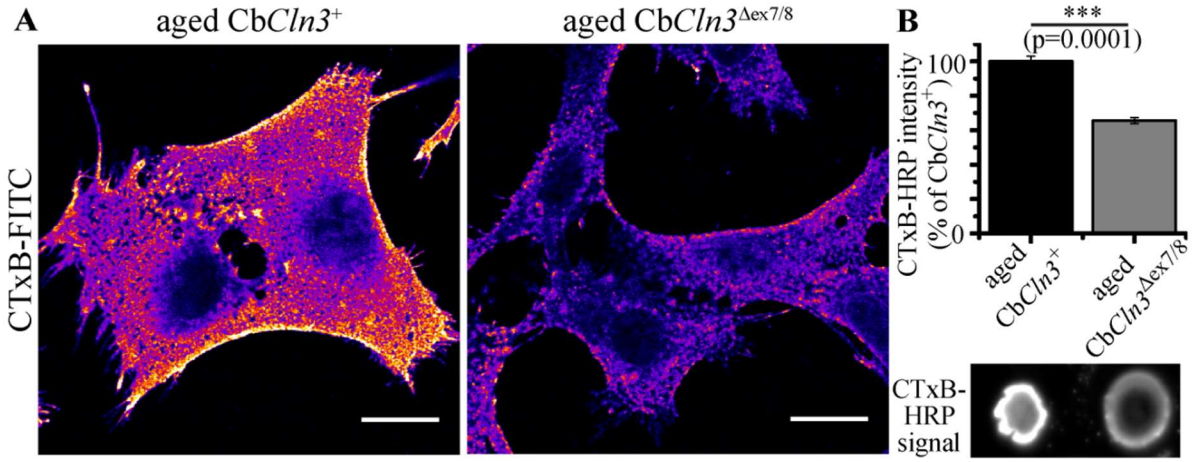

Figure 5. Levels of the ganglioside GM_1 are reduced in aged homozygous *Cln3*$^{\Delta ex7/8}$ cerebellar cells. **A,** Confocal microscopy images of aged aged Cb*Cln3*$^{+}$ and aged Cb*Cln3*$^{\Delta ex7/8}$ labeled with CTxB-FITC. Scale bar 20 µm. **B,** Biochemical quantification of ganglioside GM_1 amount by dot blots of total cell lysates of aged Cb*Cln3*$^{+}$ and aged Cb*Cln3*$^{\Delta ex7/8}$ cells incubated with CTxB-HRP. Data are the mean ± SEM of one representative experiment.

Finally, the ability of CTxB-FITC to bind GM_1 may be influenced by the cholesterol amount within the membrane, which can lead to a 'masking' effect (196). However, no increase in the colocalization between CTxB-FITC and the cholesterol-binding agent filipin could be detected (Figure 9A). To detect potentially 'masked' GM_1, Cb*Cln3*$^{+}$ and Cb*Cln3*$^{\Delta ex7/8}$ cells were treated with 10 mM methyl-β-cyclodextrin (MβCD) for 10 min to remove cholesterol from the PM. Subsequently, the cells were fixed and stained with CTxB-FITC. No change in CTxB-FITC signal intensity could be detected between MβCD-treated and untreated cells (data not shown), confirming the above described decrease in GM_1 levels of Cb*Cln3*$^{\Delta ex7/8}$ cells.

1.2 Levels of ganglioside GM_2 are increased in homozygous *Cln3*$^{\Delta ex7/8}$ cerebellar cells

Visualization of ganglioside GM_2 in Cb*Cln3*$^{+}$ and Cb*Cln3*$^{\Delta ex7/8}$ cells was achieved using a polyclonal antibody against GM_2. The observed distribution revealed a mainly perinuclear signal. The quantification of widefield microscopy images showed a significant increase of the GM_2 signal in Cb*Cln3*$^{\Delta ex7/8}$ cells to 140.2 ± 7.3% of Cb*Cln3*$^{+}$ cells (Figure 6).

To prove that the phenotype described above is not caused by a clonal variation, two individual experiments were performed measuring the anti-GM_2 signal intensity in the 7c1-3 clone of Cb*Cln3*$^{+}$ cells and the 4c1-3 clone of homozygous Cb*Cln3*$^{\Delta ex7/8}$ cells (data

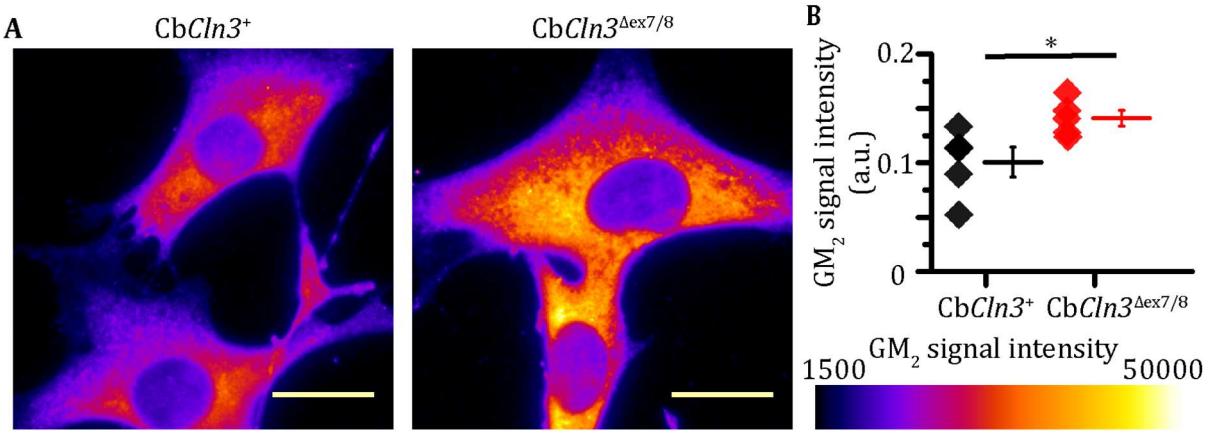

Figure 6. Levels of ganglioside GM_2 are increased in homozygous *Cln3*$^{\Delta ex7/8}$ cerebellar cells. **A,** Widefield microscopy images of Cb*Cln3*$^{+}$ and Cb*Cln3*$^{\Delta ex7/8}$ cells labeled with a polyclonal antibody against ganglioside GM_2. Scale bar 20 µm. Images are representative of five individual experiments. **B,** Quantification of anti-GM_2 signal intensity measured with CellProfiler software. Data are shown as the means ± SEM of five individual experiments. Each dot represents the mean of one experiment. Unpaired Student's t-test was applied to determine statistical significance.

not shown). Consistent with the experiments described above, the 4c1-3 Cb*Cln3*$^{\Delta ex7/8}$ cell clone showed a clear increase of 157.2 ± 17.8% in anti-GM_2 signal intensity when compared to the 7c1-3 Cb*Cln3*$^{+}$ cell clone.

1.3 Levels of ganglioside GD_{1a} are not altered in homozygous Cln3Δex7/8 cerebellar cells.

A mouse monoclonal antibody against the ganglioside GD_{1a} was used to visualize the amount of GD_{1a} in Cb*Cln3*$^{+}$ and Cb*Cln3*$^{\Delta ex7/8}$ cells. The localization of GD_{1a} resembled thereby stainings of intracellular vesicles of the degradative machinery as lysosomes and autophagosomes. No difference in signal intensity could be detected between widefield microscopy images of Cb*Cln3*$^{+}$ and Cb*Cln3*$^{\Delta ex7/8}$ cells (Figure 7).

To examine whether the phenotype described above is caused by a clonal variation, two individual experiments were performed measuring the anti-GD_{1a} signal intensity in the 7c1-3 clone of Cb*Cln3*$^{+}$ cells and the 4c1-3 clone of homozygous Cb*Cln3*$^{\Delta ex7/8}$ cells (data not shown). In contrast to the experiments described above, both, the 4c1-3 Cb*Cln3*$^{\Delta ex7/8}$ cell clone showed a clear reduction in anti-GD_{1a} signal intensity to 63.4 ± 1.3% when compared to the 7c1-3 Cb*Cln3*$^{+}$ cell clone ($p<0.05$).

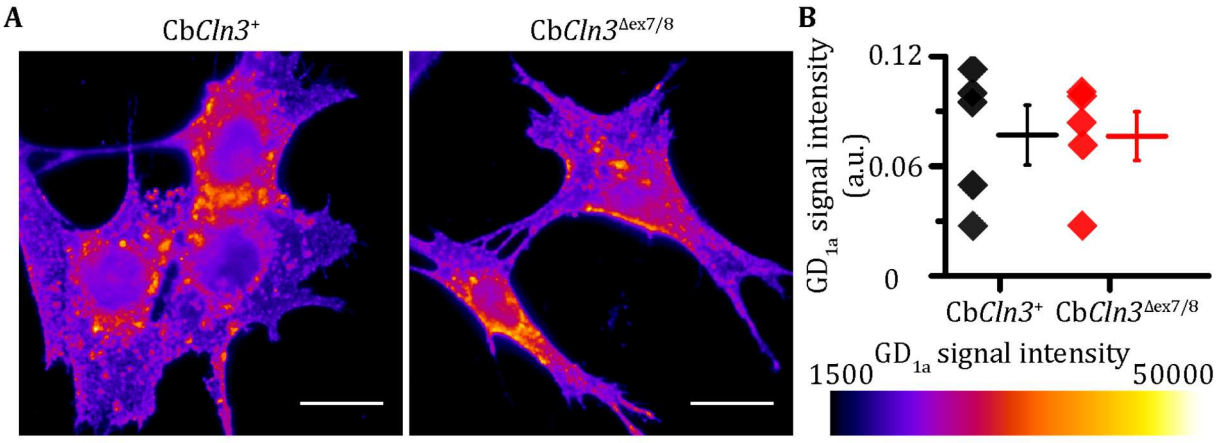

Figure 7. Levels of ganglioside GD_{1a} are not altered in homozygous *Cln3*$^{\Delta ex7/8}$ cerebellar cells.
A, Widefield microscopy images of Cb*Cln3*$^{+}$ and Cb*Cln3*$^{\Delta ex7/8}$ labeled with a polyclonal antibody against ganglioside GD_{1a}. Scale bar 20 µm. Images are representative of five individual experiments.
B, Quantification of anti-GD_{1a} signal intensity measured with CellProfiler software. Data are shown as the means ± SEM of five individual experiments. Each dot represents one experiment. Unpaired Student's t-test was applied to determine statistical significance.

2. Endocytosis and intracellular trafficking of GM_1

2.1 External GM_1 supplementation does not affect cell viability

The prominent decrease in GM_1 levels in Cb*Cln3*$^{\Delta ex7/8}$ cells led to the question whether supplementation of GM_1 would have an effect on cellular viability. Three different doses of GM_1 were applied to non-aged cerebellar cells for 24 hours. Metabolic cell activity was measured by MTT assay. Cb*Cln3*$^{\Delta ex7/8}$ cells exhibited with 78.7 ± 3.9% a significantly lower metabolic activity than Cb*Cln3*$^{+}$ cells. Supplementation of GM_1 did not induce a significant change in the metabolic activity of either genotype (Figure 8), representing neither a positive nor negative effect on the cell viability. In order to test whether and how much GM_1 was incorporated into the PM, cells were labeled with CTxB-FITC and the signal intensity measured. No difference could be detected between cells with and without external GM_1 administration (data not shown).

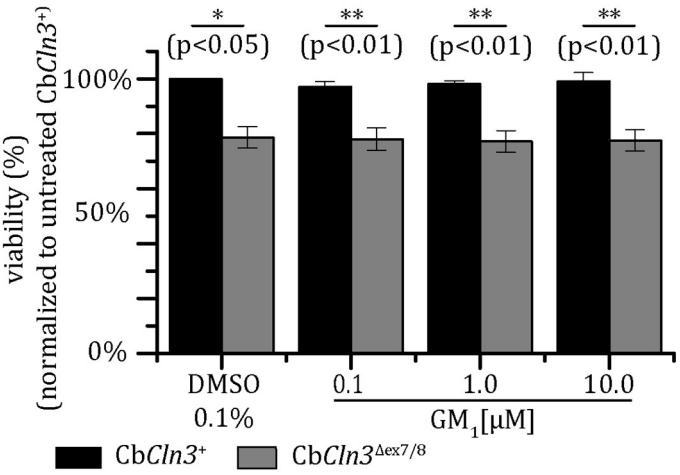

Figure 8. Effect of external GM_1 supplementation on cell viability assayed by MTT test.
All doses were applied in 4 replicates for 24 h and results normalized to untreated Cb*Cln3*$^{+}$ wells. Data are shown as means ± SEM of three independent experiments. One-way ANOVA was used to determine statistical significance between treatment groups.

2.1 Homozygous Cb*Cln3*$^{\Delta ex7/8}$ cells contain less Caveolin-1, but localization to membrane microdomains remains unchanged

The absence of an effect of external GM_1 supplementation on the cell viability gave rise to the hypothesis that a dysfunction in endocytic pathways may affect the proper uptake of GM_1. As sphingolipid segregation was implicated in the biogenesis of caveolae (197), caveolin-1 protein levels were determined via immunoblot analysis on cell lysates of non-aged cerebellar cells. As shown in Figure 9B, caveolin-1 levels were clearly decreased in homozygous Cb*Cln3*$^{\Delta ex7/8}$ cells to 50.9 ± 3.5% of Cb*Cln3*$^{+}$ cells.

Furthermore, CLN3 was previously implicated in the transport of caveolin-1 to the PM (76). In order to assess its functionality in membrane microdomains, the colocalization of caveolin-1 with the microdomain-markers GM_1, detected by CTxB-FITC, and cholesterol, detected by filipin, was determined in homozygous Cb*Cln3*$^{\Delta ex7/8}$ and Cb*Cln3*$^{+}$ cells (Figure 9A). Mander's colocalization coefficients were computed to characterize the degree of overlap for each colocalization partner separately. No alterations in Mander's coefficients could be detected in Cb*Cln3*$^{\Delta ex7/8}$ cells when compared to CbCln3^{+} cells. Hence, there are potentially less caveolae, but their membrane composition remains the same.

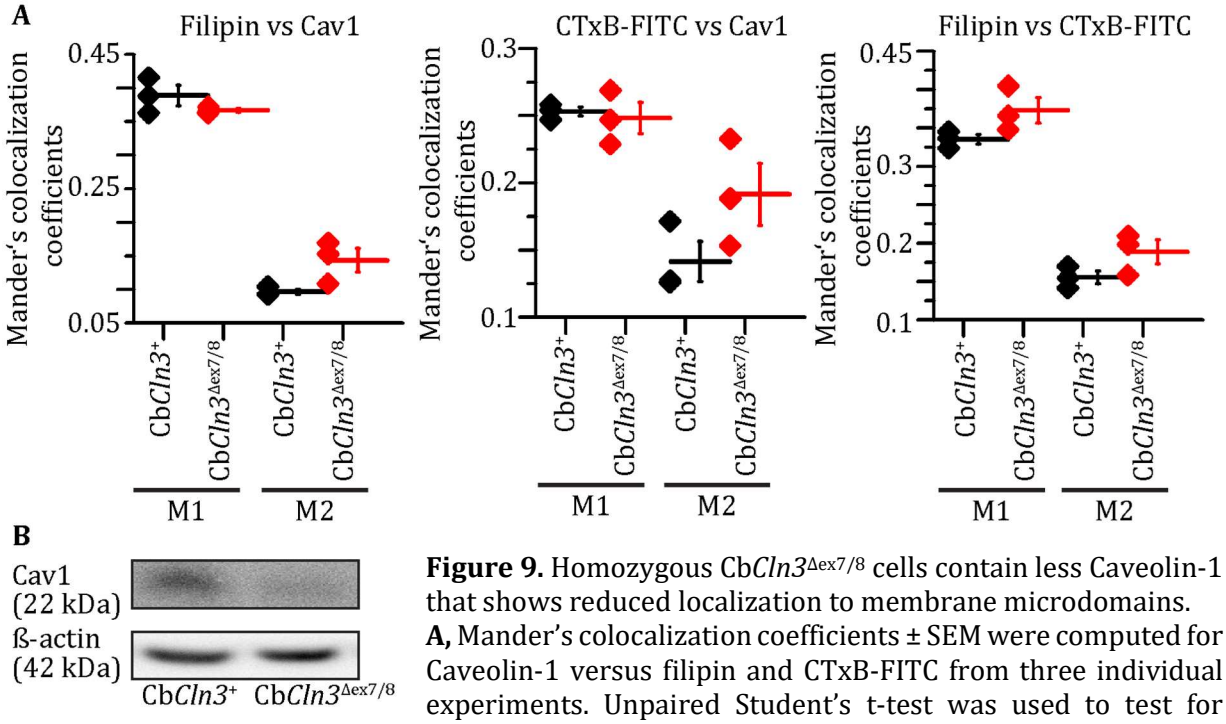

Figure 9. Homozygous Cb*Cln3*$^{\Delta ex7/8}$ cells contain less Caveolin-1 that shows reduced localization to membrane microdomains. **A,** Mander's colocalization coefficients ± SEM were computed for Caveolin-1 versus filipin and CTxB-FITC from three individual experiments. Unpaired Student's t-test was used to test for statistical significance. **B,** Western blot analysis of total cell lysates of proliferating and aged Cb*Cln3*$^{+}$ and Cb*Cln3*$^{\Delta ex7/8}$ cells showing Caveolin-1 and β-actin (loading control) immunoblots. Caveolin-1 levels were clearly decreased in homozygous Cb*Cln3*$^{\Delta ex7/8}$ cells compared to Cb*Cln3*$^{+}$ cells. Representative blot of six individual experiments.

2.2 Intracellular trafficking of GM_1 is altered in homozygous Cb*Cln3*$^{\Delta ex7/8}$ cells

Besides reduced endocytosis, a disrupted intracellular transport of GM_1 may prevent GM_1 from reaching its proper subcellular destination. In order to assess trafficking of GM_1 in Cb*Cln3*$^{+}$ and Cb*Cln3*$^{\Delta ex7/8}$ cells, pulse-chase experiments were performed with CTxB-FITC. For this, the cells were incubated with 2 µg/ml CTxB-FITC and fixed after a chase time of 0, 5, 15 or 30 min, respectively. In Cb*Cln3*$^{+}$ cells, the CTxB-FITC signal was initially concentrated on the cell surface. After 5 min of chase, Cb*Cln3*$^{+}$ cells showed a bright CTxB-

FITC signal dispersed over the PM and in discrete fluorescent punctate structures (0.074 ± 0.003 vesicles/µm² cell area). These structures are referred hereafter as "endocytic vesicles" without representing a discrete endosomal compartment. At later time points, a fraction of the CTxB-FITC signal concentrated on perinuclear compartments with Golgi-like appearance. In contrast to this, Cb*Cln3*$^{\Delta ex7/8}$ cells presented an initially weak CTxB-FITC PM staining and as of the 5-min time point a high proportion of cells showed perinuclear staining (32.5 ± 6.4% in Cb*Cln3*$^{\Delta ex7/8}$ cells versus 13.1 ± 2.3% in Cb*Cln3*$^{+}$ cells)

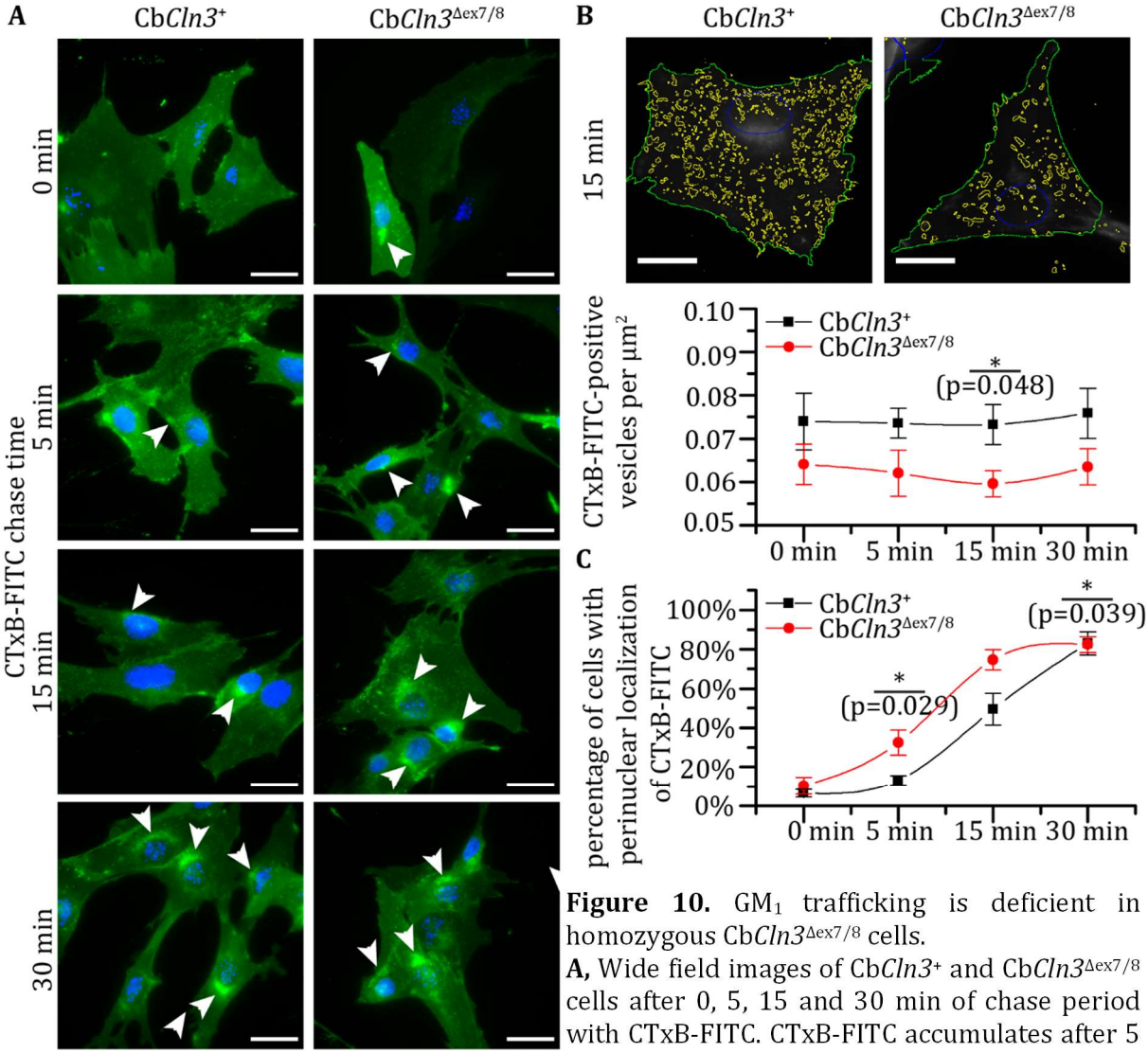

Figure 10. GM_1 trafficking is deficient in homozygous Cb*Cln3*$^{\Delta ex7/8}$ cells.
A, Wide field images of Cb*Cln3*$^{+}$ and Cb*Cln3*$^{\Delta ex7/8}$ cells after 0, 5, 15 and 30 min of chase period with CTxB-FITC. CTxB-FITC accumulates after 5 min in Cb*Cln3*$^{\Delta ex7/8}$ cells to a greater extent in perinuclear structures (arrowheads). Scale bar 25 µm. **B,** Superimposition (top) of wide field images of Cb*Cln3*$^{+}$ and Cb*Cln3*$^{\Delta ex7/8}$ cells after 15 min chase period with CTxB-FITC and outlines of cell border (green), nucleus (blue) and endocytic vesicles (yellow). Quantification (bottom) of CTxB-FITC-positive vesicles per µm² ± SEM of four individual experiments. Unpaired Student's t-test was used to test for statistical significance. Scale bar 20 µm. **C,** Quantification of percentual perinuclearly concentrated CTxB-FITC signal ± SEM of four individual experiments. Unpaired Student's t-test was used to test for statistical significance.

(Figure 10). Endocytic vesicles were also present in Cb*Cln3*$^{\Delta ex7/8}$ cells and with 0.062 ± 0.005 vesicles per µm^2 not significantly different from Cb*Cln3*$^+$ cells. After a chase time of 15 min, 74.6 ± 5.1% of the Cb*Cln3*$^{\Delta ex7/8}$ cells showed an accumulation of CTxB-FITC in the perinuclear region in comparison to 49.4 ± 8.1% of the Cb*Cln3*$^+$ cells (Figure 10) and the number of endocytic vesicles was clearly decreased with 0.060 ± 0.003 vesicles/µm^2 in Cb*Cln3*$^{\Delta ex7/8}$ cells versus 0.073 ± 0.005 vesicles/µm^2 in Cb*Cln3*$^+$ cells ($p<0.05$).

2.3 Accumulation of GM_1 in the trans-Golgi apparatus in homozygous Cb*Cln3*$^{\Delta ex7/8}$ cells

To verify the Golgi-like appearance of the CTxB-FITC signal in Cb*Cln3*$^{\Delta ex7/8}$ cells, colocalization analysis was performed between CTxB-FITC after a 15-minutes chase period and markers of the *trans*- and *cis*-Golgi apparatus (TGN46 and gm130,

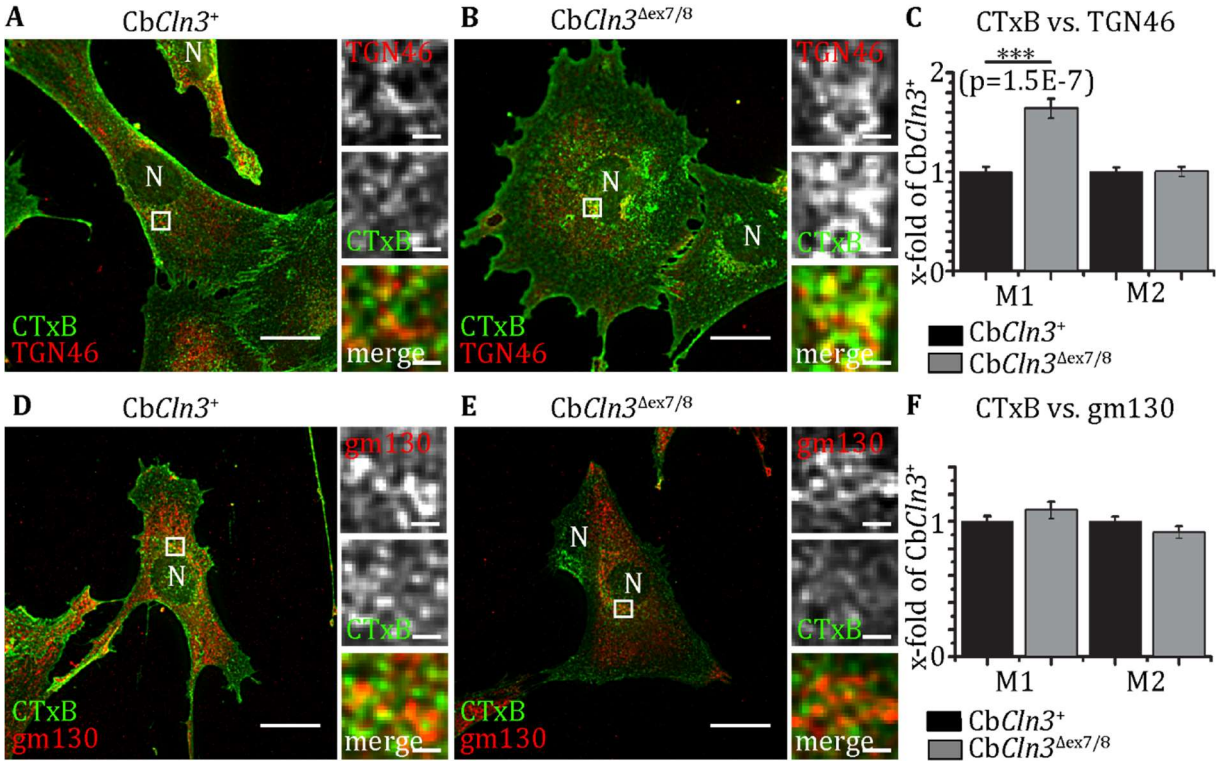

Figure 11. Accumulation of ganglioside GM_1 within the trans-Golgi apparatus.
Deconvolved focus plane wide field microscopy images of **A, D,** Cb*Cln3*$^+$ and **B, E,** Cb*Cln3*$^{\Delta ex7/8}$ cells after a 15 min chase period with CTxB-FITC. Scale bar 20 µm. Colocalization with markers of the **A, B,** trans- (TGN46) and **D, E,** cis- (gm130) Golgi apparatus after labeling with the respective antibodies. Detailed sections of the marker (top), the CTxB-FITC signal (middle) and their superimposition (bottom) are shown for each image. Scale bar 1.5 µm. Mander's colocalization coefficients ± SEM were computed for CTxB-FITC versus **C,** TGN46 and **F,** gm130 from three individual experiments. Unpaired Student's t-test and Fisher's combination of p-values were used to test for statistical significance.

respectively) (Figure 11). Mander's colocalization coefficients were computed to characterize the degree of overlap for each colocalization partner separately. A marked 1.64 ± 0.56 fold increase in Mander's coefficient M1 could be observed in Cb*Cln3*$^{\Delta ex7/8}$ cells for the colocalization between CTxB-FITC with TGN46, while no significant change was seen in M2 of this colocalization pair, nor in the colocalization between CTxB-FITC and gm130.

2.4 Ganglioside GM_1 is redirected towards degradation

Provided that CTxB-FITC uptake represents a readout for GM_1 trafficking in the cells, it is possible that the recycling of GM_1 to the PM is blocked in the TGN of Cb*Cln3*$^{\Delta ex7/8}$ cells and redirected towards degradative compartments. In order to test whether endogenous GM_1

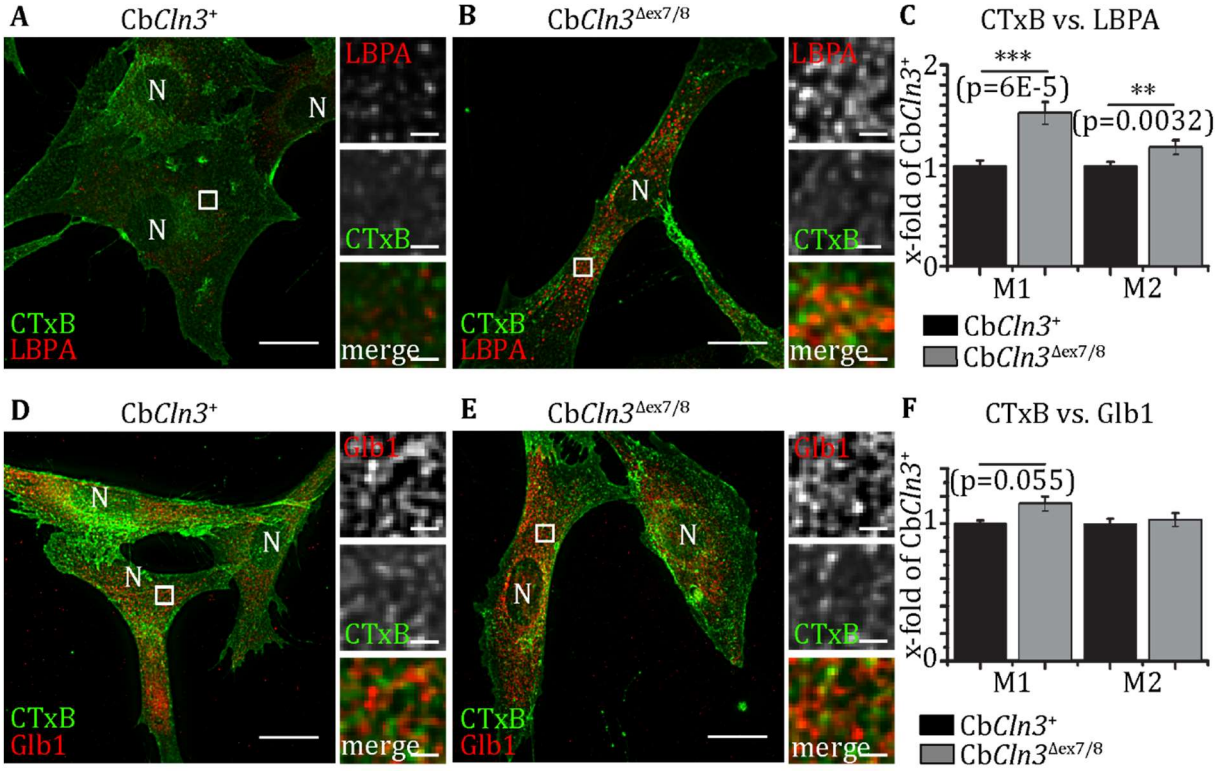

Figure 12. Increased turnover of ganglioside GM_1 within degradative compartments. Deconvolved focus plane wide field microscopy images of **A, D,** Cb*Cln3*$^{+}$ and **B, E,** Cb*Cln3*$^{\Delta ex7/8}$ cells after a 15 min chase period with CTxB-FITC. Scale bar 20 µm. Colocalization with **A, B,** late endosomal (LBPA) and **D, E,** lysosomal (β-gal) compartments after labeling with the respective antibodies. Detailed sections of the marker (top), the CTxB-FITC signal (middle) and their superimposition (bottom) are shown for each image. Scale bar 1.5 µm. Mander's colocalization coefficients ± SEM were computed for CTxB-FITC versus **C,** LBPA and **F,** β-galactosidase from three individual experiments. Unpaired Student's t-test and Fisher's combination of p-values were used to test for statistical significance.

was subjected to higher turnover, fixed Cb*Cln3*$^{+}$ and Cb*Cln3*$^{\Delta ex7/8}$ cells were double-stained with CTxB-FITC and a polyclonal anti-LC3B antibody as marker for autophagic vesicles. Colocalization analysis was performed and Mander's colocalization coefficients were computed to characterize the degree of overlap for each colocalization partner separately. Cb*Cln3*$^{\Delta ex7/8}$ cells revealed a significant increase in Mander's coefficients M1 and M2 to 1.67 ± 0.23-fold ($p<0.01$) and 1.98 ± 0.19–fold ($p<0.001$) compared to Cb*Cln3*$^{+}$ cells, respectively (data not shown). Further immunofluorescence analyses showed an elevated colocalization of CTxB-FITC after a 15-minutes chase period with two markers of the catabolic pathway of GM_1, β-galactosidase (Glb1) and LBPA (Figure 12). Mander's colocalization coefficients were computed to characterize the degree of overlap for each colocalization partner separately. For the colocalization between CTxB-FITC and LBPA a 1.52 ± 0.11-fold and a 1.18 ± 0.07-fold increase of Mander's coefficients M1 and M2, respectively, was measured in Cb*Cln3*$^{\Delta ex7/8}$ cells. The colocalization between CTxB-FITC and Glb1 revealed a potential, but not significant rise in Mander's coefficients M1 (1.14 ± 0.05-fold; $p=0.055$). No change could be detected in Mander's coefficient M2.

3. Cellular components involved in the turnover of GM_1

3.1 Homozygous Cb*Cln3*$^{\Delta ex7/8}$ cells express increased amounts of GM_1 metabolizing enzymes, β-galactosidase

In order to understand the cause for the decreased GM_1 levels in Cb*Cln3*$^{\Delta ex7/8}$ cells, the expression of genes related to GM_1 metabolism was analyzed using previously generated array data in this cell model (193). The gene expression of three GM_1 catabolizing enzymes, GM_2-activating protein (Gm2A), β-galactosidase (Glb1) and GM_1 sialyltransferase (St3gal2), were increased in Cb*Cln3*$^{\Delta ex7/8}$ cells when compared to Cb*Cln3*$^{+}$ cells (Figure 13A, Table 2). One Glb1 probe set with a lower expression level showed no significant increase in the relative expression level.

As the main enzyme responsible for lysosomal GM_1 degradation, Glb1 is of particular interest (195). Therefore, its activity was measured by monitoring the turn-over of chromogenic X-gal by the lysosomal β-galactosidase at pH 4.5 in fixed cell preparations. Only low levels of β-galactosidase activity could be detected in proliferating Cb*Cln3*$^{+}$ and

Cb*Cln3*$^{\Delta ex7/8}$ cells without significant difference (Figure 13B, C). Aging the cells by confluent growth for 7 days increased the lysosomal β-galactosidase activity as demonstrated by the modest color reaction in Cb*Cln3*$^{+}$ cells and an intense reaction in Cb*Cln3*$^{\Delta ex7/8}$ cells (Figure 13B, C). To investigate a relation between the intense color reaction and elevated β-galactosidase enzyme level, Western analysis was performed on cell lysates of non-aged and aged cerebellar cells. Only lysates from aged Cb*Cln3*$^{\Delta ex7/8}$ cells displayed a band of 64 kDa, representing the mature and active form of lysosomal Glb1 (Figure 13D). The protein amount of Glb1 in proliferating cells was under detection limit and precipitation with trichloroacetic acid (TCA) did not yield the required concentration (data not shown). However, quantification of the signal intensity in Cb*Cln3*$^{\Delta ex7/8}$ and Cb*Cln3*$^{+}$ cells immunolabeled with a monoclonal antibody against Glb1 displayed already a clear increase in two of three experiments performed (data not shown). Here, the signal intensity of Cb*Cln3*$^{\Delta ex7/8}$ cells was elevated to 129.9 ± 0.8% of Cb*Cln3*$^{+}$ cells. Thus, the decrease in GM_1 levels seen in aged Cb*Cln3*$^{\Delta ex7/8}$ cells is likely to correlate with the elevated protein levels of Glb1.

Table 2. Relative expression levels of GM_1 metabolizing enzyme genes in Cb*Cln3* cells.
Relative expression levels for Affymetrix probes representing the three GM1 metabolizing enzyme genes, Glb1, St3gal2 and Gm2a, are shown. Consistent with the decreased GM1 levels, a statistically significant upregulation is seen for all three enzyme genes. One Glb1 probe set with a lower expression level shows no significant increase in the relative expression level.

Gene symbol	Enzyme	Affymetrix Probe ID	mean expression level ((± SD)		Fold change	Student's T-test
			Cb*Cln3*$^{+}$	Cb*Cln3*$^{\Delta ex7/8}$		
Glb1	β-galactosidase	1416205_at	7.6 (0.03)	8.4 (0.21)	1.7	0.003
Glb1	β-galactosidase	1435795_at	5.3 (0.40)	5.2 (0.27)	-1.1	0.766
St3gal2	GM_1 sialyltransferase	1421890_at	7.6 (0.26)	8.8 (0.44)	2.2	0.018
St3gal2	GM_1 sialyltransferase	1421891_at	9.3 (0.11)	10.3 (0.29)	2.2	0.005
St3gal2	GM_1 sialyltransferase	1421892_at	8.4 (0.41)	9.4 (0.34)	2	0.033
Gm2a	GM_2 activator protein	1448241_at	9.3 (0.16)	10.0 (0.29)	1.7	0.019
Gm2a	GM_2 activator protein	1416188_at	8.5 (0.15)	9.3 (0.44)	1.7	0.043

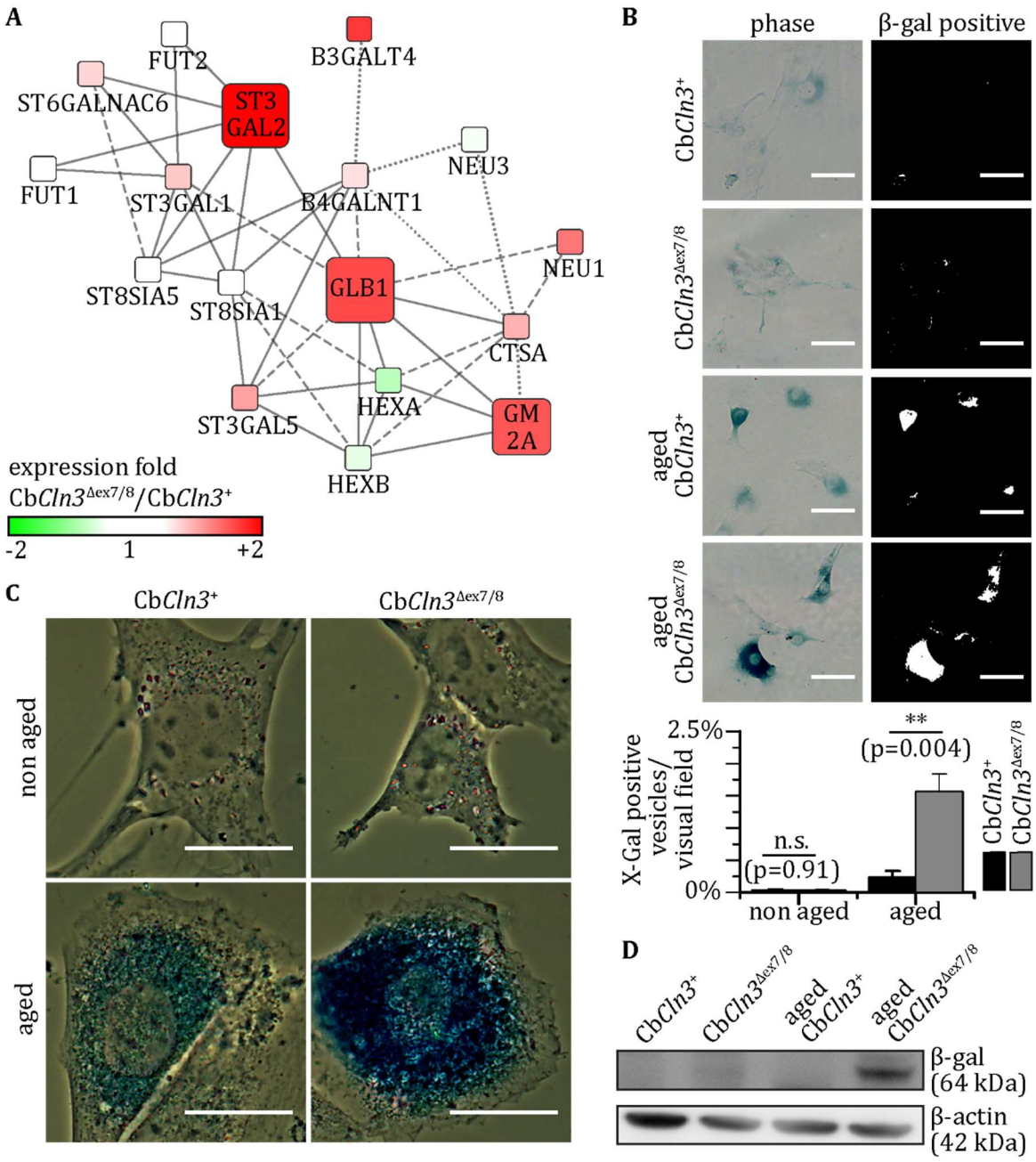

Figure 13. Increased amounts of GM_1 metabolizing enzyme, Glb1, in homozygous Cb*Cln3*$^{\Delta ex7/8}$ cells upon confluent aging.

A, Analysis of the expression of genes connected to GM_1 metabolism based on previously generated expression data by Cao *et al.* (193). Statistical significance increases with size of nodes. **B,** Enzyme activity of the lysosomal β-galactosidase at pH 4.5 measured by the turn-over of chromogenic X-gal. Images for quantification were taken with a 10x Zeiss Plan Neofluar objective. Positive β-galactosidase signal was identified and quantified using CellProfiler module UnmixColors. Data represent mean ± SD of four independent experiments. Unpaired Student's t-test was applied to determine statistical significance. Scale bar 50 µm. **C,** Representative images of **B** taken with a 63x Zeiss Plan Neofluar objective for detailed analysis of the localization of positive β-galactosidase signal. Scale bar 20 µm. **D,** Western blot analysis of total cell lysates of proliferating and aged Cb*Cln3*$^{+}$ and Cb*Cln3*$^{\Delta ex7/8}$ cells showing Glb1 and β-actin (loading control) immunoblots. Representative blot of four individual experiments.

3.2 Levels of PPCA are increased in homozygous *Cln3*$^{\Delta ex7/8}$ cerebellar cells

The enzyme activity of Glb1 is not only controlled by its protein levels. An important factor is the functional integrity of the multimeric complex Glb1 is part of in lysosomes. Among others, this complex contains cathepsin A, a protein that plays an important role in the protection of Glb1 from intralysosomal proteolysis (198, 199).

A polyclonal antibody against the protective protein cathepsin A (PPCA) was used to visualize the amount of PPCA in Cb*Cln3*$^{+}$ and Cb*Cln3*$^{\Delta ex7/8}$ cells (Figure 14A). The quantification of widefield microscopy images showed no difference in anti-PPCA signal intensity between the two genotypes (Figure 14B). However, Western analysis performed on cell lysates of non-aged cerebellar cells revealed a clear increase of PPCA protein levels in Cb*Cln3*$^{\Delta ex7/8}$ cells (Figure 14D). Additionally, Western analysis on cell lysates of aged

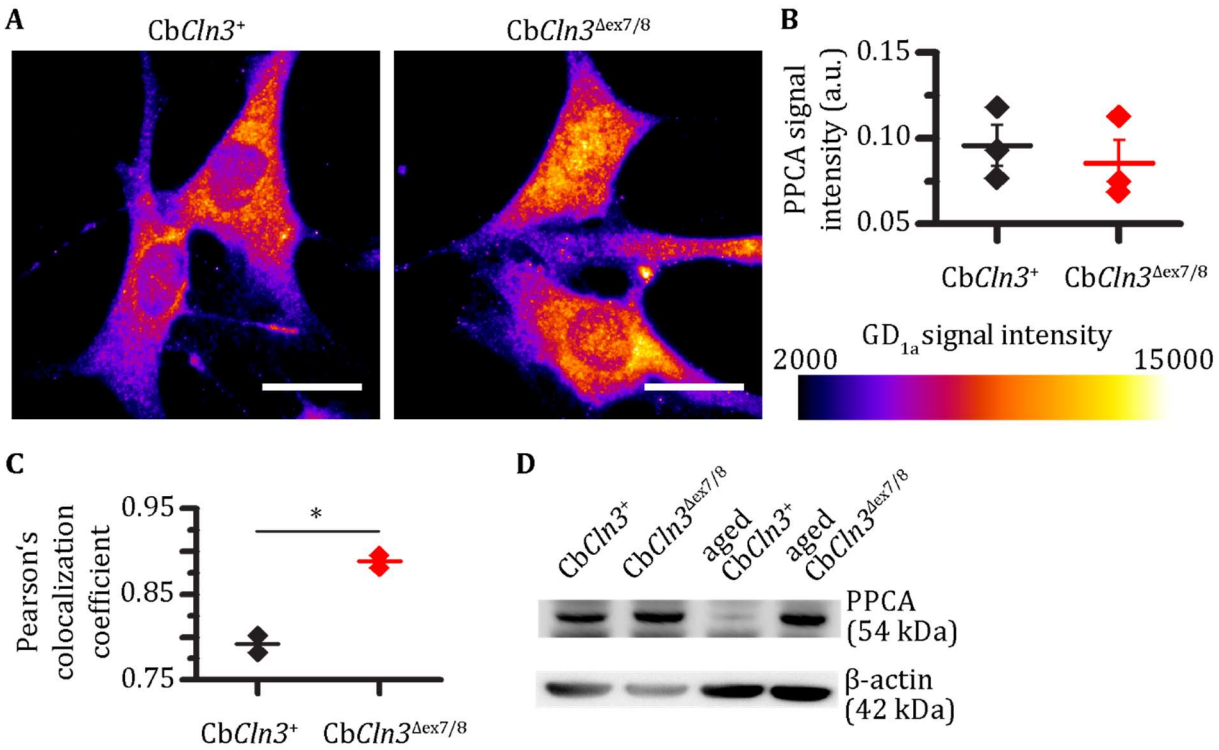

Figure 14. Levels of PPCA are increased in homozygous *Cln3*$^{\Delta ex7/8}$ cerebellar cells.
A, Widefield microscopy images of Cb*Cln3*$^{+}$ and Cb*Cln3*$^{\Delta ex7/8}$ cells labeled with a polyclonal anti-PPCA antibody. Scale bar 25 µm. Images are representative of three individual experiments. **B,** Quantification of PPCA signal intensity measured with CellProfiler software. Grubb's test was used to detect outliers. Unpaired Student's t-test was used to test for statistical significance. **C,** Quantification of Pearson's correlation coefficients between PPCA and Glb1 measured with CellProfiler software. Grubb's test was used to detect outliers. Unpaired Student's t-test was used to test for statistical significance. Two individual experiments. **D,** Western blot analysis of total cell lysates of proliferating and aged Cb*Cln3*$^{+}$ and Cb*Cln3*$^{\Delta ex7/8}$ cells showing PPCA and β-actin (loading control) immunoblots. Representative blot of three individual experiments.

cerebellar cells revealed a strong decrease in PPCA levels in Cb*Cln3*$^{+}$ cells during aging. This decrease was not found in aged Cb*Cln3*$^{\Delta ex7/8}$ cells, pointing to a prolonged stabilization of Glb1. In order to estimate the integrity of the GM_1-degrading multimeric complex, Pearson's colocalization coefficient was measured for Cb*Cln3*$^{+}$ and Cb*Cln3*$^{\Delta ex7/8}$ cells immunolabeled with anti-PPCA and anti-Glb1 antibodies. In Cb*Cln3*$^{\Delta ex7/8}$ cells, Pearson's colocalization coefficient was increased with 0.89 ± 0.01 when compared to Cb*Cln3*$^{+}$ cells with 0.79 ± 0.01 (Figure 14C). A single experiment measuring Pearson's colocalization coefficient in aged cells, showed a further decrease in aged Cb*Cln3*$^{+}$ cells to 0.66 ± 0.02, while it remained 0.86 ± 0.01 in Cb*Cln3*$^{\Delta ex7/8}$ cells.

3.3 Homozygous Cb*Cln3*$^{\Delta ex7/8}$ cells show increased amounts of lysosomal and late endosomal LBPA

Besides the integrity of the multimeric complex, the enzyme activity of Glb1 in living cells depends additionally on its binding ability to GM_1 containing membranes, a factor that cannot be determined in cell lysates. However, it was shown previously that elevated levels of LBPA favor the membrane binding of β-galactosidase (135). Immunofluorescence staining and 3D confocal microscopy were performed in order to visualize the distribution of LBPA in Cb*Cln3*$^{+}$ and Cb*Cln3*$^{\Delta ex7/8}$ cells. For both genotypes, LBPA signal partially colocalized with Lysotracker® Red DND-99 positive acidic lysosomes and late endosomes (data not shown), and Rab7 positive late and sorting endosomes (Figure 15). In line with earlier observations (67), lysosomes of Cb*Cln3*$^{\Delta ex7/8}$ appeared smaller and less intensively stained with Lysotracker Red than in control Cb*Cln3*$^{+}$ cells. Conversely, LBPA-containing vesicles appeared small in Cb*Cln3*$^{+}$ cells with a mean of 1.23 ± 0.08 μm^2, while those seen in Cb*Cln3*$^{\Delta ex7/8}$ cells were larger (1.60 ± 0.08 μm^2; p=0.01; Figure 16A, B). Furthermore, homozygous Cb*Cln3*$^{\Delta ex7/8}$ cells showed with 57.7 ± 1.9 vesicles per cell a decrease in vesicle number when compared to Cb*Cln3*$^{+}$ cells with 100.2 ± 14.0 vesicles per cell. However, normalization to cell area compensated this reduction and in total, the cell area covered by LBPA-positive vesicles was 46.5 ± 10.0% bigger in homozygous Cb*Cln3*$^{\Delta ex7/8}$ cells ($p<0.01$; Figure 16B). Regarding the localization of LBPA vesicles within the cell, no difference could be detected in the absolute or relative distance to the nucleus between both genotypes (Figure 16B). Finally, no difference was

measured in LBPA signal intensity between Cb*Cln3*$^{+}$ and Cb*Cln3*$^{\Delta ex7/8}$ (Figure 16B). This suggests that LBPA levels are elevated due to an increase in the size of late endosomes, but not accumulating in these structures. Anyway, this results in enhanced turnover of GM_1 ganglioside.

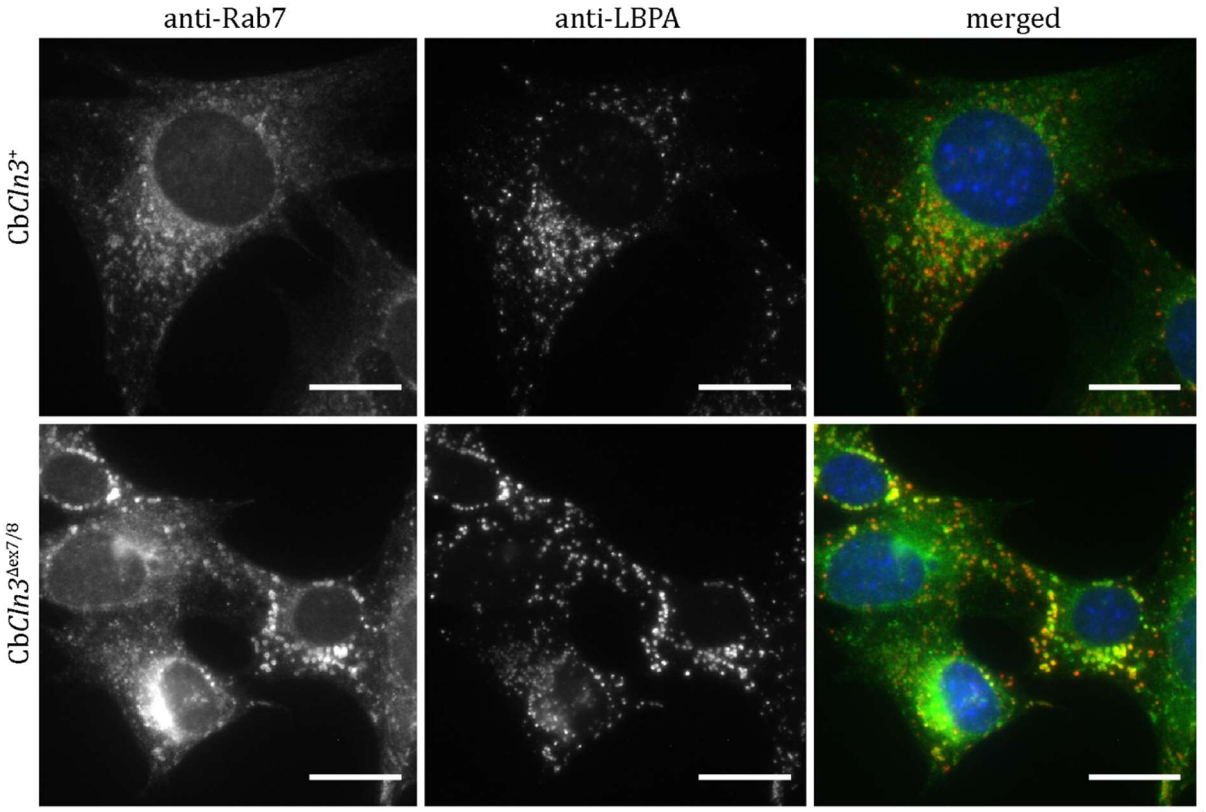

Figure 15. Colocalization of LBPA with Rab7, a marker for late and sorting endosomes.
Wide field microscopy images of Cb*Cln3*$^{+}$ and Cb*Cln3*$^{\Delta ex7/8}$ cells captured with a Zeiss Axioskop 2 and labeled with mouse monoclonal anti-LBPA antibody (middle column) and rabbit polyclonal anti-Rab7 antibody (left column) and their superimposition (right column). Scale bar 25 µm.

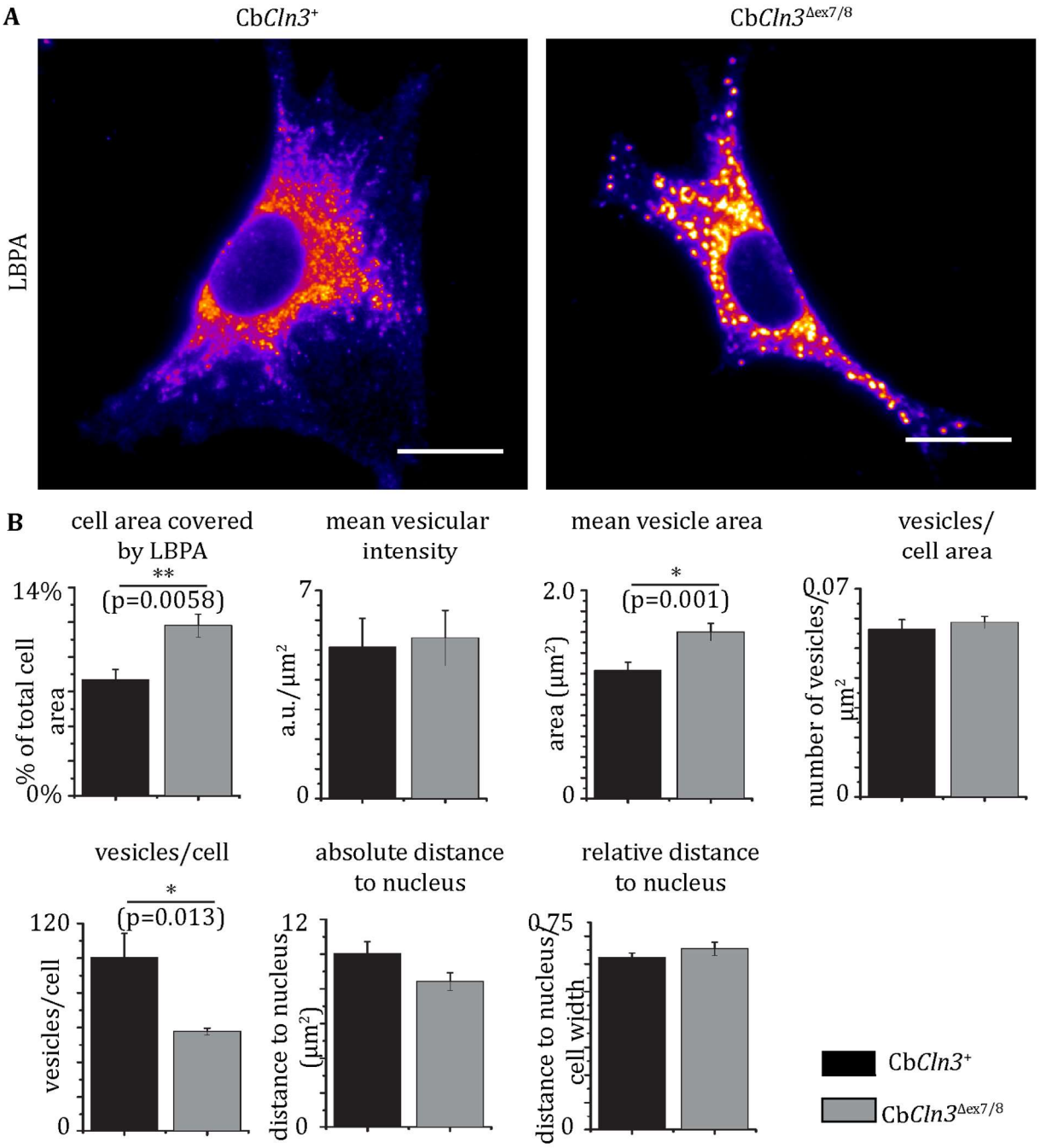

Figure 16. Increased amounts of lysosomal and late endosomal LBPA in homozygous Cb*Cln3*$^{\Delta ex7/8}$ cells.

A, Wide field microscopy images of Cb*Cln3*$^{+}$ and Cb*Cln3*$^{\Delta ex7/8}$ cells labeled with mouse monoclonal anti-LBPA antibody. Scale bar 20 µm. Representative images of three individual experiments. **B**, Quantification of the cell area fraction covered by LBPA, signal intensity, mean vesicle area, number of LBPA vesicles per cell area and per cell and absolute/relative distance of LBPA vesicles to the nucleus determined using CellProfiler. Unpaired Student's t-test was used to test for statistical significance.

3.4 Neuraminidase 1 levels are not altered in homozygous Cb*Cln3*$^{\Delta ex7/8}$ cells, but enzyme activity could be elevated

Cathepsin A and β-galactosidase are enzymes involved in the turnover of GM_1 to GM_2. In order to get a holistic view on the metabolism of GM_1 ganglioside, protein levels and localization of α-neuraminidase (Neu1), the enzyme responsible for the formation of GM_1

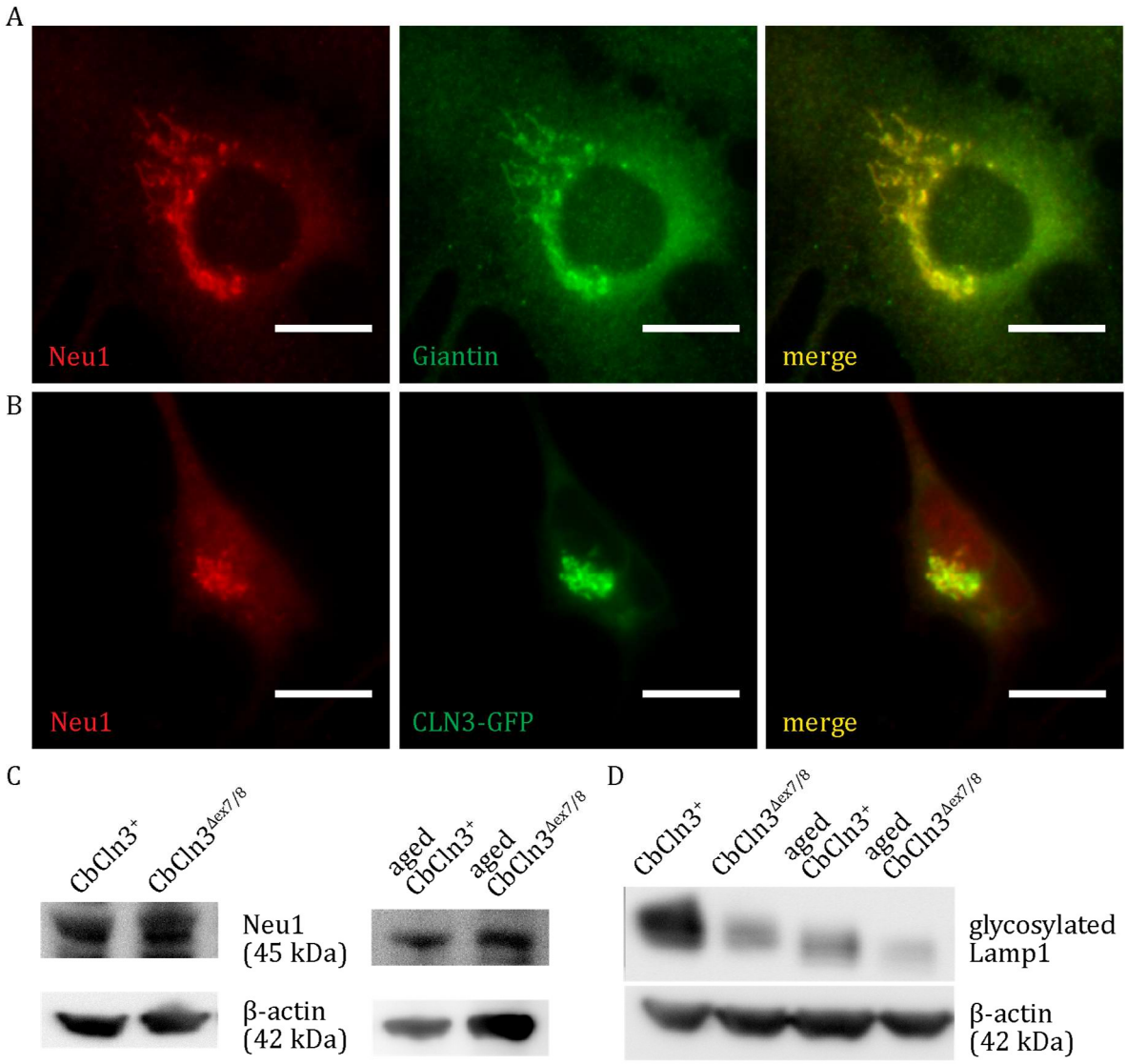

Figure 17. Colocalization of Neu1 with **A,** Giantin, a Golgi apparatus marker and **B,** overexpressed CLN3-GFP.
Wide field microscopy images of Cb*Cln3*$^{+}$ cells labeled with a rabbit polyclonal anti-Neu1 antibody (left column), a mouse monoclonal anti-Giantin antibody (**A**, middle column) or expressing CLN3-GFP (**B**, middle column) and their superimpositions (right column). Scale bar 15 µm. **C,** Western blot analysis of total cell lysates of proliferating and aged Cb*Cln3*$^{+}$ and Cb*Cln3*$^{\Delta ex7/8}$ cells showing Neu1 and β-actin (loading control) immunoblots. Representative blot of three individual experiments for proliferating cells and preliminary experiment of aged cells. **D,** Western blot analysis of total cell lysates of proliferating and aged Cb*Cln3*$^{+}$ and Cb*Cln3*$^{\Delta ex7/8}$ cells showing Lamp1 and β-actin (loading control) immunoblots. Representative blot of two individual experiments.

from GD_{1a}, were investigated. Western analysis performed on cell lysates of proliferating and aged cerebellar cells revealed no difference between the protein levels of Neu1 in Cb*Cln3*$^{+}$ and Cb*Cln3*$^{\Delta ex7/8}$ cells (Figure 17C). Immunofluorescence stainings with a polyclonal anti-Neu1 antibody revealed no clear difference between the staining patterns of Cb*Cln3*$^{+}$ and Cb*Cln3*$^{\Delta ex7/8}$ cells. The highest signal intensity of Neu1 was shown in the Golgi apparatus of cerebellar granule neuronal precursor cells where it colocalized with Giantin (Figure 17A) and overexpressed CLN3-GFP (Figure 17B). In a preliminary experiment, FRET analysis was performed in Cb*Cln3*$^{+}$ and Cb*Cln3*$^{\Delta ex7/8}$ cells. Transiently transfected CLN3-GFP and an AlexaFluor®546-labeled secondary donkey anti-rabbit antibody detecting the primary anti-Neu1 antibody were used to determine whether CLN3 directly interacts with Neu1. Quantification of FRET efficacy indicated no FRET between the two fluorophores (data not shown).

However, Western analysis visualizing the protein levels of lysosome-associated membrane protein 1 (Lamp1), a substrate of Neu1, revealed a shift in Lamp1 migration (Figure 17D). Proliferating Cb*Cln3*$^{\Delta ex7/8}$ cells showed a lower molecular weight band of Lamp1 in comparison to Cb*Cln3*$^{+}$ cells. Furthermore, protein levels of Lamp1 were reduced in Cb*Cln3*$^{\Delta ex7/8}$ cells. This finding was supported by a preliminary experiment showing a decrease of Lamp1 signal intensity in Cb*Cln3*$^{\Delta ex7/8}$ cells immunolabeled with a polyclonal antibody against Lamp1 (data not shown). Aging the cells by confluent growth for 7 days lowered the glycosylation status of Lamp1 even further.

3.5 Homozygous Cb*Cln3*$^{\Delta ex7/8}$ cells show a potential increase in HRas activity

The upregulation of lysosomal glycohydrolases was previously shown to correlate with Ras activation in Alzheimer's disease fibroblasts (200), raising the question if this is also the case in the Cb*Cln3*$^{\Delta ex7/8}$ knock-in cell model. The localization of HRas to membrane microdomains is thereby essential in order to exert its function as GTPase. It was determined by colocalization analysis with CTxB-FITC as its ligand GM_1 represents a commonly used microdomain marker. Mander's colocalization coefficients were computed to characterize the degree of overlap for each colocalization partner separately. Cb*Cln3*$^{\Delta ex7/8}$ cells revealed a slight, but significant increase of 17.7 ± 1.0% in Mander's

coefficient M2 for the colocalization pair CTxB-FITC and HRas ($p<0.05$; Figure 18). This implicates that a bigger fraction of HRas is located in membrane microdomains. As HRas was shown to require GTP-dependent segregation from microdomains to become active (201), this may result in a potential activity decrease. In contrast, Mander's coefficient M1 was slightly decreased to 86.1 ± 2.4%, supporting the hypothesis that less GM_1 reaches the PM in Cb*Cln3*$^{\Delta ex7/8}$. Therefore, the upregulation of β-galactosidase is rather not triggered by HRas activity.

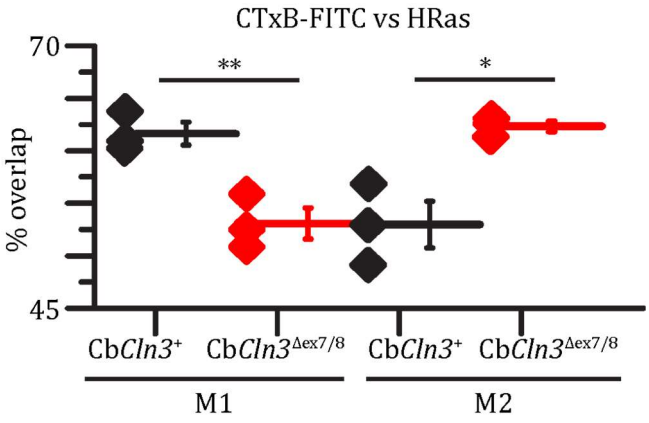

Figure 18. Homozygous Cb*Cln3*$^{\Delta ex7/8}$ cells show a potential decrease in HRas activity. Mean Mander's colocalization coefficients (vertical lines) ± SEM (whiskers) were computed for CTxB-FITC versus HRas from three individual experiments. Each data point represents one experiment. Unpaired Student's t-test was used to test for statistical significance.

4. Correlation to CLN3

4.1 GM_1 amount on the plasma membrane correlates with CLN3

To investigate the contribution of functional CLN3 to intracellular GM_1 trafficking and its disruption in Cb*Cln3*$^{\Delta ex7/8}$ cells, the intensity of CLN3 antibody staining was correlated with the amount of CTxB-FITC uptake. As shown in Figure 19, CTxB-FITC uptake positively correlated with the endogenous CLN3 levels of Cb*Cln3*$^{+}$ cells (Pearson's $R^2=0.29801$). In Cb*Cln3*$^{\Delta ex7/8}$ cells, such a correlation was absent (Pearson's $R^2=0.00452$). This suggests a role for functional CLN3 in the maintenance of the GM_1 content on the PM.

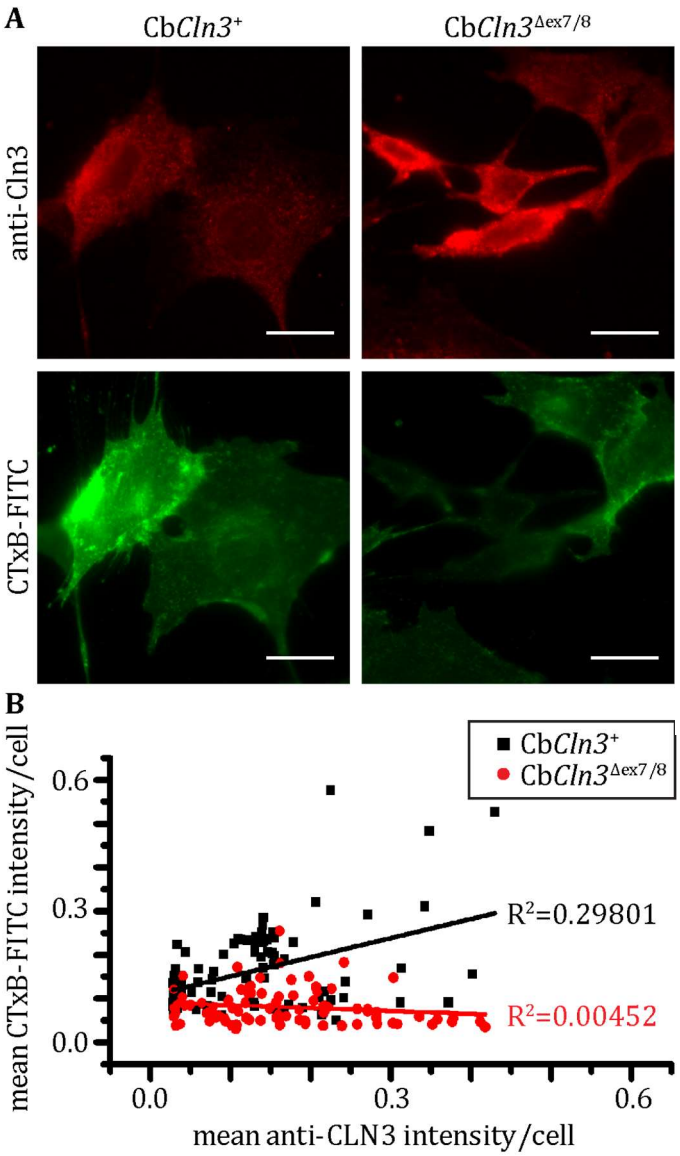

Figure 19. Correlation analysis between CTxB-FITC and CLN3.
A, Widefield microscopy images of PFA-fixed Cb*Cln3*$^{+}$ and Cb*Cln3*$^{\Delta ex7/8}$ cells after a 5 min chase period with CTxB-FITC and labeled with rabbit polyclonal anti-CLN3 antibody. Scale bar 20 µm. **B,** Scatter plot showing mean CTxB-FITC signal intensity versus mean CLN3 signal intensity. Every data point represents one cell from three individual experiments. Regression models were calculated with OriginPro 9 and are statistically different from each other at the 0.05 significance level.

4.2 Absence of FRET between CTxB-FITC and CLN3-DyLight™549

The correlation between CLN3 and the GM_1 amount on the PM raised the question whether a direct interaction occurs between CLN3 and GM_1. Förster resonance energy transfer (FRET) analysis was performed in Cb*Cln3*$^{+}$ and Cb*Cln3*$^{\Delta ex7/8}$ cells using CTxB-FITC and an anti-CLN3 antibody directly labeled with DyLight™549. Quantification of FRET efficacy indicated no FRET between the two fluorophores (data not shown).

4.3 Expression of functional CLN3 in Cb*Cln3*$^{\Delta ex7/8}$ cells restores GM_1 amount on the plasma membrane.

The lack of a direct interaction between CLN3 and GM_1 focused the further investigation on the question whether functional CLN3 modulates the route of GM_1 to the PM. Cb*Cln3*$^{+}$ and Cb*Cln3*$^{\Delta ex7/8}$ cells were either transiently transfected with a wild-type CLN3-myc construct or with a red fluorescent protein (RFP) vector as negative control and subjected to a 5 min pulse-chase treatment with 0.2 µg/ml CTxB-FITC. Transfection efficiency was generally low in Cb*Cln3*$^{\Delta ex7/8}$ cells with RFP. Transient transfection analysis revealed that functional CLN3-myc, but not RFP, increases the signal intensity of CTxB-FITC in Cb*Cln3*$^{\Delta ex7/8}$ cells 2.17 ± 0.08-fold to the level of Cb*Cln3*$^{+}$ cells ($p<0.05$; Figure 20). This increase implies an elevation of the amount of GM_1 present on the PM prior to pulse-chase labeling with CTxB-FITC. In contrast, Cb*Cln3*$^{+}$ cells showed no significant difference in CTxB-FITC signal intensity after transient transfection of CLN3-myc when compared to RFP.

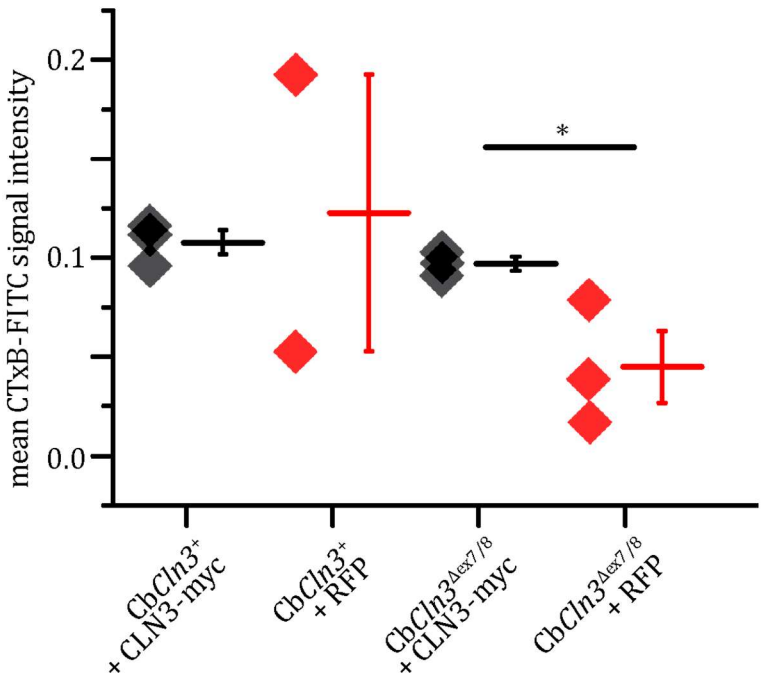

Figure 20. Expression of functional CLN3 in Cb*Cln3*$^{\Delta ex7/8}$ cells restores GM_1 amount on the plasma membrane. Quantification of CTxB-FITC signal intensity after a 5 min chase period of cells transiently transfected with RFP control vector or CLN3-myc. Intensities were measured using CellProfiler software. Data represent mean (vertical lines) ± SEM (whiskers) from three independent experiments. Grubb's test was used to detect outliers. Unpaired Student's t-test was used to test for statistical significance.

4.1 GM_1 vesicles – Rescue experiment

The possibility of functional CLN3 to increase the amount of GM_1 on the PM of Cb*Cln3*$^{\Delta ex7/8}$ cells, raised the question whether it affected the transport or amount of GM_1-positive vesicles. Therefore, the appearance of these vesicles was examined in Cb*Cln3*$^{+}$ and Cb*Cln3*$^{\Delta ex7/8}$ cells either transiently transfected with a wild-type CLN3-myc construct or with a red fluorescent protein (RFP) vector as negative control.

Cb*Cln3*$^{+}$cells transfected with the RFP control vector showed a mean anti-GM_1 signal intensity of 3.7 ± 0.7 a.u./µm^2, while transient transfection with CLN3-myc elevated the signal intensity to 5.2 ± 0.3 a.u./µm^2 (Figure 21B). However, this difference was not significant (p=0.09). Due to the very low transfection efficiency for RFP in Cb*Cln3*$^{\Delta ex7/8}$ cells, the standard deviation was too high to detect a change for the mean signal intensity in Cb*Cln3*$^{\Delta ex7/8}$ cells transfected with CLN3-myc or RFP, respectively. Furthermore, no

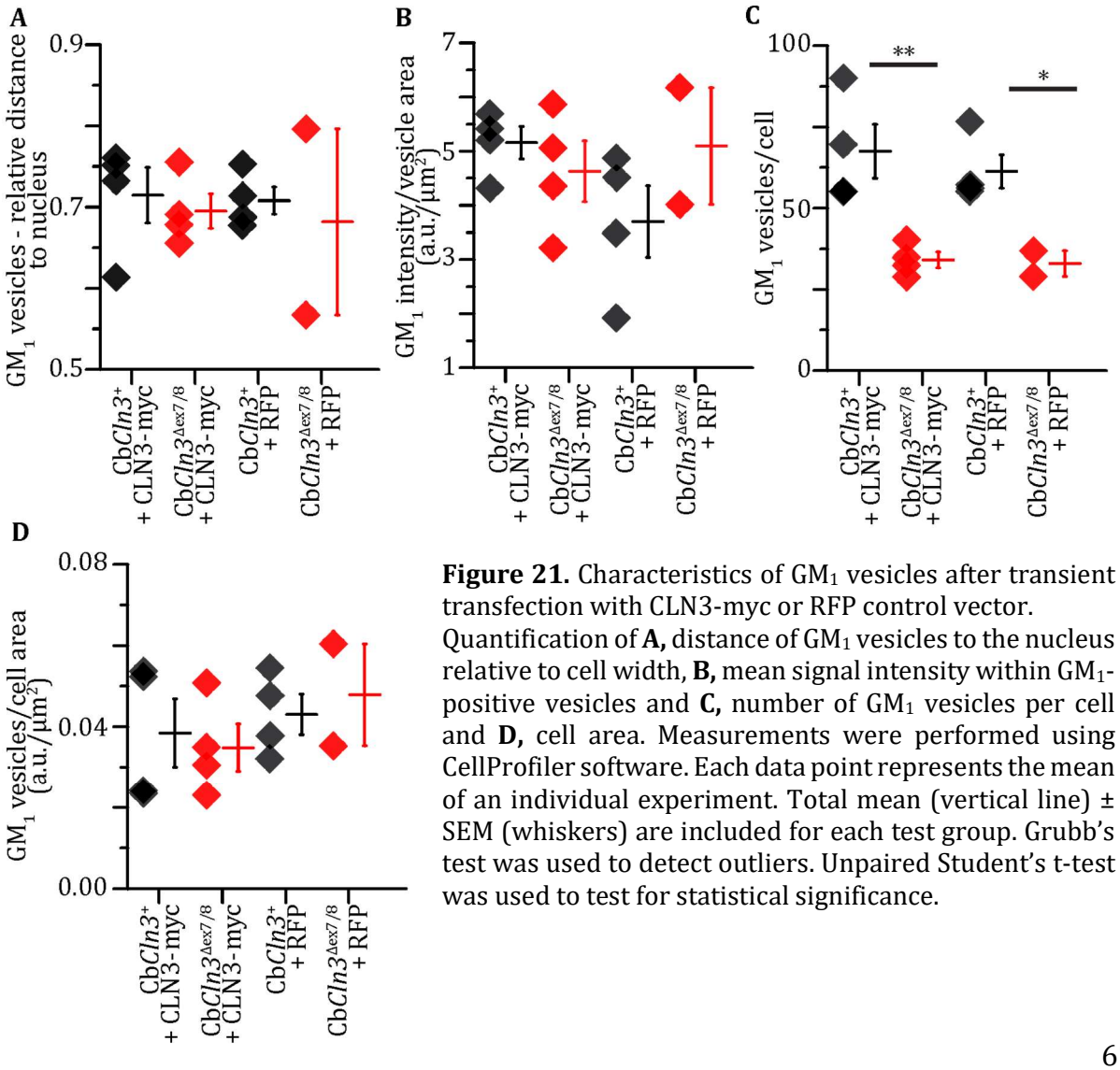

Figure 21. Characteristics of GM_1 vesicles after transient transfection with CLN3-myc or RFP control vector. Quantification of **A,** distance of GM_1 vesicles to the nucleus relative to cell width, **B,** mean signal intensity within GM_1-positive vesicles and **C,** number of GM_1 vesicles per cell and **D,** cell area. Measurements were performed using CellProfiler software. Each data point represents the mean of an individual experiment. Total mean (vertical line) ± SEM (whiskers) are included for each test group. Grubb's test was used to detect outliers. Unpaired Student's t-test was used to test for statistical significance.

significant difference was measured in the distance of GM_1 vesicles to the nucleus relative to the cell width (Figure 21A).

The number of GM_1 vesicles per cell was significantly lower in Cb*Cln3*$^{\Delta ex7/8}$ cells when compared to Cb*Cln3*$^{+}$ cells, but normalization to the cell area suppressed this effect. Transient transfection with CLN3-myc had no effect on this parameter.

VII. DISCUSSION

1. Are GM_1 levels decreased in homozygous Cb*Cln3*$^{\Delta ex7/8}$ cells?

1.1 Detection of ganglioside GM_1 with CTxB-FITC

Core of this study is the severe loss of GM_1 from Cb*Cln3*$^{\Delta ex7/8}$ cellular membranes. Due to financial aspects, FITC-labeled beta-subunit of cholera toxin (CTxB-FITC) was used to detect GM_1 as it is widely accepted as a specific marker (202–205). However, to eliminate possible concerns regarding its applicability, two additional experiments were conducted to confirm the decrease in GM_1 level. The first issue was presented by Kuziemko *et al*. (206) who described lower binding affinities of CTxB for other gangliosides that may lead to misinterpretation of the data. Therefore, double stainings with CTxB-FITC and an anti-GM_1 antibody were performed showing the similarity in their staining patterns along with a strong decrease in their signal intensity in Cb*Cln3*$^{\Delta ex7/8}$ cells. Although the signal intensity of CTxB-FITC was higher towards the cell periphery, the structures stained by both methods remained the same. This discrepancy may be caused by the pentameric nature of CTxB, leading to less accurate representation of the GM_1 amount than an anti-GM_1-antibody. Second, Mahfoud *et al*. stated that a major fraction of GSLs might be undetectable by their ligands due to cholesterol-mediated conformation changes of their carbohydrate group (196). Hence, alterations in the cholesterol level of Cb*Cln3*$^{\Delta ex7/8}$ cells may present falsely as a decrease in GM_1 levels. Dot blot analysis of GM_1 levels negated this hypothesis. However, to definitely exclude the possibility, cells were treated with MβCD disproving such a 'masking' effect. Furthermore, no change was shown in the colocalization between CTxB-FITC and cholesterol. These results provide confirmatory evidence that the decrease in GM_1 levels is specific and put the underlying mechanism into focus of further investigation.

1.2 CLN3 reduces the degradation of GM_1 in a concentration-dependent manner

A first step to understand how the CLN3 protein is regulating the cellular GM_1 pool required the specification whether the observed decrease is uniformly distributed over the cell or if certain compartments are affected stronger than others. As the major part of ganglioside GM_1 localizes to the PM, it was also the source of the biggest loss (approximately 50% of the GM_1 amount) in Cb*Cln3*$^{\Delta ex7/8}$ cells. In contrast, the loss on the inner membranes had to be less severe as the reduction in total GM_1 amount accounted only 30%. This implicates a blockage in the anterograde transport of GM_1 containing vesicles, and possibly, in their fusion with the plasma membrane. In line with that, a recent study by Tecedor *et al.* reported that protein transport, membrane transport and, in particular, the trafficking of GM_1 from TGN to PM are deficient in immortalized mouse brain endothelial cells lacking CLN3 (76). Furthermore, the present study showed a positive correlation between cell surface GM_1 and the cellular amount of full-length CLN3, but not the truncated protein. The more CNL3 was present in these cells, the higher their surface GM_1 pool and transfection of full-length CLN3 in Cb*Cln3*$^{+}$ showed a trend to an increased mean signal intensity of GM_1-positive vesicles. Furthermore, the transfection of Cb*Cln3*$^{\Delta ex7/8}$ cells with full-length CLN3 restored the GM_1 levels on the PM to the amount in Cb*Cln3*$^{+}$ cells. Nevertheless, no accumulation of GM_1 was found on the inner membranes of homozygous Cb*Cln3*$^{\Delta ex7/8}$ cells, suggesting that the retardation is secondary to a general decrease in GM_1 levels.

However, a role of CLN3 in the biosynthesis of GM_1 remains elusive because no FRET could be measured between CLN3 and GM_1. However, this does not necessarily exclude interaction. The antibody used in the present study is against the predicted cytoplasmic N-terminus of CLN3, whereas GM_1 was reported to be localized mainly on the outer leaflet of the PM. Unfortunately, there is no efficient extracellular anti-CLN3 antibody available so far and overexpressed CLN3 localizes mainly to the Golgi compartment as described in section VI.3.4. Although FITC and DyLight™549 were previously shown to be a very effective FRET pair (207), the distance between the bound FITC-tag of CTxB and the DyLight™549-tag of the anti-CLN3 antibody might be over 10 nm. As FRET efficiency is very sensitive to the distance, the probability to measure FRET in this dimension decreases drastically. Based on the data obtained, we assume that functional CLN3

reduces the degradation of GM_1 indirectly. A possible mechanism may be the impact of CLN3 on sphingolipid transport (49, 208). The increase in GM_1 levels resulting from elevated CLN3 levels may stimulate the performance of the cellular sorting machinery as described in section IV.5.3.1 and thereby enhance the transport of GM_1 and other membrane components to the PM.

2. Implications of the ganglioside metabolism on the drop in GM_1 levels

The observed reduction in ganglioside GM_1 levels in Cb*Cln3*$^{\Delta ex7/8}$ cells may be caused by different alterations in the ganglioside metabolism. Although possible, reduced synthesis of GM_1 was neglected because biosynthetic enzymes of the sphingolipid metabolism are seldom the cause for diseases in human (209). Also, the analysis of the gene expression database by Cao *et al.* (193) rather excluded such alterations. Therefore, the observed drop in GM_1 levels is likely to result from an increased degradation. Lysosomal β-galactosidase (Glb1) is the main enzyme responsible for GM_1 turnover (195) and hence, the leading candidate for further investigation in the present study. The alterations may be thereby directly Glb1-dependent in case of changes in the protein levels or enzyme activity, indirectly Glb1-dependent in case of changes upstream of Glb1 or Glb1-independent in case the degradation of GM_1 is increased by other factors. The present study considered all three possibilities as discussed in the following sections.

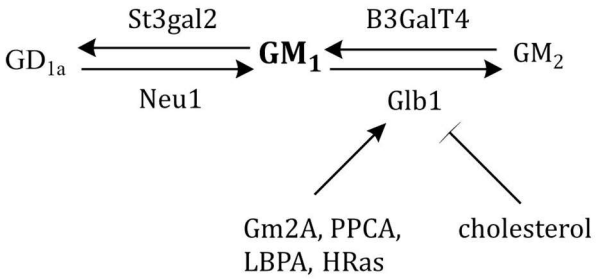

Figure 22. Turnover of GM_1.
Overview of enzymes directly involved in GM_1 turnover. For Glb1 protein stimulating and inhibiting factors are displayed.

2.1 Are Glb1 levels elevated in proliferating cells?

In line with the expectations, aged Cb*Cln3*$^{\Delta ex7/8}$ cells presented with a clear increase in expression, protein levels and enzyme activity of Glb1. In proliferating cells, the presence of Glb1 was shown in the gene expression database by Cao *et al.* (193), but only one of the two probe sets representing Glb1 revealed elevated levels in Cb*Cln3*$^{\Delta ex7/8}$ cells. Although both probes were related to the same gene, the deviation may have several explanations. Different isoforms, splice variants, paralogues or a polymorphism in the investigated sample could lead to different results. In case of a highly similar gene family, another member may cross-hybridize with the probe set or one probe set may be better designed than the other resulting in a higher binding affinity. So far, this data could not be confirmed biochemically, because the Glb1 levels measured by Western blot analysis and the enzyme activity assay were under detection limit. A more sensitive method as enzyme-linked immunosorbent assay (ELISA) may provide here biochemical results. However, the quantification of the signal intensity in immunofluorescence samples of proliferating Cb*Cln3*$^{+/+}$ and Cb*Cln3*$^{\Delta ex7/8}$ cells lends support to the claim that elevated Glb1 protein levels represent an early disease phenotype.

2.2 Contribution of other factors to the decreased GM_1 levels

As described above, Glb1 levels and enzyme activity in proliferating Cb cells were too low to allow a clear statement about its potential elevation. Therefore, other factors may contribute to the observed decrease in GM_1 levels, for example, other GM_1 metabolizing enzymes as St3gal2, a sialyltransferase that catalyzes the biosynthesis of GD_{1a}. All three probe sets of St3gal2 in the gene expression database revealed an increase in mRNA levels resulting in enhanced GM_1 turnover by a Glb1-independent pathway (193). Another option are factors enhancing Glb1 activity through direct interference. These factors can be divided into three subcategories: first, members of the multimeric enzyme complex Glb1 is part of, second, factors that modulate the physico-chemical properties of GM_1-containing membranes and third, upstream effectors of Glb1. Representatives of all three categories were examined in the present study and are discussed in detail in the subsequent chapters.

2.2.1 Multimeric enzyme complex

The synergistic action of multiple hydrolases co-operating in the stepwise degradation of a specific molecule is often achieved by assembly of a multimeric enzyme complex. Glb1 is part of such a complex together with its protective protein, the serine carboxypeptidase Cathepsin A (PPCA) and optionally Neu1 (198, 210). In this constellation, PPCA plays a role as scaffold protein or molecular chaperone for the subcellular localization and activation of both glycosidases (211, 212). Although no increase in PPCA mRNA expression could be detected by Cao *et al*. (193), examination of the protein levels by Western blot analysis in the present study revealed a clear upregulation in homozygous Cb*Cln3*$^{\Delta ex7/8}$ cells. Furthermore, the colocalization between Glb1 and PPCA increased as shown by Pearson's colocalization coefficient resulting in further stabilization of Glb1. However, in confluency-aged Cb*Cln3*$^{+}$ cells the protein levels of PPCA decreased severely. This is in line with the lack of PPCA staining in human cerebellar granule cells from postmortem brains of healthy individuals, where confluent growth is natural (213). Consistently, the degradation of ganglioside GM_1 might be decreased, resulting in higher levels of GM_1 typical for adult brains. In contrast, PPCA protein levels in homozygous Cb*Cln3*$^{\Delta ex7/8}$ cells remained continuously elevated. This may represent a lack of developmental change or be a sign of early cellular senescence as the activity of Glb1 increases drastically during aging (214). This aberration may also affect the catalytic activity of PPCA. A consequence may be altered processing of PPCA substrates, for example Lamp2a and oxytocin. Decreased Lamp2a levels were shown to inhibit chaperone mediated autophagy (215), a phenotype also present in another ATPsubC-accumulating lysosomal storage disease, mucolipidosis type IV (216). Further investigation here may reveal a common mechanism. In addition, decreased levels of the anti-stress hormone oxytocin may result in anxiety-like behavior as observed regularly in JNCL patients (217) and recently by our group in homozygous Cb*Cln3*$^{\Delta ex7/8}$ mice (218).

For completeness, protein levels and localization of Neu1, the other prevalent member of the Glb1 complex, were examined. Although Neu1 is not directly involved in GM_1 turnover, it is influencing its intracellular levels by desialylation of GD_{1a}. The consensus view in the current literature states that the catalytic activity of Neu1 remains only sustained when it associates with PPCA and Glb1 in the multimeric enzyme complex (210, 212). Despite all

expectations, in the present study, the immunofluorescent staining pattern of Neu1 localized to the Golgi compartment in both, Cb*Cln3*$^{+}$ and homozygous Cb*Cln3*$^{\Delta ex7/8}$ cells, where it did not colocalize with PPCA and Glb1. However, application in HeLa cells displayed the expected localization of Neu1 in lysosomes suggesting an aberrant distribution in cerebellar granule cells or a reduced specificity of the antibody for murine Neu1. However, this study is the first to analyze the distribution of Neu1 in cerebellar granule cells using an unbiased approach. Although Pitto *et al*. (219) found a sialidase to be present in lysosomal and PM fractions of this cell type, there is neither data regarding the Golgi, nor was the concrete isoform of Neu1 specified. Also alignment of the peptide immunogen used to produce this antibody by BLAST revealed no other proteins with acceptable homology (personal communication with the technical support of Sigma-Aldrich®). The remaining possibility is that not all modification states are detected with the antibody used. In case the peptide immunogen represents a sequence that is glycosylated in catalytically active Neu1 in mice, the antibody might recognize only its inactive state. This would result in the staining pattern detected in the present study as newly synthesized Neu1 traverses the Golgi before being activated. Suitably, no change was detected in the protein levels of Neu1 using the same antibody in Western blot analysis. However, this left the question open whether there were changes in activated Neu1 levels. Deglycosylation of the cell lysates or usage of a different anti-Neu1 antibody in future experiments may provide an answer to this question.

Nevertheless, the decrease in protein size detected for the Neu1-substrate Lamp1 in homozygous Cb*Cln3*$^{\Delta ex7/8}$ cells points to an increase in Neu1 activity. This is supported by the alteration of ganglioside GD_{1a} levels, another substrate of Neu1. Although signal intensity of the anti-GD_{1a} antibody was decreased only in immunofluorescence samples of the 4c1-3 clone of homozygous Cb*Cln3*$^{\Delta ex7/8}$ cells, high performance liquid chromatography (HPLC) data obtained in collaboration with the laboratory of Dr. F. Platt (Department of Pharmacology, University of Oxford, UK) confirmed the reduction in GD_{1a} levels in the 6a3-2 Cb*Cln3*$^{\Delta ex7/8}$ clone when compared to Cb*Cln3*$^{+}$ cells (manuscript under preparation).

Taken together, the evaluation of the Glb1-containing multimeric complex shows a synergistic activity of its individual components towards a ganglioside pattern dominated by less complex a-series gangliosides.

2.2.2 Factors modulating physico-chemical accessibility of ganglioside GM_1

Another factor modulating the enzyme activity of Glb1 are non-catalytic proteins acting directly on the glycolipid substrate. The main representatives of this category are accessory proteins, stabilizers and substrate sensors. Although the cofactor Gm2A was only shown to extract ganglioside GM_2 from membranes, it has a positive effect on the degradation of GM_1 (220). Presumably, this happens by disturbance of the lipid organization after insertion of Gm2A into the bilayer and/or by a shift of the substrate/product ratio (135). In the gene expression database both probe sets of Gm2A presented an increase in mRNA levels in homozygous Cb*Cln3*$^{\Delta ex7/8}$ cells (193) substantiating the increase in Glb1 enzyme activity.

Furthermore, the present study investigated the localization and distribution of the late endosomal lipid LBPA. LBPA enhances the binding of both β-galactosidase and activator proteins to substrate-carrying membranes, leading to a higher turnover rate of GM_1 (135). A clear increase in the size of LBPA-positive vesicles was demonstrated in the present study. The lack of a concomitant increase in signal intensity excludes, thereby, the possibility that the observed enlargement is a light scattering artefact. However, previous studies analyzing LBPA levels in JNCL range from no changes to a reduction in the synthesis of LBPA in lipid rafts and total lipid content of JNCL brains (111, 221, 222). Moreover, Hobert and Dawson observed that overexpression of wild-type CLN3P resulted in increased LBPA synthesis while overexpression of mutant CLN3P-L170P produced an opposite effect. They consequently proposed a role for CLN3 in the synthesis of LBPA (111). Additionally, Meikle *et al*. reported an increase of total LBPA levels in the plasma of JNCL patients (223), where it does not have any effect on Glb1. The present study is the first to indicate higher LBPA levels in homozygous Cb*Cln3*$^{\Delta ex7/8}$ cells. The discrepancies between the previous studies and our current results may be caused by the methodology used or lie in the use of a single cell type as opposed to post-mortem brain tissue. This is

of special interest as the ganglioside pattern differs between various cell types and some cells are earlier affected in JNCL than others, indicating that LBPA levels may also be highly variable. However, an increase in LBPA is in line with the decrease in mature cathepsin D and defective transport of CI-M6PR cargo described for JNCL cells, both associated previously with an enrichment of LBPA in multilamellar bodies (224, 225). Anyway, the increase in LBPA levels could be confirmed in the future by high-performance thin layer chromatography (HPTLC), allowing additionally to investigate the distribution of different fatty acyl species in LBPA (226). Since Meikle *et al*. showed that the concentration of monounsaturated $C_{18:1}/C_{18:1}$ LBPA species is decreased in the plasma (223), a similar alteration is conceivable in the intracellular pool. This may affect the ability of the cell to efficiently partition cholesterol within the membranes (227), thereby affecting the formation and function of lipid rafts and leading to further dysfunctions.

2.3 Enhanced HRas activity may up-regulate Glb1 protein levels

Emiliani *et al*. provided evidence that the up-regulation of Glb1 and other lysosomal glycohydrolases in skin fibroblasts from AD patients correlated positively with Ras activation (200). This up-regulation was suggested to be caused by activation of p38 mitogen-activated protein kinase. Suitably, CLN3 was previously suggested to act as a regulator of palmitoylated proteins (105, 106). In this context, the data presented here provides a possibility that the observed increase in Glb1 activity may be triggered by the activation status of palmitoylated Ras isoforms. Unfortunately, Emiliani *et al.* did not provide any information which Ras isoform performs this activity. Therefore, the present study concentrated on the localization of two different Ras isoforms, NRas and HRas, in Cb*Cln3*$^{+}$ and homozygous Cb*Cln3*$^{\Delta ex7/8}$ cells. For NRas, no alteration could be detected (data not shown) and previous data of our group showed no difference in total protein levels or membrane localization of HRas (228). However, computation of Mander's colocalization coefficients for HRas and CTxB-FITC revealed a slightly increased localization of HRas to GM_1-positive lipid rafts (M2) implicating a higher percentage of constitutively inactive HRas (201). Therefore, the upregulation of β-galactosidase is rather not triggered by HRas activity.

3. Role of CLN3 in ganglioside biosynthesis/turnover

3.1 What is currently known about (glyco-)sphingolipids in JNCL?

Sphingolipids that were previously shown to be affected in immortalized JNCL patient lymphoblasts are sphingomyelin, galactosyl- and glucosylceramide (208). Among others, these three bioactive lipids are known to accumulate also in prosaposin deficiency (209), that affects several steps of the biosynthetic pathway of GSLs. A similar multifocal intrusion may be conceivable for CLN3. Furthermore, the *de novo* synthesis pathway of ceramide, a bioactive lipid at the hub of sphingolipid metabolism, was shown to be influenced by CLN3 (229).

3.1.1 CLN3 harbors a putative galactosylceramide-binding domain

As described above (section IV.3.2), CLN3 exhibits a highly conserved VYFAE amino acid motif, homologous to and structurally compatible with the galactosylceramide-binding (GalCer) domain of amyloid precursor protein, V3-loop of HIV-1 surface-glycoprotein gp120 and PrpSC, the infectious variant of prion protein (49, 230). In fact, full length CLN3 colocalized with GalCer in the Golgi apparatus, TGN and lipid rafts of normal fibroblasts, whereas in CLN3-deficient cells GalCer levels were particularly increased within the fragmented Golgi apparatus while being absent from the PM (208). Being a major sphingolipid component of myelin and lipid rafts, mislocalization of GalCer affects neuronal function, protein-protein interactions and signaling (231). Expression of wild type CLN3 in these cells led to a restoration to the regular levels of GalCer and extracellular application of GalCer to CLN3-deficient lymphoblasts was shown to restore the cellular growth, suggesting a role for CLN3 in anterograde transport of GalCer (49).

3.1.2 CLN3 deficiency leads to elevated levels of proapoptotic (DH)ceramide

CLN5 disease (previously CLN9) was suggested to result from a defect of a sphinganine acyltransferase regulator protein, resulting in subsequent impairment of dihydroceramide (DHCer) biosynthesis (15). Clinical features of these CLN5 patients are identical to those with JNCL, leading to the assumption CLN3 might exert a similar role.

However, in contrast to CLN5, CLN3 deficient mouse brain tissue was shown to contain increased levels of ceramide (49). Since thin-layer chromatography (TLC) is not capable to distinguish between both species, the measurement may actually represent DHCer (229). Suitably, DHCer was shown to induce the formation of LC3-positive puncta and Cao *et al.* reported an upregulation of autphagosome formation in homozygous Cb*Cln3*$^{\Delta ex7/8}$ cells (99, 232). Furthermore, previous results of our group revealed that fenretinide, a DHCer activator, increased LC3-positive puncta in homozygous Cb*Cln3*$^{\Delta ex7/8}$ cells even further (Anton Petcherski, manuscript under preparation), supporting the correlation between autophagosome formation and DHCer levels.

Additionally, DHCer exerts also a proapoptotic role as direct precursor in the biosynthesis of ceramide, which induces 'leakiness' of the mitochondrial membrane at physiological conditions and regulates the splicing of caspase-9 and Bcl-X. Furthermore, ceramide activates apoptotic signal pathways through interaction with caspase-8, cathepsin D and TNF's in lipid rafts (233, 234). Partly, this pathway is based on the decrease of mitochondrial membrane potential (235), a phenotype observed previously in homozygous Cb*Cln3*$^{\Delta ex7/8}$ cells (Anton Petcherski, unpublished data). Suitably, suppression of CLN3 in tumor cells by antisense-RNA increased ceramide and Bcl2 levels and thereby cell death (236). Stable CLN3 overexpression in NT2 cells, on the other hand, was shown to reduce ceramide levels to less than half of that of controls (229, 237). Taken together, this indicates an antiapoptotic function of CLN3 by the regulation of (DH)ceramide levels.

3.2 Involvement of other members of the a-series ganglioside metabolism

Ganglioside metabolism is a complex organization of interleaving and interdependent processes, leading under disease conditions often to changes in more than one ganglioside species. In order to work out a comprehensive overview of the alterations present in the ganglioside metabolism of homozygous Cb*Cln3*$^{\Delta ex7/8}$ cells, the examination was extended to the other gangliosides before focusing on the potential role of CLN3. Thereby, the focus was set to some gangliosides typical for cerebellar cells, which include mainly members of the a-series: GM_3, GM_2, GM_1, GD_{1a}, GD_{1b}, O-Ac-GT_{1b}, GT_{1b} (195).

As described in section VII.2.2.1, no evidence was found that the decrease in GM_1 is caused by impaired degradation of GD_{1a}. Therefore, the next step was to examine the other product of GM_1 turnover, ganglioside GM_2. Although an increase in signal intensity was detected in immunofluorescence samples of homozygous Cb*Cln3*$^{\Delta ex7/8}$ cells, HPLC data obtained in collaboration with the laboratory of Dr. F. Platt did not confirm any difference (manuscript under preparation). A possible reason for the observed discrepancy might be an accumulation of GM_2 in certain cellular compartments without an increase in its total amount. This is possible due to the light scattering effect; the higher the signal intensity in a certain area, the bigger it appears. In this way, mere analysis of immunofluorescence samples may lead to misinterpretation of the data. However, it requires further investigation to confirm a potential accumulation and its cause.

In the absence of a good antibody, the levels of ganglioside GM_3 were only examined by HPLC analysis by the group of Dr. F. Platt. Homozygous Cb*Cln3*$^{\Delta ex7/8}$ cells revealed a severe increase of ganglioside GM_3 when compared to Cb*Cln3*$^{+}$ cells (manuscript under preparation). In combination with the lack of a significant increase in GM_2 levels, this is very untypical since secondary GSL accumulation in lysosomal storage disorders is often represented by modest accummulation of GM_3 and GM_2 ganglioside. A possible explanation may be an increase in the activity of GM_3 synthase or a decrease in the activity of GM_2 synthase, although the majority of sphingolipid metabolizing enzymes affected in human diseases reside in the degradative machinery (209). Consequently, the flux through the a-series ganglioside pathway would be reduced. In fact, GM_2/GD_2 synthase deficiency was described in a single patient with impaired motor development, seizures and premature death in infancy. The genetic basis of this patient remains unproven because the phenotype is more severe than in normal B4GalNT1 deficiency (238, 239). Interestingly, he accumulated only ganglioside GM_3 in brain and liver. However, the disease course is not similar to the one of JNCL either and Glb1 activity measured in leukocytes and liver of the patient was unchanged. Furthermore, subsequent examination of the ganglioside levels of fetal bovine serum used in the study revealed the source of ganglioside GM_3 as not innate to the cell. This lends support to the claim that GM_3 may have become trapped somewhere within the cell or at the membrane. In the future, repetition of the measurements with cells grown in GM_3-free serum may help to clarify if

the accumulation occurs due to a defect in GM_3 degradation or if the flux of GSL transport is impaired.

3.3 Is the decrease in GM_1 a compensatory reaction of the cell?

Despite the generally positive and neuroprotective effects of GM_1 reported so far, an overload of GM_1 is as detrimental for the organism as its lack. Therefore, it remains possible that the decreased GM_1 levels in Cb*Cln3*$^{\Delta ex7/8}$ cells are not the cause for the successive pathology, but a rescue effort of the cells due to increased GM_1 susceptibility. Recently, Wu *et al.* indicated an activation of the unfolded protein response in cells transfected with the *CLN3*$^{\Delta ex7/8}$ cDNA, a reaction also caused by GM_1 loading in wild-type neurospheres (240, 241). Similarly, the increased ceramide levels in CLN3 deficient mouse brains may be caused by an increase in TNFα that occurs also concomitantly with disease progression in GM_1 gangliosidosis mice (242, 243). Also the formation of meganeurites and enhanced autophagy were observed in both, GM_1 gangliosidosis models and JNCL (99, 244–246). However, these paradox findings are not restricted to GM_1 levels. Regarding the increase in PPCA levels in homozygous Cb*Cln3*$^{\Delta ex7/8}$ cells reported in the present study, it is of note that the early loss of cerebellar Purkinje cells is not only reported in JNCL, but also in PPCA knock-out mice (73, 247, 248). Furthermore, in both cases lysosomal storage material is found in these cells (247). Therefore, it is possibly not the direction of the shift that leads to JNCL pathology, but the inability of the cells to retain a balanced ganglioside pattern.

4. How does CLN3 affect the distribution of GM_1?

In context of the ample support for a role of CLN3 in the anterograde and retrograde trafficking in the last years (54), a defect in GSL trafficking may be a good candidate for the alterations in ganglioside metabolism described above.

4.1 Externally administered GM_1 does not reach its site of action to exert neuroprotection

Ganglioside GM_1 is reported to exert a neuroprotective role. In 1990, primary cultures of cerebellar granule cells were exposed to a brief application of glutamate resulting in delayed neuronal death (249). This excitotoxicity could be prevented by pretreating the cells with GM_1. Furthermore, GM_1 was shown to block Aβ-induced cytotoxicity (249, 250). Suitably, GM_1 levels were found to be decreased in patients with AD, Parkinsons's disease (PD) and Huntington's disease (HD). Small clinical trials of GM_1 administration to PD and HD patients showed an overall improvement of motor function (251–253). The upregulation of GM_1 and GD_{1a} ganglioside levels by the elimination of GD_3 synthase in an Alzheimer's disease (AD) model resulted in improved memory and reduced plaque load (254). Additionally, administration of GM_1 in a striatal cell model of HD restored ganglioside levels protecting the cells from apoptosis by activation of the pro-survival PI3K/AKT pathway (252). A potential mechanism underlying this improvement in PD is the ability of GM_1 to inhibit α-synuclein aggregation in vitro. Suitably, some PD patients presented elevated levels of anti-GM_1 antibody, possibly precluding GM_1 to carry out its function (255, 256). Finally, the administration of GM_1 ganglioside to patients was shown to be generally safe (257), besides a few cases of peripheral neuropathy caused by the production of anti-GM_1 antibodies (257). Also, gangliosides were shown to cross the blood-brain barrier and to enter the foetus via the placenta, providing thereby the prospect of an early and uncomplicated treatment (258, 259). Based on this ample amount of indications, administration of GM_1 was expected to improve cell viability of homozygous Cb*Cln3*$^{\Delta ex7/8}$ cells and beyond that to rescue potentially some disease phenotypes.

Against all expectations, external supplementation of GM_1 to Cb*Cln3*$^{+}$ and Cb*Cln3*$^{\Delta ex7/8}$ cells showed no effect on their viability irrespective which concentration was used. Furthermore, no difference in CTxB-FITC signal intensity could be detected between cells with and without external GM_1 administration, questioning the efficiency of its uptake. A putative reason for the lack of additional signal may be here the fast turnover of the surplus of GM_1, although the time span is rather not plausible. On average, first degradation products appear 10-15 minutes after the pulse and metabolic salvage events

start within the subsequent 15 minutes (120). Nevertheless, not all ganglioside is processed immediately. Although the half-life is difficult to measure, the values reported in literature range from several hours to days dependent on the type of cell and ganglioside investigated (reviewed in 120). For example, Riboni *et al*. measured a half-life of 6.5 hours for exogenously administered [^{3}H-NeuAc]-GM_1 in differentiated rat cerebellar cells (260). Hence, 1 hour of pulse time should not cause problems in the detection. Anyway, a complete lack of incorporation of ganglioside GM_1 into the PM is very unlikely. Valsecchi *et al*. and Riboni *et al*. showed cultured cerebellar granule cells to take up radiolabeled GM_1 at a concentration of 0.1 µM and 1 µM, respectively (261, 262). Furthermore, Brown *et al.* reported that GM_1 inserts spontaneously into phospholipid bilayer vesicles (263). Both findings support the theory that the absence of an effect after GM_1 administration is not caused by insufficient uptake. Possibly, the amount of GM_1 taken up by the cells is concealed by the pentameric nature of CTxB. In future experiments, usage of boron dipyromethenedifluoride (BODIPY)- or radio-labeled GM_1 that allow the detection of trace amounts of GM_1 may be beneficial.

The absence of an effect may have also other reasons. Eventually not the total GM_1 level, but its localization within the cell or the route of delivery may have a high impact on the cell's fate (264). Already in 2004, Tessitore *et al*. presented mislocalized GM_1 to activate ER-chaperones and to trigger neuronal apoptosis (241). Furthermore, Nishio *et al*. showed that PC12 cells transfected with a GM_1/GD_{1b}/GA_1 synthase gene exhibited higher levels of GM_1 ganglioside, but reacted differently to nerve growth factor stimulation than cells supplied with exogenous GM_1 (265). Also systemic delivery of GM_1 to transgenic mice overexpressing APP caused a decrease in soluble Aβ levels while exogenous GM_1 administration increased Aβ secretion (266, 267). Hence, external supplementation of Cb*Cln3*$^{\Delta ex7/8}$ cells with ganglioside GM_1 might lead to an increase of its concentration on the PM, but it does not implicate a proper trafficking to its site of action. Future experiments may investigate the effects of an internal increase of GM_1 levels after transfection with GM_1 synthase. Alternatively, inhibition of ganglioside degradation with chloroquine may be beneficial (144, 268).

*4.1.1 Caveolar endocytosis is disrupted in homozygous Cb*Cln3$^{\Delta ex7/8}$ *cells*

Regarding the possible mislocalization of administered GM_1, the first mechanism investigated was the internalization of its ligand CTxB-FITC. In 1998, Orlandi and Fishman reported that the endocytosis of CTxB occurs via a special type of lipid rafts that builds small invaginations at the PM, referred to as caveolae (269). In these strucutres, GM_1 labeled with CTxB was reported to concentrate four-fold (270). Although it remains uncertain whether endogenous lipids not bound to toxins behave in the same way, Parton *et al.* showed that the accumulation was not due to the pentameric nature of CTxB (271). Sonnino *et al*. proposed that GM_1 could be responsible for the curvature of caveolae by separation from the inner cholesterol and caveolin-1-rich domain (118). However, the present study showed that the colocalization degree between caveolin-1 and CTxB-FITC-labeled GM_1, as well as caveolin-1 and filipin-labeled cholesterol remains unaffected in homozygous Cb*Cln3*$^{\Delta ex7/8}$ cells. This indicates that the existing caveolae are functional. In future experiments, usage of BODIPY-labeled GM_1 may clarify the exact disposition of the administered ganglioside in this constellation. Pools of accumulated caveolar GM_1 could be then distinguished from diffusely distributed GM_1 by changing the emitted wavelength from green to red due to excimer formation with increased concentration. This may allow a more detailed insight about the amount of GM_1 available for endocytosis in homozygous Cb*Cln3*$^{\Delta ex7/8}$ cells. Although this data makes a direct role of CLN3 in the composition of caveolae rather unlikely, CLN3 may be involved in the initiation of caveolae internalization. In fact, Puri *et al*. found no evidence for domain formation before the internalization of sphingolipids is initialized (272), suggesting that the uptake of administered GM_1 needs possibly a further impulse. As described by Marks *et al*. the initiation of caveolae formation may occur via interaction of the oligosaccharide headgroup of the ganglioside with specific proteins (273), a similar mechanism to the apical sorting of glycoproteins via their N-glycan chains (168). A good candidate for this interaction partner may be caveolin-1, as Persaud-Sawin *et al*. reported that it colocalizes with the full-length CLN3 protein (49).

Suitably, in the present study, homozygous Cb*Cln3*$^{\Delta ex7/8}$ cells were shown to contain only half of the caveolin-1 protein amount of Cb*Cln3*$^{+}$ cells. This is in line with the observation of Tecedor *et al.* in microvascular endothelial CLN3-null cells, who implicated CLN3 in the

transport of caveolin-1 (76). The resulting loss in caveolae leads to the impaired endocytosis described already in 2004 by Fossale *et al*. (67). Furthermore, caveolin-1 deficiency in cells causes an impaired mitochondrial function, resulting from cholesterol storage in the mitochondrial membrane. This leads to increased membrane potential, reduced efficiency of the respiratory chain, reduction of the intrinsic antioxidant defense and therefore, to higher apoptotic susceptibility and neuronal death (274). The decrease in caveolin-1 levels may be also related to the decreased cell size of homozygous Cb*Cln3*$^{\Delta ex7/8}$ cells that was observed previously in our group (228). Sinha *et al.* reported that caveolae reformation contributes to the recovery from osmotic-induced swelling and plays a role in the mechanism of regulatory volume decrease (275). On the whole, the reduction in caveolin-1 protein levels is likely to preclude the transport of externally administered GM_1 to its site of action in homozygous Cb*Cln3*$^{\Delta ex7/8}$ cells and affect simultaneously other cellular pathways. This provides a valid reason why the cellular viability was not altered after external GM_1 supplementation.

4.1.2 GM_1 may be internalized by several endocytosis routes

In the current endocytosis model, cholera toxin is internalized via caveolae and transported in early endosomes from the PM to the TGN, from where it traverses the Golgi to its target compartment, the endoplasmic reticulum (276). However, the uptake of CTxB in HeLa cells and hippocampal neurons was shown to occur sometimes via clathrin-dependent endocytosis (277, 278) suggesting aberrant trafficking. In fact, some reports in cell models of sphingolipid storage diseases showed an alternative route of CTxB to endosomal structures, revealing that an imbalance in the membrane GSL composition can strongly influence its targeting (272, 279, 280). Puri *et al*. described that the endocytic mechanism involved in sphingolipid internalization is divided into two Golgi targeting pathways, a clathrin-dependent and –independent route (272). These pathways may intermix at some point along the endocytic route and undergo lipid-based sorting (reviewed in 119, 164, 281, 282). Furthermore, some studies suggested the existence of non-caveolar, non-clathrin endocytic processes (269, 283). In general, the different endocytic mechanisms may coexist and be divided by their purposes. The three most important would be then the directed internalization induced by the binding of ligands,

the uptake for degradation purposes and salvage processes responsible for the basic recycling and remodeling of the membrane (120). The contribution of the latter was largely underestimated so far. Steinmann *et al*. reported that per hour half of the PM is internalized and recycled in non-dividing cells and Sofer *et al*. could show that most of an internalized short acyl chain analogue of GM_1 is directly recycled back to the PM without being processed (142, 284). Hence, the recycling of gangliosides plays an important role in the maintenance of the dynamic state of the plasma membrane. Unfortunately, the methodological limitations in studying the mechanisms of endogenous lipid transport (detailed in 285) prevented so far a better characterization of the specific routes of CTxB trafficking according to their purpose.

In the present study, pulse-chase experiments were performed using CTxB-FITC bound to GM_1 ganglioside on the PM before imaging its distribution within the cell after a certain time span. Already after 5 minutes of pulse, CTxB-FITC accumulated within late endosomes and the TGN of homozygous Cb*Cln3*$^{\Delta ex7/8}$ cells, whereas it remained longer

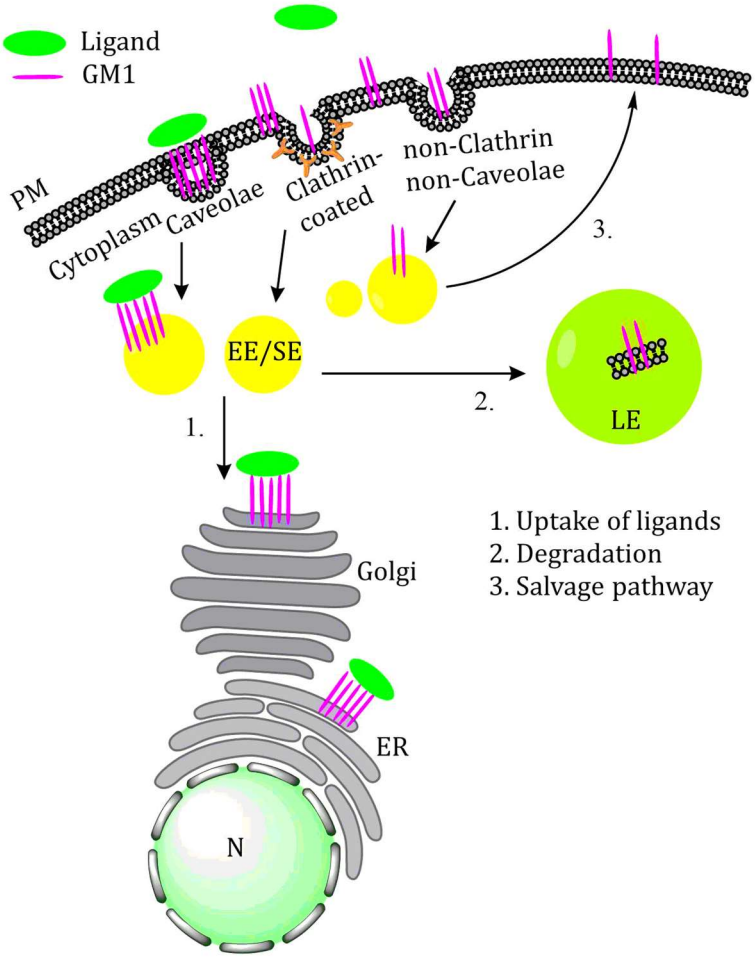

Figure 23. Scheme of alternative endocytosis routes for GM_1.

Ganglioside GM_1 is taken up from the plasma membrane by different endocytic mechanisms that coexist and depend on the purpose of uptake. The three most important purposes are directed internalization induced by the binding of extracellular ligands (1.), the uptake for degradation purposes (2.) and salvage processes responsible for the basic recycling and remodeling of the membrane (3.). The endocytic mechanisms include caveolar, clathrin-dependent as well as caveolae- and clathrin-independent pathways. However, the relation between uptake mechanism, endocytic route and purpose of endocytosis is not well characterized yet.

distributed over the PM and in unspecified endocytic vesicles in Cb*Cln3*$^{+}$ cells. Considering the disruption of caveolar endocytosis described above, these results point to a shift in the endocytosis of CTxB/GM_1 to an alternative internalization route. Possibly, the initial targeting process directing CTxB into one or another pathway is affected by the mutation in the CLN3 gene.

4.2 Putative role of CLN3 in lipid sorting from TGN to PM

As detailed in section IV.3.5, CLN3 and its yeast orthologue *btn1* have been recently assigned a multitude of functions in and around the Golgi and TGN, predominantly in protein sorting and the maintenance of membrane properties (76–78, 88). However, the probability of CLN3 being a residual Golgi protein is rather low. Structural Golgi proteins were reported to be five amino acid residues shorter in their transmembrane domains, preventing them to leave the Golgi (286, 287). Additionally, they comprise a high percentage of phenylalanine (286). Both characteristics are not found in CLN3. Nevertheless, the present study confirmed the presence of CLN3 in the Golgi, where it colocalized with Giantin. A reason may be that CLN3 exerts a function where it has to transfer the Golgi, without being indigenous to it. As the Golgi complex represents the central sorting station for lipids and membrane proteins in the cell, it is intimately connected to endocytic, secretory and recycling pathways (288). In fact, Tecedor *et al*. reported that ectopically expressed CLN3-mCherry colocalizes with GM_1 and buoyant regions of TGN membranes, but shows only proximity to the Golgi marker gm130 without direct colocalization (76). A similar distribution was seen here for the trafficking route of CTxB-FITC in homozygous Cb*Cln3*$^{\Delta ex7/8}$ cells. After 15 min of chase time, the lack of functional CLN3 led to increased colocalization of CTxB-FITC with TGN46, whereas no difference could be detected for the *cis*-Golgi marker gm130. In regard of the potential role of CLN3 in salvage pathways, this blockage may be caused by the regulation of Rab7 as described in the next section. The consequence would be redirection of accumulated GM_1-bound CTxB towards degradative compartments, explaining the additional colocalization increase of CTxB with LBPA and potentially Glb1 and the upregulation of the degradative machinery of GM_1.

Another finding favoring a role of CLN3 in lipid recycling to the PM is the involvement of the CLN3 yeast orthologue Btn1 in the polarization of sterol-rich membrane domains and polarized cell growth reported by Codlin *et al*. (61). This kind of sorting requires an accurately controlled turnover and directed transport of sphingolipids. Of particular interest in this context, is the colocalization of CLN3 with Neu1 that was reported to exert a function as negative regulator of lysosomal exocytosis via Lamp1 (289). Although no FRET could be measured between CLN3 and Neu1 and the data on Neu1 protein levels and enzyme activity remains inconclusive as described in section VII.2.2.1, its substrate Lamp1 was shown to be hyposialylated in homozygous Cb*Cln3*$^{\Delta ex7/8}$ cells. As a consequence, protein levels were also reduced due to an impaired protection from lysosomal proteases. Since Lamp1 plays a pivotal role in the docking of lysosomes to the PM, its hyposialylation leads to decreased exocytosis that may contribute to the observed disruption of anterograde transport (76, 289, 290). This strengthens previous observations that CLN3 regulates TGN to plasma membrane transport by acting on a protein upstream of Neu1. Since Neu1 is not an integral membrane protein, its yet unidentified membrane-associated partner may be a good candidate here (291).

4.3 Rab7 regulates the intracellular trafficking route of CTxB via cholesterol

The amount of cholesterol was shown to influence the initial uptake mechanism of the GSL-binding toxins ricin and CTxB (272, 292). While low levels promoted Golgi targeting of the endocytosed vesicles, accumulation of cholesterol led to a shift towards 'cytoplasmic punctae' (272). A similar regulation may lead to the observed accumulation of CTxB in the TGN and late endosomes of homozygous Cb*Cln3*$^{\Delta ex7/8}$ cells. Although filipin stainings revealed no difference between Cb*Cln3*$^{+}$ and homozygous Cb*Cln3*$^{\Delta ex7/8}$ cells (data not shown), its specificity for cholesterol was now shown to be questionable (293). Furthermore, the detection of filipin was problematic due to its low excitation wavelength of 340-380 nm, while the available laser-line used was at 405 nm, and its fast photobleaching. Other methods, for example gas chromatography-mass spectrometry, would provide more conclusive results, but so far, no direct measurement of cholesterol levels was performed on cerebellar cells. However, Westermarck *et al*. reported that the cholesterol levels in the plasma of JNCL patients were reduced and previous work in our

group suggested a decrease of cholesterol synthesis in homozygous Cb*Cln3*$^{\Delta ex7/8}$ cells (228, 294). As a consequence, the internalization of CTxB-FITC may be directed towards the TGN instead of being recycled to the PM. The resulting lack of GM_1 on the PM in combination with the defect in anterograde transport reported by Tecedor *et al*. (76), points to a disrupted salvage pathway of ganglioside GM_1.

Suitably, CLN3 was shown to interact with Rab7, which coordinates the transport of late endosomes towards centrosomes and lysosomes, and mediates recycling between late and early endosomes (295, 296). Furthermore, Rab7 was shown to be a regulator of vimentin phosphorylation and assembly (297) and an intact vimentin intermediate filament network is essential for ganglioside metabolism (120, 157). The direction of transport depends thereby on the motor protein associated to Rab7. Hölttä-Vuori *et al*. reported that Rab proteins regulate cholesterol-trafficking circuits as compartment-specific molecular switches (298). In line with this, overexpression of Rab7 was shown to decrease cholesterol levels and to correct the Golgi targeting of LacCer and CTxB in Niemann-Pick Type C cells (279). In case of homozygous Cb*Cln3*$^{\Delta ex7/8}$ cells, levels of membrane-bound Rab7 might be elevated leading to a decrease in cholesterol levels and the observed Golgi targeting of internalized CTxB. This would suggest a role for CLN3 in the regulation of Rab7 membrane localization, thereby influencing retro- and anterograde transport. Finally, low cholesterol levels might contribute to the upregulated degradation of GM_1 through an increase in the membrane-perturbing capability of saposins (299, 300).

5. How do the changes in ganglioside levels lead to disease phenotypes?

An impressive number of cellular processes is regulated by gangliosides and other sphingolipids. In particular, they play a major role in intra- and intercellular interactions during the development of the nervous system. In this period the ganglioside pattern changes towards more complex gangliosides and the extent of metabolic processing increases (262). Although the highest expression of CLN3 in rat brains was measured around birth, the juvenile onset of JNCL may be related to an intrinsic role it plays in unique neuronal cell populations later in the development (301). Besides this temporal parameter, also spatial factors play a role. The different ganglioside patterns in brain and

extra-neural tissues may explain why CLN3 is expressed ubiquitously, but JNCL pathology is restricted to the CNS.

5.1 Vacuolated lymphocytes and microglia activation may be caused by GM_3 accumulation

In 2003, Jeyakumar *et al*. suggested that microglia activation in GM_1 and GM_2 gangliosidosis mouse models initially occurs in regions with high extent of ganglioside storage (242). Suitably, the inflammatory response was also shown to be disturbed in a Cln3-deficient mouse model due to a failure of normal morphological transformation of the glia cells upon activation (302, 303). The reason may be the putative accumulation of GM_3 described in section VII.3.2 since GM_3 represents together with GD_3 the predominant gangliosides during embryogenesis (304). While GM_3 turnover rates are low, the cells may compensate for the delay in degradation, but substantial developmental changes like the shift to more complex gangliosides may lead to detrimental consequences due to the overload with GM_3. Suitably, GM_3 and other gangliosides were reported to cluster on the surface of lymphocytes in human peripheral blood. Hence, the presence of vacuolated lymphocytes in JNCL patients may also be caused by disrupted GM_3 turnover (29, 305). This is supported by the coinciding appearance of lymphocyte vacuolation and secondary GM_3 storage in an α-mannosidosis guinea pig model (306).

5.2 Putative correlation between the expression of CLN3 and ganglioside GD_{1a} during development

NCLs are a group of disorders that share common symptoms, indicating that the proteins affected in these diseases interrelate in so far unidentified cellular mechanisms. A recent study by Fabritius *et al*. concentrated hereby on the identification of cell types that show simultaneous expression of NCL-causing genes (307). CLN3 was shown to be spatially and temporally co-expressed with the soluble lysosomal proteins CLN2 and CLN5 in germinal epithelium, ventrical regions, cerebellum and hippocampus of developing mouse brains. These regions were reported to be major sites of neurogenesis (308–310). Interestingly, the expression of specific ganglioside patterns has been also associated with discrete

neuronal cell types in the cerebellum and hippocampus. For example, a higher expression of GD_{1a} was found in cerebellar granule cells and the dentate gyrus during development (311, 312). Therefore, the decrease in the GD_{1a} levels of homozygous Cb*Cln3*$^{\Delta ex7/8}$ cells reported in the present study leads to the assumption that these developmental changes are disturbed by the truncated CLN3 protein. A putative consequence may be the destabilization of the long-term axon-myelin interface that was shown to be mediated by the interaction of GD_{1a}/GT_{1a} with the myelin-associated glycoprotein (MAG) in cerebellar granule cells and hippocampal neurons (reviewed in 171). The concomitant inhibition of axonal outgrowth depends, thereby, on the activation of the small GTPase RhoA whose protein levels were shown to be reduced in previous observations of our group (228, 313). Furthermore, the increased vulnerability of cultured CLN3$^{-/-}$ cerebellar granule cells to AMPA-type glutamate receptor-mediated toxicity may be caused by a loss of this interaction as MAG was shown to protect axons from short-term neurotoxic insults (314, 315). In future, a detailed examination of CLN3 and GD_{1a} expression patterns may provide further information on the existence of a potential correlation.

5.1 Loss of GM_1 disrupts axon-glia interaction in homozygous Cb*Cln3*$^{\Delta ex7/8}$ cells

As described in detail in section VII.4.1, GM_1 is the major ganglioside known to exert a neuroprotective role (191). A partial reduction of GM_1 would lead to profound impacts on the nervous system of JNCL patients. Thereby, some cell types would be more affected than others due to the differential cellular expression of GM_1. For example, human motor nerve myelin was shown to contain more GM_1 (15% of total ganglioside) than sensory nerve cells (5%) (316), suggesting a role for GM_1 in the axon-glia interaction in these cells. Suitably, Autti *et al*. described severe loss of myelin in JNCL patients (317, 318), although levels of myelin basic protein were shown to be unchanged. Similar findings were made in *Cln8*-deficient mouse brains and *Cln5* knock-out mice (319, 320), presenting again a common mechanism affected in different NCLs. Furthermore, autoantibodies to GM_1 were shown to be present in the autoimmune neuropathy Guillain-Barré syndrome, where they label paranodal regions and disrupt nodes of Ranvier (177). The resulting mislocalization of potassium channels leads to slowed nerve conduction (177). In JNCL, this adverse effect may be even amplified as calsenilin, an interaction partner of CLN3, was previously shown

to regulate the localization of A-type voltage-gated potassium channels (321). The observed deterioration of the CNS in JNCL may be therefore a consequence of the impaired axon-glia interaction through loss of ganglioside GM_1 as stabilizer.

5.2 Involvement of GM_1 in the intracellular Ca^{2+} transport

GM_1 has an intrinsic ability to bind Ca^{2+} and is assumed to be an inhibitor of an L-type voltage-dependent calcium channel (322). This theory results from an observed increase in the endogeneous Ca^{2+} concentration in neuroblastoma N18 cells after application of CTxB. Furthermore, Wu *et al*. reported GM_1 to regulate the Ca^{2+} transfer to the ER (185, 323, 324). The study demonstrated that GM_1 has an opposite effect to GM_3 on the activity of the Ca^{2+}-ATPase of the sarcoplasmic reticulum (SERCA). Using intrinsic and time-resolved fluorescence and fluorescence quenching, the conformational changes of SERCA induced by GM_1 and GM_3 were compared. The obtained results indicated that GM_1 could make SERCA packed less compactly in the hydrophilic domain but more compact in the hydrophobic domain, while GM_3 makes the enzyme more compact in both, the hydrophilic and hydrophobic domain. Therefore, downregulation of GM_1 and upregulation of GM_3, as described in the present study, would lead to an increase in SERCA activity. The resulting cardiac hypertrophy has also been reported for JNCL patients (325, 326).

Furthermore, GM_1 was also shown to play a role at mitochondria-associated ER-membranes (MAMs) that are the place of Ca^{2+} transfer from the ER to mitochondria and enriched in GSLs (327). Brailovskaya *et al*. reported in 2014 that GM_1 protects PC12 cells from oxidative stress by increasing the rates of mitochondrial respiration and an increased energetic potential of inner mitochondrial membranes (328). A decrease in GM_1 levels may result in elevated degradation of respiratory chain members as the mitochondrial ATP synthase, whose highly hydrophobic subunit C presents the major storage component in JNCL (329).

Interestingly, also CLN8 was previously shown to shuttle between the ER and ER-Golgi intermediate complex and to regulate mitochondrial Ca^{2+} buffering (16, 330). Therefore, the role of GM_1 in Ca^{2+} regulation described here may provide a common pathway between CLN8 and CLN3 in intracellular Ca^{2+} transport.

5.3 Potential shift to GD_3 synthesis may lead to mitochondrial abnormalities

Although GD_3 levels were not measured in this study, GD_3 synthesis is a competitive pathway to GM_1 generation due to their origin from GM_3 (331). Hence, a shift in the ganglioside pattern is likely. As GD_3 directly targets mitochondria, the abnormalities reported in this compartment may be caused by a potential elevation (332). For example, elevation of GD_3 was shown to be sufficient to dissipate the mitochondrial membrane potential (264), leading consequently to the pro-apoptotic release of cytochrome c and caspase-9. In line with that, previous results in our group revealed a decreased mitochondrial membrane potential in homozygous Cb*Cln3*$^{\Delta ex7/8}$ cells (Anton Petcherski, data not published). Furthermore, Fossale *et al*. reported an elongation of mitochondria in homozygous Cb*Cln3*$^{\Delta ex7/8}$ cells (67) that may result from the ability of GD_3 to change the membrane viscosity of mitochondria (264). Therefore, future investigation of the ganglioside metabolism in JNCL should include the expansion to other series than a.

5.4 Biochemical overlap between JNCL, Alzheimer's disease and aging

Regarding the group of NCLs, Svennerholm *et al*. reported already in 1987 an altered brain ganglioside pattern in CLN1 disease (333). However, the disruption of ganglioside metabolism may provide also a biochemical overlap between neuronal disorders with different etiologies. For example, the enlargement of LBPA vesicles, described in the present study, markedly resembles the endosomal enlargement and increased number of lysosomes seen in AD neurons and prosaposin-deficiency (334, 335). Suitably, lysosomal glycohydrolases (among them Glb1) were found to be up-regulated in skin fibroblasts and cultured fibroblasts from AD patients (200, 336). Furthermore, Golabek *et al*. suggested full-length CLN3 to be a physiological regulator of APP metabolism (87). In line with that, a recent study reported that the amyloid-β (Aβ) fibrillogenesis is mediated by the binding of Aβ to GM_1 in detergent resistant microdomains and can be inhibited by administration of insulin (337). When insulin receptors are defective, as it is the case in AD, a specific Aβ-type (sAPP) accumulates in GM_1 positive vesicles of presynaptic areas and leads to aggregation of amyloid plaques (338). Therefore, AD is referred to as brain-specific type 3 diabetes (339). The underlying mechanism of this insulin-mediated sAPP secretion is regulated by phosphatidylinositol-3 kinase (PI3K) and triggers the PI3K/Akt/mTor

pathway, a signaling pathway involved in apoptosis and autophagy regulation (340). Notably, the same pathway is affected by lithium that inhibits inositol-monophosphatase (IMPase) and leads to degradation of accumulated ATPsubC, decreased autofluorescence and restoration of the abnormal Ca^{2+} levels in $CLN3^{\Delta ex7/8}$ knock-in cerebellar cells (100). Furthermore, the accumulation of GM_2 and GM_3, described for homozygous Cb*Cln3*$^{\Delta ex7/8}$ cells in the present study, was shown to inactivate the epidermal growth factor and insulin receptors, resulting in a decreased insulin sensitivity (341–343). Thereby GM_3 competes functionally with Cav-1 by binding a lysine residue just above the transmembrane domain of the insulin receptor (341). As insulin resistance and brain ceramide are also increased during aging, another parallel might be drawn here to JNCL. Of special interest is here the observed upregulation of Glb1 as a sign for premature senescence (344, 345). However, further experiments are needed to validate this connection. A first step may be the measurement of the membrane fluidity because an increase of the C20 fatty acyl species of GM_1 and GD_1 in the aging hippocampus was shown to result in a decrease in fluidity, making the cells more prone to degeneration (175, 264).

VIII. CONCLUSIONS

The first goal of the present study was the establishment of a comprehensive overview about the contribution of a-series gangliosides to JNCL pathology. The resulting quintessence is the observed synergistic activity of many individual components towards less complex gangliosides. Hereby, the severe loss of ganglioside GM_1 plays a central role. It is caused by the combined action of the GM_1-degrading multimeric enzyme complex (Glb1, PPCA and Neu1) and further stimulation by altered physicochemical membrane properties. The latter one encompasses an increase in LBPA levels that enhances the binding of Glb1 to GM_1-carrying membranes and stimulation of the membrane-perturbing capability of saposins by GM2a and potentially low cholesterol levels. The successive pathology results from the loss of neuroprotection provided by GM_1 and GD_{1a}. Destabilization of the axon-myelin interface and defective Ca^{2+} homeostasis are, thereby, the main characteristics. Furthermore, the combined effect of decreased GM_1 and increased GM_3 levels leads to an upregulation of SERCA and results in cardiac hypertrophy. Also the mitochondrial function is heavily affected by the lack of GM_1. A consequence may be the degradation of mitochondrial respiratory chain members, resulting in the previously observed accumulation of ATPsubC in the storage material of JNCL patients. Taken all together, the altered ganglioside pattern in homozygous Cb*Cln3*$^{\Delta ex7/8}$ cells may derive from a failed adaption to new conditions during the development or be a sign of early senescence. Both may explain the delayed onset of JNCL.

The second goal of this study was the identification of cellular mechanisms leading to the altered ganglioside profile and investigation of a potential role of CLN3. As described before, there is strong evidence that CLN3 modulates a process or condition that is essential in many cellular pathways and that is related to lipid metabolism. As shown in the present study, the alteration of ganglioside patterns by regulation of glycohydrolases via HRas is rather unlikely, as well as a role for CLN3 in the composition of caveolae. The similarity to a process that exerts a multifocal intrusion ability as prosaposin deficiency, emphasizes rather a function early in the ganglioside biosynthesis, in salvage processes or GSL transport. A hypothesis supporting the first is the close similarity of JNCL and some cases of CLN5 disease, suggesting a role for CLN3 in DHCer biosynthesis. Both are accompanied by the accumulation of LC3 punctae, decreased mitochondrial membrane

potential and ceramid-induced apoptosis. Alternatively, a dysfunction of salvage processes and/or GSL transport is favored by the recurring observation of an impaired flux of vesicular structures in JNCL models. The impaired endocytosis of administrated GM_1 described here depicts a role for CLN3 in the initiation of caveolae formation. However, the still present uptake of CTxB-FITC in pulse-chase experiments accompanied by different routing and the reported blockage of the anterograde transport of GM_1 and GalCer, suggest that the impaired endocytosis is only part of a more complex problem. This is supported by the possible stagnation in both, GM_2 distribution and processing of ingested GM_3. Nevertheless, no full blockage of intracellular transport was reported and GM_1 was not shown to accumulate on inner membranes while being absent from the PM. Therefore, the correlation between CLN3 amount and anterograde transport of GM_1 suggests that the impaired flux is secondary to a decrease in GM_1 levels. This is possible regarding the composition of GSLs in membranes as fundamental part of a lipid-based sorting machinery guiding the intracellular transport as described in section IV.5.3.1. The severe lack of GM_1 combined with alterations in the levels of other lipids may disrupt membrane dynamics and lead to a reorganization of cellular processes. The expansion of the degradative system described in the present study by the enlargement of LBPA-positive vesicles and the redirection of endocytosed CTxB-FITC towards late endosomes and lysosomes, may be an attempt of the cell to handle these circumstances. Therefore, this study suggests a potential role for CLN3 in the TGN as part of the central lipid sorting machinery, explaining its colocalization with Neu1 and Giantin and the exclusion of the *cis*-Golgi from the observed trafficking defects.

IX. FUTURE AIMS

Future work may expand the analysis performed in this study to other ganglioside series and their precursors, although there aren't many robust methods for doing this yet. Among others, the level and distribution of GD_3 may be of interest as it is next to GM_3 the other big antagonist of GM_1. Alterations in GD_3 may lead to the mitochondrial abnormalities observed in JNCL as described in section VII.5.3. In general, a thorough biochemical analysis would be useful to get deeper insights into the topic. For example, HPTLC analysis would allow to investigate the distribution of gangliosides under the aspect of different fatty acyl species as they play an important role in the packing density of membranes. Furthermore, additional HPLC runs may help to distinguish between ceramide and DHCer and provide, in general, more precise data than dot blot analysis as they are not dependent on the quality of antibodies. Besides expansion to other gangliosides, the investigation of overlapping processes between JNCL and the other NCLs as well as with neuronal disorders of different etiologies (for example AD, PD and HD) may provide an opportunity to narrow down the function of CLN3 by extracting the phenotypes that are unique to CLN3 deficiency. The same accounts for the determination, which of the observed phenotypes are present in human patients. As an example, the splicing mechanism of Glb1 to elastin binding protein is not conserved in mice, leading possibly to a different phenotype than the upregulation of Glb1 in mouse Cb*Cln3*$^{\Delta ex7/8}$ cells.

Finally, repetition of the administration of GM_1 to homozygous Cb*Cln3*$^{\Delta ex7/8}$ cells using GM_1-BODIPY instead of CTxB-FITC may provide a better understanding of the affected mechanism that precludes a neuroprotective effect. In parallel, the elevation of endogenous GM_1 levels in these cells should be tested either by transfection of GM_1 synthase or by impairment of ganglioside degradation using chloroquine. Of particular interest would be here the impact on the cellular lipid sorting machinery. A potential improvement of the endocytic flux would be in line with the conclusions of this study.

I. DEUTSCHE ZUSAMMENFASSUNG

Die Störung des intrazellulären Transports von Gangliosid GM_1 in einem genetisch akkuraten Model der neurodegenerativen lysosomalen Speicherkrankheit Juvenile Neuronale Ceroid Lipofuszinose (JNCL)

1. Einleitung

Bei Juveniler Neuronaler Ceroid-Lipofuszinose (JNCL) handelt es sich um eine seltene lysosomale Speicherkrankheit im Kindesalter. Sie führt zum frühzeitigen Tod in der dritten Lebensdekade und die derzeit mögliche Behandlung ist rein symptomatisch. JNCL entsteht aufgrund autosomal rezessiver Mutationen im sogenannten *CLN3* Gen. 85% der Patienten weisen dabei eine 1,02 kb große Deletion auf, bei welcher die Exone 7 und 8 mitsamt der sie umgebenden Intron-DNA fehlen ($CLN3^{\Delta ex7/8}$). Trotz der Entdeckung dieses Gendefekts vor über 20 Jahren, konnten bisher weder die Struktur, Funktion, noch die Lokalisation des dazugehörigen CLN3 Proteins aufgeklärt werden. Die bisherige Forschung weist jedoch auf einen von CLN3 gesteuerten Mechanismus hin, der dazu in der Lage ist, viele zelluläre Prozesse gleichzeitig zu beeinflussen. Bisher nachgewiesene Veränderungen betreffen unter anderem die lysosomale Ansäuerung, den lysosomalen Arginin-Import, Prozesse der Membranfusion, den vesikulären Transport, die Organisation des Zytoskeletts, Autophagie, Apoptose und die Proteolipidmodifikation anderer Proteine. Gute Kandidaten für die Funktion von CLN3, die diese Vielfalt an Veränderungen abdecken, wären somit der Lipidmetabolismus, als auch der antero- und retrograde Transport. Welche Rolle CLN3 dort jedoch genau zukommt, bleibt weiterhin ein Rätsel. Diese Studie beschäftigt sich daher mit speziellen bioaktiven Glycosphingolipiden, sogenannten Gangliosiden, die als regulierendes Zwischenglied fungieren könnten. Insbesondere Ganglioside der a-Serie wurden dabei schon häufiger mit den in JNCL gestörten Zellprozessen in Zusammenhang gebracht. So spielen sie eine wesentliche Rolle in der Immunomodulation, Rezeptoraktivität, an Kontaktstellen zwischen Zellen, sowie zwischen Zellen und ihrer Umgebung. Zusätzlich sind sie an der Entwicklung und Versorgung des Gehirns beteiligt, wo sie unter anderem für das

Neuritenwachstum, Heilungsprozesse nach Verletzungen, sowie das Überleben der Zellen verantwortlich sind. Eine der Hauptfunktionen von Gangliosiden ist jedoch die Regulierung von Membrantransportvorgängen wie der Endozytose und Autophagie. Die zugrundeliegenden Mechanismen sind bisher jedoch weitgehend unbekannt. Eine der Haupttheorien, wie Ganglioside die oben genannten Vorgänge beeinflussen, beschäftigt sich mit ihrer Fähigkeit die physiko-chemischen Membraneigenschaften zu verändern und somit sowohl Fusions-/Trennungsvorgänge zu beeinflussen, als auch eine wesentliche Rolle im lipidbasierten Sortiermechanismus zu spielen. Da es sich hierbei um einen graduellen, im Wesentlichen selbstregulierenden Prozess handelt, könnte eine Störung des Gangliosidsystems zu multifokalen Störungen in den Zellen führen. Die Veränderungen würden dabei hauptsächlich die Aktivität von Membranproteinen, deren Transportgeschwindigkeit, sowie die endgültige Lokalisation beeinflussen.

2. Zielsetzung der vorliegenden Studie

Eine Störung des Gangliosidmetabolismus wurde bereits bei vielen lysosomalen Speicherkrankheiten als pathogener Faktor eingestuft; welche Rolle Gangliosiden im Krankheitsverlauf von NCLs zukommt, ist bisher jedoch kaum erforscht. Insbesondere Gangliosiden der a-Serie wurde eine Rolle in der Entwicklung und dauerhaften Versorgung des Gehirns zugesprochen. Dort sind sie unter anderem für Membrantransportvorgänge verantwortlich. Um die Zusammenhänge zwischen diesen Funktionen und deren Störungen während der Krankheitsentwicklung bei JNCL Patienten zu aufzudecken, beschäftigt sich die vorliegende Studie mit der Analyse zentraler Enzyme und Metaboliten des Synthesewegs von Gangliosiden der a-Serie in einem Zellmodel von JNCL. Dabei wurden folgende Zielsetzungen verfolgt:

- Ein detaillierter Überblick über die Unterschiede im Gangliosid-Muster der a-Serie zwischen homozygoten Cb*Cln3*$^{+}$ und Cb*Cln3*$^{\Delta ex7/8}$ Zellen.
- Die Identifikation und Charakterisierung von Enzymen und Metaboliten, welche für die gefundenen Unterschiede verantwortlich sind.
- Die Beschreibung der zugrundeliegenden zellulären Mechanismen.
- Die Untersuchung, welche potentielle Rolle CLN3 im Zusammenhang mit den beschriebenen Veränderungen des Gangliosid-Metabolismus spielt.

3. Ergebnisse und Schlussfolgerung

Im ersten Teil der vorliegenden Forschungsarbeit wurden die zentralen Enzyme und Metaboliten der a-Serie-Ganglioside in einem murinen Zellmodel von JNCL analysiert. Das Kernstück der Untersuchung stellen dabei die gesenkten Level des neuroprotektiven Gangliosids GM_1 in homozygoten Cb*Cln3*$^{\Delta ex7/8}$ Zellen dar. Diese werden durch einen verstärkt agierenden Enzymkomplex verursacht, welcher aus drei Enzymen besteht: neuraminidase 1 (Neu1), welche GD_{1a} zu GM_1 abbaut, β-Galactosidase (Glb1), die GM_1 zu GM_2 umwandelt, und dem protektiven Protein Cathepsin A (PPCA). Für Glb1 konnten dabei erhöhte Proteinlevel, sowie eine gesteigerte Enzymaktivität, in homozygoten Cb*Cln3*$^{\Delta ex7/8}$ Zellen nachgewiesen werden, deren Proliferation durch Erreichen der Konfluenz gestoppt wurde. Bei prolifererierenden Cb*Cln3*$^{\Delta ex7/8}$ Zellen befanden sich diese Messwerte jedoch unter der Nachweisgrenze. Deshalb wurden weitere Faktoren untersucht, die die Menge von GM_1 direkt durch eine Steigerung der Glb1-Aktivität oder Glb1-unabhängig senken. Zu den Glb1-unabhängigen Faktoren gehört dabei die von Cao *et al.* beschriebene Steigerung der St3Gal2 mRNA Level. Ein Glb1-abhängiger Faktor hingegen ist der in der vorliegenden Arbeit beschriebene Anstieg des speziellen Lipids LBPA, welches die Bindung von Glb1 an GM_1-haltige Membranen erleichtert und somit den GM_1-Abbau fördert. Hinzu kommt die längerfristige Stabilisierung von Glb1 durch erhöhte PPCA Level. Auch eine mögliche Steigerung der Neu1 Aktivität, auf welche die Abnahme der Lamp1 Sialylierung, sowie niedrigere GD_{1a} Mengen hinweisen fördern den Eindruck einer Verschiebung des Gangliosidmusters zu Gunsten der weniger komplexen Ganglioside. Die Anreicherung von GM_2 und GM_3 in homozygoten Cb*Cln3*$^{\Delta ex7/8}$ Zellen, bestätigen diesen Eindruck. Der daraus resultierende Verlust an Neuroprotektion könnte die Grundlage der multifokalen Pathologie von JNCL sein.

Der zweite Teil dieser Studie beschäftigt sich mit den zellulären Mechanismen, die hinter den Veränderungen des Gangliosidmusters stehen und der dazugehörigen Rolle von CLN3. Dabei konnte eine positive Korrelation zwischen der Menge von CLN3 in der Zelle und dem anterograden Transport von GM_1 zur Plasmamembran nachgewiesen werden. Diese Korrelation entfällt im Falle der *CLN3*$^{\Delta ex7/8}$-Mutation und führt zu einer schwächeren Färbung der Plasmamembran mit dem GM_1-Marker CTxB-FITC. Die Transfektion der Zellen mit dem vollständigen CLN3 Protein konnte die Intensität der CTxB-FITC Färbung wiederherstellen. Basierend auf der neuroprotektiven Rolle von GM_1,

ist die damit einhergehende Steigerung der GM_1 Menge möglicherweise für die, in früheren Studien veröffentlichte, Wiederherstellung der zellulären Prozesse verantwortlich. Daher wurde erwartet, dass eine Behandlung der homozygoten Cb*Cln3*$^{\Delta ex7/8}$ Zellen mit GM_1 ihre Lebensdauer erhöht und möglicherweise einige andere pathogene Phänotypen korrigiert. Dies konnte jedoch nicht beobachtet werden. Der Grund dafür liegt vermutlich in der verminderten caveolaren Endozytose von GM_1, sowie dem Fehltransport des aufgenommenen GM_1 zum trans-Golgi Netzwerk (TGN), von wo aus es Richtung Abbaukompartimente umgeleitet wird. Beides spricht für eine generelle Verlangsamung des intrazellulären Durchflusses bei CLN3-Ausfall. Der in dieser Studie erbrachte Nachweis von CLN3 im TGN weist deshalb auf eine Rolle von CLN3 im lipid-basierten Sortiermechanismus hin. Bei dessen Störung kommt es zu Veränderungen der Membrankomposition, was wiederum Auswirkungen auf die regulatorischen Funktionen vieler Membranproteine haben kann. Die dadurch entstehenden parallelen Schädigungen verschiedener zellulärer Prozesse entspräche der multifokalen Pathologie in JNCL.

4. Ausblick

Um die aktuelle Studie zu vervollständigen, wäre eine Wiederholung der Versuche zur GM_1 Verabreichung wünschenswert. Hierbei sollte jedoch GM_1-BODIPY anstatt von CTxB-FITC verwendet werden, da bereits geringe aufgenommene Mengen auf diese Art und Weise nachgewiesen werden könnten. Weiterhin ermöglicht es eine bessere Verfolgung der Endozytose-Route um mögliche Blockaden oder alternative Transportwege aufzudecken. Ebenfalls von Interesse wäre, ob eine Erhöhung der endogenen GM_1 Level zu anderen Ergebnissen führen würde als die äußere Verabreichung. Dies könnte entweder über eine Transfektion der homozygoten Cb*Cln3*$^{\Delta ex7/8}$ Zellen mit einer GM_1-Synthase geschehen oder über die Hemmung des Abbaus von Gangliosiden mittels Chloroquin. Von besonderem Interesse wäre dabei der Effekt auf den zellulären lipidbasierten Sortiermeachanismus, da eine potentielle Erhöhung des endozytischen Durchflusses im Einklang mit den Schlussfolgerungen der vorliegenden Studie wäre.

Da sich die Ergebnisse der vorliegenden Arbeit im Wesentlichen auf die a-Serie der Ganglioside beschränken, wäre der nächste Schritt eine Ausweitung der Untersuchung auf Ganglioside anderer Serien, sowie deren Vorläufermoleküle. An erster Stelle steht

dabei eine ausführliche biochemische Analyse. Die Verwendung der HPTLC Technologie erlaubt, zum Beispiel, eine detailliertere Klassifizierung der Ganglioside in Abhängigkeit von den gebundenen Fettsäurespezies. Neben den Oligosaccharidketten, spielen diese eine wesentliche Rolle für die Funktion des jeweiligen Gangliosids, da die Struktur der Fettsäuren Auswirkungen auf die Packungsdichte der sie enthaltenden Membran hat. Weiterhin wären zusätzliche HPLC Untersuchungen hilfreich, da sie präzisere Ergebnisse liefern als die bisher genutzte Dot Blot Technik. Zum einen wird dies durch ihre Unabhängigkeit von der Qualität der verwendeten Antikörper ermöglicht, zum anderen sind mit HPLC auch feinere Unterscheidungen möglich, wie die zwischen Ceramid und DHCer. Insgesamt, wäre eine Weiterentwicklung der bisher verfügbaren Methoden zur Untersuchung von Gangliosiden wünschenswert, da der derzeitige Stand der Technik viele Fragen ungeklärt lässt.

Bei der Wahl der untersuchten Gangliosidspezies, sollte ein besonderes Augenmerk auf die Level und intrazelluläre Verteilung von GD_3 gelegt werden, da es sich hierbei nicht nur um ein aus GM_3 entstehendes Konkurrenzprodukt zu GM_1 handelt, sondern auch um dessen Antagonist auf funktioneller Ebene. Wie in Absatz VII.5.3 beschrieben, könnten Veränderungen in GD_3 zu den in JNCL beobachteten mitochondrialen Veränderungen führen.

Einen weiteren wichtigen Schritt stellt die Kartierung überlappender Prozesse zwischen JNCL und anderen NCLs, sowie anderer neuronaler Krankheiten, wie zum Beispiel AD, PD oder HD, dar. Diese Vorgehensweise liefert einerseits ein besseres Bild der Funktionsvielfalt einzelner Ganglioside, ermöglicht aber auch die Eingrenzung spezifischer Funktionen von CLN3 durch das Herausfiltern der für JNCL einzigartigen Phänotypen. Dasselbe gilt für die Klärung, welche der gefundenen Phänotypen in menschlichen Patienten wiederzufinden sind. Der Splicing Mechanismus von Glb1 zum Elastin Binding Protein ist, zum Beispiel, in Mäusen nicht konserviert. Dies könnte in JNCL Patienten zu anderen Ergebnissen als der hier beobachteten Hochregulierung von Glb1 in murinen Cb*Cln3*$^{\Delta ex7/8}$ Zellen führen und muss deshalb in beiden Organismen verglichen werden.

II. REFERENCES

1. Rider, J. A., and Rider, D. L. (1988) Batten disease: past, present, and future. *Am. J. Med. Genet. Suppl.* **5**, 21–6

2. Uvebrant, P., and Hagberg, B. (1997) Neuronal Ceroid Lipofuscinoses in Scandinavia: Epidemiology and Clinical Pictures. *Neuropediatrics* **28**, 6–8

3. Haltia, M. (2006) The neuronal ceroid-lipofuscinoses: From past to present. *Biochim. Biophys. Acta - Mol. Basis Dis.* **1762**, 850–856

4. Zeman, W., and Dyken, P. (1969) Neuronal ceroid-lipofuscinosis (Batten's disease): relationship to amaurotic family idiocy? *Pediatrics* **44**, 570–83

5. Mole, S. E. (2004) The Genetic Spectrum of Human Neuronal Ceroid-lipofuscinoses. *Brain Pathol.* **14**, 70–76

6. Tyynelä, J., Cooper, J. D., Khan, M. N., Shemilts, S. J. A., and Haltia, M. (2004) Hippocampal pathology in the human neuronal ceroid-lipofuscinoses: distinct patterns of storage deposition, neurodegeneration and glial activation. *Brain Pathol.* **14**, 349–57

7. Verkruyse, L. A., and Hofmann, S. L. (1996) Lysosomal Targeting of Palmitoyl-protein Thioesterase. *J. Biol. Chem.* **271**, 15831–15836

8. Hofmann, S. L., Lee, L. A., Lu, J.-Y., and Verkruyse, L. A. (1997) Palmitoyl-Protein Thioesterase and the Molecular Pathogenesis of Infantile Neuronal Ceroid Lipofuscinosis. *Neuropediatrics* **28**, 27–30

9. Sleat, D. E., Donnelly, R. J., Lackland, H., Liu, C.-G., Sohar, I., Pullarkat, R. K., and Lobel, P. (1997) Association of Mutations in a Lysosomal Protein with Classical Late-Infantile Neuronal Ceroid Lipofuscinosis. *Science (80-.).* **277**, 1802–1805

10. Sohar, I., Sleat, D. E., Jadot, M., and Lobel, P. (2002) Biochemical Characterization of a Lysosomal Protease Deficient in Classical Late Infantile Neuronal Ceroid Lipofuscinosis (LINCL) and Development of an Enzyme-Based Assay for Diagnosis and Exclusion of LINCL in HUman Specimens and Animal Models. *J. Neurochem.* **73**, 700–711

11. Sleat, D. E., Lackland, H., Wang, Y., Sohar, I., Xiao, G., Li, H., and Lobel, P. (2005) The human brain mannose 6-phosphate glycoproteome: A complex mixture composed of multiple isoforms of many soluble lysosomal proteins. *Proteomics* **5**, 1520–1532

12. Sleat, D. E., Zheng, H., and Lobel, P. (2007) The human urine mannose 6-phosphate glycoproteome. *Biochim. Biophys. Acta - Proteins Proteomics* **1774**, 368–372

13. Sleat, D. E., Della Valle, M. C., Zheng, H., Moore, D. F., and Lobel, P. (2008) The Mannose 6-Phosphate Glycoprotein Proteome. *J. Proteome Res.* **7**, 3010–3021

14. Haddad, S. El, Khoury, M., Daoud, M., Kantar, R., Harati, H., Mousallem, T., Alzate, O., Meyer, B., and Boustany, R.-M. N. (2012) CLN5 and CLN8 protein association with ceramide synthase: Biochemical and proteomic approaches. *Electrophoresis* **33**, 3798–3809

15. Schulz, A., Mousallem, T., Venkataramani, M., Persaud-Sawin, D.-A., Zucker, A., Luberto, C., Bielawska, A., Bielawski, J., Holthuis, J. C. M., Jazwinski, S. M., Kozhaya, L., Dbaibo, G. S., and Boustany, R.-M. N. (2005) The CLN9 Protein, a Regulator of Dihydroceramide Synthase. *J. Biol. Chem.* **281**, 2784–2794

16. Winter, E., and Ponting, C. P. (2002) TRAM, LAG1 and CLN8: members of a novel family of lipid-sensing domains? *Trends Biochem. Sci.* **27**, 381–383

17. Gao, H., Boustany, R.-M. N., Espinola, J. A., Cotman, S. L., Srinidhi, L., Antonellis, K. A., Gillis,

T., Qin, X., Liu, S., Donahue, L.-R., Bronson, R. T., Faust, J. R., Stout, D., Haines, J. L., Lerner, T. J., and MacDonald, M. E. (2002) Mutations in a Novel CLN6-Encoded Transmembrane Protein Cause Variant Neuronal Ceroid Lipofuscinosis in Man and Mouse. *Am. J. Hum. Genet.* **70**, 324–335

18. Sharp, J. D., Wheeler, R. B., Parker, K. A., Gardiner, R. M., Williams, R. E., and Mole, S. E. (2003) Spectrum of CLN6 mutations in variant late infantile neuronal ceroid lipofuscinosis. *Hum. Mutat.* **22**, 35–42

19. Teixeira, C. A. F., Espinola, J. A., Huo, L., Kohlschütter, J., Persaud-Sawin, D.-A., Minassian, B. A., Bessa, C. J. P., Guimarães, A., Stephan, D. A., Sá Miranda, M. C., MacDonald, M. E., Ribeiro, M. G., and Boustany, R.-M. N. (2003) Novel mutations in the CLN6 gene causing a variant late infantile neuronal ceroid lipofuscinosis. *Hum. Mutat.* **21**, 502–508

20. Siintola, E., Topcu, M., Aula, N., Lohi, H., Minassian, B. A., Paterson, A. D., Liu, X.-Q., Wilson, C., Lahtinen, U., Anttonen, A.-K., and Lehesjoki, A.-E. (2007) The Novel Neuronal Ceroid Lipofuscinosis Gene MFSD8 Encodes a Putative Lysosomal Transporter. *Am. J. Hum. Genet.* **81**, 136–146

21. Smith, K. R., Dahl, H. H. M., Canafoglia, L., Andermann, E., Damiano, J., Morbin, M., Bruni, A. C., Giaccone, G., Cossette, P., Saftig, P., Grötzinger, J., Schwake, M., Andermann, F., Staropoli, J. F., Sims, K. B., Mole, S. E., Franceschetti, S., Alexander, N. A., Cooper, J. D., Chapman, H. A., Carpenter, S., Berkovic, S. F., and Bahlo, M. (2013) Cathepsin F mutations cause Type B Kufs disease, an adult-onset neuronal ceroid lipofuscinosis. *Hum. Mol. Genet.* **22**, 1417–1423

22. Warrier, V., Vieira, M., and Mole, S. E. (2013) Genetic basis and phenotypic correlations of the neuronal ceroid lipofusinoses. *Biochim. Biophys. Acta - Mol. Basis Dis.* **1832**, 1827–1830

23. Yoshikawa, M., Uchida, S., Ezaki, J., Rai, T., Hayama, A., Kobayashi, K., Kida, Y., Noda, M., Koike, M., Uchiyama, Y., Marumo, F., Kominami, E., and Sasaki, S. (2002) CLC-3 deficiency leads to phenotypes similar to human neuronal ceroid lipofuscinosis. *Genes Cells* **7**, 597–605

24. Kasper, D., Planells-Cases, R., Fuhrmann, J. C., Scheel, O., Zeitz, O., Ruether, K., Schmitt, A., Poët, M., Steinfeld, R., Schweizer, M., Kornak, U., and Jentsch, T. J. (2005) Loss of the chloride channel ClC-7 leads to lysosomal storage disease and neurodegeneration. *EMBO J.* **24**, 1079–1091

25. Mole, S. E., Williams, R. E., and Goebel, H.-H. (2011) *The Neuronal Ceroid Lipofuscinoses (Batten Disease)*, Oxford University Press, New York, USA

26. Claussen, M., Heim, P., Knispel, J., Goebel, H. H., and Kohlschütter, A. (1992) Incidence of neuronal ceroid-lipofuscinoses in West Germany: Variation of a method for studying autosomal recessive disorders. *Am. J. Med. Genet.* **42**, 536–538

27. Cardona, F., and Rosati, E. (1995) Neuronal ceroid-lipofuscinoses in Italy: An epidemiological study. *Am. J. Med. Genet.* **57**, 142–143

28. Rakheja, D., Narayan, S. B., and Bennett, M. J. (2007) Juvenile neuronal ceroid-lipofuscinosis (Batten disease): a brief review and update. *Curr. Mol. Med.* **7**, 603–608

29. Gillis, W. S., Bennett, M. J., Galloway, J. H., Cartwright, I. J., Hosking, G. P., and Smith, C. M. L. (1987) Lipid abnormalities in Batten's disease. *J. Inherit. Metab. Dis.* **10**, 329–332

30. Schuurmans Stekhoven, J. H., van Haelst, U. J. G. M., Joosten, E. M. G., and Loonen, M. C. B. (1977) Ultrastructural study of the vacuoles in the peripheral lymphocytes in juvenile amaurotic idiocy. *Acta Neuropathol.* **38**, 137–142

31. Mole, S. E., Williams, R. E., and Goebel, H.-H. (2005) Correlations between genotype,

ultrastructural morphology and clinical phenotype in the neuronal ceroid lipofuscinoses. *Neurogenetics* **6**, 107–126

32. Jalanko, A., and Braulke, T. (2009) Neuronal ceroid lipofuscinoses. *Biochim. Biophys. Acta - Mol. Cell Res.* **1793**, 697–709

33. Lerner, T. J., Boustany, R.-M. N., Anderson, J. W., D'Arigo, K. L., Schlumpf, K., Buckler, A. J., Gusella, J. F., and Haines, J. L. (1995) Isolation of a novel gene underlying batten disease, CLN3. *Cell* **82**, 949–957

34. Mitchison, H. M., Munroe, P. B., O'Rawe, A. M., Taschner, P. E. M., de Vos, N., Kremmidiotis, G., Lensink, I. L., Munk, A. C., D'Arigo, K. L., Anderson, J. W., Lerner, T. J., Moyzis, R. K., Callen, D. F., Breuning, M. H., Doggett, N. A., Gardiner, R. M., and Mole, S. E. (1997) Genomic Structure and Complete Nucleotide Sequence of the Batten Disease Gene,CLN3. *Genomics* **40**, 346–350

35. Cotman, S. L., Vrbanac, V., Lebel, L.-A., Lee, R. L., Johnson, K. A., Donahue, L.-R., Teed, A. M., Antonellis, K. A., Bronson, R. T., Lerner, T. J., and MacDonald, M. E. (2002) Cln3(Deltaex7/8) knock-in mice with the common JNCL mutation exhibit progressive neurologic disease that begins before birth. *Hum. Mol. Genet.* **11**, 2709–2721

36. Chattopadhyay, S., and Pearce, D. A. (2000) Neural and Extraneural Expression of the Neuronal Ceroid Lipofuscinoses Genes CLN1, CLN2, and CLN3: Functional Implications for CLN3. *Mol. Genet. Metab.* **71**, 207–211

37. Järvelä, I., Sainio, M., Rantamäki, T., Olkkonen, V. M., Carpén, O., Peltonen, L., and Jalanko, A. (1998) Biosynthesis and intracellular targeting of the CLN3 protein defective in Batten disease. *Hum. Mol. Genet.* **7**, 85–90

38. Golabek, A. A., Kaczmarski, W., Kida, E., Kaczmarski, A., Michalewski, M. P., and Wisniewski, K. E. (1999) Expression Studies of CLN3 Protein (Battenin) in Fusion with the Green Fluorescent Protein in Mammalian Cellsin Vitro. *Mol. Genet. Metab.* **66**, 277–282

39. Ezaki, J., Takeda-Ezaki, M., Koike, M., Ohsawa, Y., Taka, H., Mineki, R., Murayama, K., Uchiyama, Y., Ueno, T., and Kominami, E. (2003) Characterization of Cln3p, the gene product responsible for juvenile neuronal ceroid lipofuscinosis, as a lysosomal integral membrane glycoprotein. *J. Neurochem.* **87**, 1296–1308

40. Kyttälä, A., Ihrke, G., Vesa, J., Schell, M. J., and Luzio, J. P. (2003) Two Motifs Target Batten Disease Protein CLN3 to Lysosomes in Transfected Nonneuronal and Neuronal Cells. *Mol. Biol. Cell* **15**, 1313–1323

41. Nugent, T., Mole, S. E., and Jones, D. T. (2008) The transmembrane topology of Batten disease protein CLN3 determined by consensus computational prediction constrained by experimental data. *FEBS Lett.* **582**, 1019–1024

42. Ratajczak, E., Petcherski, A., Ramos-Moreno, J. M., and Ruonala, M. O. (2014) FRET-Assisted Determination of CLN3 Membrane Topology. *PLoS One* **9**, e102593

43. Michalewski, M. P., Kaczmarski, W., Golabek, A. A., Kida, E., Kaczmarski, A., and Wisniewski, K. E. (1999) Posttranslational Modification of CLN3 Protein and Its Possible Functional Implication. *Mol. Genet. Metab.* **66**, 272–276

44. Storch, S., Pohl, S., and Braulke, T. (2004) A Dileucine Motif and a Cluster of Acidic Amino Acids in the Second Cytoplasmic Domain of the Batten Disease-related CLN3 Protein Are Required for Efficient Lysosomal Targeting. *J. Biol. Chem.* **279**, 53625–53634

45. Storch, S., Pohl, S., Quitsch, A., Falley, K., and Braulke, T. (2007) C-Terminal Prenylation of the CLN3 Membrane Glycoprotein Is Required for Efficient Endosomal Sorting to

Lysosomes. *Traffic* **8**, 431–444

46. Mao, Q., Foster, B. J., Xia, H., and Davidson, B. L. (2003) Membrane topology of CLN3, the protein underlying Batten disease. *FEBS Lett.* **541**, 40–46

47. Pullarkat, R. K., and Morris, G. (1997) Farnesylation of Batten Disease CLN3 Protein. *Neuropediatrics* **28**, 42–44

48. Kaczmarski, W., Wisniewski, K. E., Golabek, A. A., Kaczmarski, A., Kida, E., and Michalewski, M. P. (1999) Studies of Membrane Association of CLN3 Protein. *Mol. Genet. Metab.* **66**, 261–264

49. Persaud-Sawin, D.-A., McNamara, J. O., Rylova, S. N., Vandongen, A., and Boustany, R.-M. N. (2004) A Galactosylceramide Binding Domain Is Involved in Trafficking of CLN3 from Golgi to Rafts via Recycling Endosomes. *Pediatr. Res.* **56**, 449–463

50. JNCL mutation database, http://www.ucl.ac.uk/ncl/cln3.shtml (date accessed 03/10/2015)

51. Järvelä, I., Lehtovirta, M., Tikkanen, R., Kyttälä, A., and Jalanko, A. (1999) Defective intracellular transport of CLN3 is the molecular basis of Batten disease (JNCL). *Hum. Mol. Genet.* **8**, 1091–1098

52. Kitzmüller, C., Haines, R. L., Codlin, S., Cutler, D. F., and Mole, S. E. (2008) A function retained by the common mutant CLN3 protein is responsible for the late onset of juvenile neuronal ceroid lipofuscinosis. *Hum. Mol. Genet.* **17**, 303–312

53. Munroe, P. B., Mitchison, H. M., O'Rawe, A. M., Anderson, J. W., Boustany, R.-M. N., Lerner, T. J., Taschner, P. E. M., de Vos, N., Breuning, M. H., Gardiner, R. M., and Mole, S. E. (1997) Spectrum of mutations in the Batten disease gene, CLN3. *Am. J. Hum. Genet.* **61**, 310–316

54. Cotman, S. L., and Staropoli, J. F. (2012) The juvenile Batten disease protein, CLN3, and its role in regulating anterograde and retrograde post-Golgi trafficking. *Clin. Lipidol.* **7**, 79–91

55. Taschner, P. E. M., de Vos, N., and Breuning, M. H. (1997) Rapid detection of the major deletion in the Batten disease gene CLN3 by allele specific PCR. *J. Med. Genet.* **34**, 955–956

56. Muzaffar, N. E., and Pearce, D. A. (2008) Analysis of NCL Proteins from an Evolutionary Standpoint. *Curr. Genomics* **9**, 115–136

57. Pearce, D. A., and Sherman, F. (1998) A yeast model for the study of Batten disease. *Proc. Natl. Acad. Sci. U. S. A.* **95**, 6915–6918

58. Gachet, Y., Codlin, S., Hyams, J. S., and Mole, S. E. (2005) btn1, the Schizosaccharomyces pombe homologue of the human Batten disease gene CLN3, regulates vacuole homeostasis. *J. Cell Sci.* **118**, 5525–5536

59. Ramirez-Montealegre, D., and Pearce, D. A. (2005) Defective lysosomal arginine transport in juvenile Batten disease. *Hum. Mol. Genet.* **14**, 3759–3773

60. Osório, N. S., Carvalho, A., Almeida, A. J., Padilla-Lopez, S., Leão, C., Laranjinha, J., Ludovico, P., Pearce, D. A., and Rodrigues, F. (2007) Nitric Oxide Signaling Is Disrupted in the Yeast Model for Batten Disease. *Mol. Biol. Cell* **18**, 2755–2767

61. Codlin, S., Haines, R. L., and Mole, S. E. (2008) btn1 Affects Endocytosis, Polarization of Sterol-Rich Membrane Domains and Polarized Growth in Schizosaccharomyces pombe. *Traffic* **9**, 936–950

62. Mitchison, H. M., Bernard, D. J., Greene, N. D. E., Cooper, J. D., Junaid, M. A., Pullarkat, R. K., de Vos, N., Breuning, M. H., Owens, J. W., Mobley, W. C., Gardiner, R. M., Lake, B. D., Taschner,

P. E. M., and Nussbaum, R. L. (1999) Targeted Disruption of the Cln3 Gene Provides a Mouse Model for Batten Disease. *Neurobiol. Dis.* **6**, 321–334

63. Katz, M. L., Shibuya, H., Liu, P.-C., Kaur, S., Gao, C.-L., and Johnson, G. S. (1999) A mouse gene knockout model for juvenile ceroid-lipofuscinosis (Batten disease). *J. Neurosci. Res.* **57**, 551–556

64. Seigel, G. M., Lotery, A., Kummer, A., Bernard, D. J., Greene, N. D. E., Turmaine, M., Derksen, T. A., Nussbaum, R. L., Davidson, B. L., Wagner, J., and Mitchison, H. M. (2002) Retinal Pathology and Function in a Cln3 Knockout Mouse Model of Juvenile Neuronal Ceroid Lipofuscinosis (Batten Disease). *Mol. Cell. Neurosci.* **19**, 515–527

65. Katz, M. L., Johnson, G. S., Tullis, G. E., and Lei, B. (2008) Phenotypic characterization of a mouse model of juvenile neuronal ceroid lipofuscinosis. *Neurobiol. Dis.* **29**, 242–253

66. Eliason, S. L., Stein, C. S., Mao, Q., Tecedor, L., Ding, S.-L., Gaines, D. M., and Davidson, B. L. (2007) A Knock-In Reporter Model of Batten Disease. *J. Neurosci.* **27**, 9826–9834

67. Fossale, E., Wolf, P., Espinola, J. A., Lubicz-Nawrocka, T., Teed, A. M., Gao, H., Rigamonti, D., Cattaneo, E., MacDonald, M. E., and Cotman, S. L. (2004) Membrane trafficking and mitochondrial abnormalities precede subunit c deposition in a cerebellar cell model of juvenile neuronal ceroid lipofuscinosis. *BMC Neurosci.* **5**, 57

68. Kremmidiotis, G., Lensink, I. L., Bilton, R. L., Woollatt, E., Chataway, T. K., Sutherland, G. R., and Callen, D. F. (1999) The Batten disease gene product (CLN3p) is a Golgi integral membrane protein. *Hum. Mol. Genet.* **8**, 523–531

69. Haskell, R. E., Derksen, T. A., and Davidson, B. L. (1999) Intracellular Trafficking of the JNCL Protein CLN3. *Mol. Genet. Metab.* **66**, 253–260

70. Kida, E., Kaczmarski, W., Golabek, A. A., Kaczmarski, A., Michalewski, M. P., and Wisniewski, K. E. (1999) Analysis of Intracellular Distribution and Trafficking of the CLN3 Protein in Fusion with the Green Fluorescent Proteinin Vitro. *Mol. Genet. Metab.* **66**, 265–271

71. Margraf, L. R., Boriack, R. L., Routheut, A. A., Cuppen, I., Alhilali, L., Bennett, C. J., and Bennett, M. J. (1999) Tissue Expression and Subcellular Localization of CLN3, the Batten Disease Protein. *Mol. Genet. Metab.* **66**, 283–289

72. Haskell, R. E., Carr, C. J., Pearce, D. A., Bennett, M. J., and Davidson, B. L. (2000) Batten disease: evaluation of CLN3 mutations on protein localization and function. *Hum. Mol. Genet.* **9**, 735–744

73. Luiro, K., Kopra, O., Lehtovirta, M., and Jalanko, A. (2001) CLN3 protein is targeted to neuronal synapses but excluded from synaptic vesicles: new clues to Batten disease. *Hum. Mol. Genet.* **10**, 2123–2131

74. Mao, Q., Xia, H., and Davidson, B. L. (2003) Intracellular trafficking of CLN3, the protein underlying the childhood neurodegenerative disease, Batten disease. *FEBS Lett.* **555**, 351–357

75. Rakheja, D., Narayan, S. B., Pastor, J. V., and Bennett, M. J. (2004) CLN3P, the Batten disease protein, localizes to membrane lipid rafts (detergent-resistant membranes). *Biochem. Biophys. Res. Commun.* **317**, 988–991

76. Tecedor, L., Stein, C. S., Schultz, M. L., Farwanah, H., Sandhoff, K., and Davidson, B. L. (2013) CLN3 Loss Disturbs Membrane Microdomain Properties and Protein Transport in Brain Endothelial Cells. *J. Neurosci.* **33**, 18065–18079

77. Codlin, S., and Mole, S. E. (2009) S. pombe btn1, the orthologue of the Batten disease gene

CLN3, is required for vacuole protein sorting of Cpy1p and Golgi exit of Vps10p. *J. Cell Sci.* **122**, 1163–1173

78. Kama, R., Kanneganti, V., Ungermann, C., and Gerst, J. E. (2011) The yeast Batten disease orthologue Btn1 controls endosome-Golgi retrograde transport via SNARE assembly. *J. Cell Biol.* **195**, 203–215

79. Vitiello, S. P., Benedict, J. W., Padilla-Lopez, S., and Pearce, D. A. (2010) Interaction between Sdo1p and Btn1p in the Saccharomyces cerevisiae model for Batten disease. *Hum. Mol. Genet.* **19**, 931–942

80. Stieber, A., Mourelatos, Z., and Gonatas, N. K. (1996) In Alzheimer's disease the Golgi apparatus of a population of neurons without neurofibrillary tangles is fragmented and atrophic. *Am. J. Pathol.* **148**, 415–426

81. Lane, J. D., Lucocq, J., Pryde, J., Barr, F. A., Woodman, P. G., Allan, V. J., and Lowe, M. (2002) Caspase-mediated cleavage of the stacking protein GRASP65 is required for Golgi fragmentation during apoptosis. *J. Cell Biol.* **156**, 495–509

82. Sakurai, A., Okamoto, K., Fujita, Y., Nakazato, Y., Wakabayashi, K., Takahashi, H., and Gonatas, N. K. (2000) Fragmentation of the Golgi apparatus of the ballooned neurons in patients with corticobasal degeneration and Creutzfeldt-Jakob disease. *Acta Neuropathol.* **100**, 270–274

83. Johnson, A. O., Lampson, M. A., and McGraw, T. E. (2001) A di-leucine sequence and a cluster of acidic amino acids are required for dynamic retention in the endosomal recycling compartment of fibroblasts. *Mol. Biol. Cell* **12**, 367–381

84. Golabek, A. A., Kida, E., Walus, M., Kaczmarski, W., Wujek, P., and Wisniewski, K. E. (2001) CLN3 disease process: missense point mutations and protein depletion in vitro. *Eur. J. Paediatr. Neurol.* **5**, 81–88

85. Holopainen, J. M., Saarikoski, J., Kinnunen, P. K. J., and Järvelä, I. (2001) Elevated lysosomal pH in neuronal ceroid lipofuscinoses (NCLs). *Eur. J. Biochem.* **268**, 5851–5856

86. Braulke, T., Geuze, H. J., Slot, J. W., Hasilik, A., and von Figura, K. (1987) On the effects of weak bases and monensin on sorting and processing of lysosomal enzymes in human cells. *Eur. J. Cell Biol.* **43**, 316–321

87. Golabek, A. A., Kida, E., Walus, M., Kaczmarski, W., Michalewski, M. P., and Wisniewski, K. E. (2000) CLN3 Protein Regulates Lysosomal pH and Alters Intracellular Processing of Alzheimer's Amyloid-β Protein Precursor and Cathepsin D in Human Cells. *Mol. Genet. Metab.* **70**, 203–213

88. Metcalf, D. J., Calvi, A. A., Seaman, M. N. J., Mitchison, H. M., and Cutler, D. F. (2008) Loss of the Batten Disease Gene CLN3 Prevents Exit from the TGN of the Mannose 6-Phosphate Receptor. *Traffic* **9**, 1905–1914

89. Sleat, D. E., Sohar, I., Pullarkat, P. S., Lobel, P., and Pullarkat, R. K. (1998) Specific alterations in levels of mannose 6-phosphorylated glycoproteins in different neuronal ceroid lipofuscinoses. *Biochem. J.* **334**, 547–551

90. Korade, Z., and Kenworthy, A. K. (2008) Lipid rafts, cholesterol, and the brain. *Neuropharmacology* **55**, 1265–1273

91. Pike, L. J. (2008) The challenge of lipid rafts. *J. Lipid Res.* **50**, S323–S328

92. Tsui-Pierchala, B. A., Encinas, M., Milbrandt, J., and Johnson, E. M. J. (2002) Lipid rafts in neuronal signaling and function. *Trends Neurosci.* **25**, 412–417

93. Luiro, K., Yliannala, K., Ahtiainen, L., Maunu, H., Järvelä, I., Kyttälä, A., and Jalanko, A. (2004) Interconnections of CLN3, Hook1 and Rab proteins link Batten disease to defects in the endocytic pathway. *Hum. Mol. Genet.* **13**, 3017–3027

94. Vesa, J., Chin, M. H., Oelgeschläger, K., Isosomppi, J., DellAngelica, E. C., Jalanko, A., and Peltonen, L. (2002) Neuronal Ceroid Lipofuscinoses Are Connected at Molecular Level: Interaction of CLN5 Protein with CLN2 and CLN3. *Mol. Biol. Cell* **13**, 2410–2420

95. Baldwin, S. A., Beal, P. R., Yao, S. Y. M., King, A. E., Cass, C. E., and Young, J. D. (2004) The equilibrative nucleoside transporter family, SLC29. *Pflügers Arch. - Eur. J. Physiol.* **447**, 735–743

96. Getty, A. L., and Pearce, D. A. (2011) Interactions of the proteins of neuronal ceroid lipofuscinosis: clues to function. *Cell. Mol. Life Sci.* **68**, 453–474

97. Uusi-Rauva, K., Luiro, K., Tanhuanpää, K., Kopra, O., Martín-Vasallo, P., Kyttälä, A., and Jalanko, A. (2008) Novel interactions of CLN3 protein link Batten disease to dysregulation of fodrin–Na+, K+ ATPase complex. *Exp. Cell Res.* **314**, 2895–2905

98. Weimer, J. M., Chattopadhyay, S., Custer, A. W., and Pearce, D. A. (2005) Elevation of Hook1 in a disease model of Batten disease does not affect a novel interaction between Ankyrin G and Hook1. *Biochem. Biophys. Res. Commun.* **330**, 1176–1181

99. Cao, Y., Espinola, J. A., Fossale, E., Massey, A. C., Cuervo, A. M., MacDonald, M. E., and Cotman, S. L. (2006) Autophagy Is Disrupted in a Knock-in Mouse Model of Juvenile Neuronal Ceroid Lipofuscinosis. *J. Biol. Chem.* **281**, 20483–20493

100. Chang, J.-W., Choi, H., Cotman, S. L., and Jung, Y.-K. (2011) Lithium rescues the impaired autophagy process in CbCln3Δex7/8/Δex7/8 cerebellar cells and reduces neuronal vulnerability to cell death via IMPase inhibition. *J. Neurochem.* **116**, 659–668

101. Fatemi, S. H., Reutiman, T. J., and Folsom, T. D. (2009) The role of lithium in modulation of brain genes: relevance for aetiology and treatment of bipolar disorder. *Biochem. Soc. Trans.* **37**, 1090–1095

102. Nair, U., Jotwani, A., Geng, J., Gammoh, N., Richerson, D., Yen, W. L., Griffith, J., Nag, S., Wang, K., Moss, T., Baba, M., McNew, J. A., Jiang, X., Reggiori, F., Melia, T. J., and Klionsky, D. J. (2011) SNARE Proteins Are Required for Macroautophagy. *Cell* **146**, 290–302

103. Haberman, A., Williamson, W. R., Epstein, D., Wang, D., Rina, S., Meinertzhagen, I. A., and Hiesinger, P. R. (2012) The synaptic vesicle SNARE neuronal Synaptobrevin promotes endolysosomal degradation and prevents neurodegeneration. *J. Cell Biol.* **196**, 261–276

104. Dawson, G., Kilkus, J., Siakotos, A. N., and Singh, I. (1996) Mitochondrial abnormalities in CLN2 and CLN3 forms of batten disease. *Mol. Chem. Neuropathol.* **29**, 227–235

105. Narayan, S. B., Rakheja, D., Tan, L., Pastor, J. V., and Bennett, M. J. (2006) CLN3P, the Batten's disease protein, is a novel palmitoyl-protein Δ-9 desaturase. *Ann. Neurol.* **60**, 570–577

106. Narayan, S. B., Tan, L., and Bennett, M. J. (2008) Intermediate levels of neuronal palmitoyl-protein Δ-9 desaturase in heterozygotes for murine Batten disease. *Mol. Genet. Metab.* **93**, 89–91

107. Chang, J.-W., Choi, H., Kim, H.-J., Jo, D.-G., Jeon, Y.-J., Noh, J.-Y., Park, W. J., and Jung, Y.-K. (2007) Neuronal vulnerability of CLN3 deletion to calcium-induced cytotoxicity is mediated by calsenilin. *Hum. Mol. Genet.* **16**, 317–326

108. Takimoto, K., Yang, E.-K., and Conforti, L. (2002) Palmitoylation of KChIP Splicing Variants Is Required for Efficient Cell Surface Expression of Kv4.3 Channels. *J. Biol. Chem.* **277**,

26904–26911

109. Buxbaum, J. D., Choi, E.-K., Luo, Y., Lilliehook, C., Crowley, A. C., Merriam, D. E., and Wasco, W. (1998) Calsenilin: A calcium-binding protein that interacts with the presenilins and regulates the levels of a presenilin fragment. *Nat. Med.* **4**, 1177–1181

110. Jo, D.-G., Kim, M.-J., Choi, Y.-H., Kim, I.-K., Song, Y.-H., Woo, H.-N., Chung, C.-W., and Jung, Y.-K. (2001) Pro-apoptotic function of calsenilin/DREAM/KChIP3. *FASEB J.* **15**, 589–591

111. Hobert, J. A., and Dawson, G. (2007) A novel role of the Batten disease gene CLN3: Association with BMP synthesis. *Biochem. Biophys. Res. Commun.* **358**, 111–116

112. Pullarkat, R. K., Kim, K. S., Sklower, S. L., and Patel, V. K. (1988) Oligosaccharyl diphosphodolichols in the ceroid-lipofuscinoses. *Am. J. Med. Genet.* **31**, 243–251

113. Hall, N. A., Thomas-Oates, J. E., Dell, A., Haltia, M., Lake, B. D., and Patrick, A. D. (1992) Stored dolichyl pyrophosphoryl oligosaccharides in Batten disease. *Am. J. Med. Genet.* **42**, 580–585

114. Padilla-Lopez, S., Langager, D., Chan, C.-H., and Pearce, D. A. (2012) BTN1, the Saccharomyces cerevisiae homolog to the human Batten disease gene, is involved in phospholipid distribution. *Dis. Model. Mech.* **5**, 191–199

115. Finn, R. D., Mistry, J., Schuster-Böckler, B., Griffiths-Jones, S., Hollich, V., Lassmann, T., Moxon, S., Marshall, M., Khanna, A., Durbin, R., Eddy, S. R., Sonnhammer, E. L. L., and Bateman, A. (2006) Pfam: clans, web tools and services. *Nucleic Acids Res.* **34**, D247–D251

116. Åberg, L. E., Autti, T., Braulke, T., Cooper, J. D., van Diggelen, O. P., Jalanko, A., Kenrick, S., Kitzmüller, C., Kohlschütter, A., Kyttälä, A., Mitchison, H. M., Mole, S. E., Niezen-de Boer, R., Punkari, M.-L., Schulz, A., Talling, M., and Williams, R. E. (2011) CLN3 in *The Neuronal Ceroid Lipofuscinoses* (Mole, S. E., ed.) pp. 110–139, Oxford University Press, New York

117. Simons, K., and Ikonen, E. (1997) Functional rafts in cell membranes. *Nature* **387**, 569–572

118. Sonnino, S., Mauri, L., Chigorno, V., and Prinetti, A. (2006) Gangliosides as components of lipid membrane domains. *Glycobiology* **17**, 1R–13R

119. van Meer, G., and Holthuis, J. C. M. (2000) Sphingolipid transport in eukaryotic cells. *Biochim. Biophys. Acta* **1486**, 145–170

120. Tettamanti, G. (2004) Ganglioside/glycosphingolipid turnover: New concepts. *Glycoconj. J.* **20**, 301–317

121. Basu, S., Schultz, A. M., Basu, M., and Roseman, S. (1971) Enzymatic synthesis of galactocerebroside by a galactosyltransferase from embryonic chicken brain. *J. Biol. Chem.* **246**, 4272–4279

122. Morell, P., and Radin, N. S. (1969) Synthesis of cerebroside by brain from uridine diphosphate galactose and ceramide containing hydroxy fatty acid. *Biochemistry* **8**, 506–512

123. Huwiler, A., Kolter, T., Pfeilschifter, J., and Sandhoff, K. (2000) Physiology and pathophysiology of sphingolipid metabolism and signaling. *Biochim. Biophys. Acta - Mol. Cell Biol. Lipids* **1485**, 63–99

124. Kuhn, R., and Wiegandt, H. (1964) Weitere Ganglioside aus Menschenhirn. *Zeitschrift für Naturforsch. B* **19**, 256–257

125. Ledeen, R. W., Yu, R. K., and Eng, L. F. (1973) Gangliosides of Human Myelin: Sialosylgalacosylceramide (G7) as a Major Component. *J. Neurochem.* **21**, 829–839

126. Hanada, K., Kumagai, K., Yasuda, S., Miura, Y., Kawano, M., Fukasawa, M., and Nishijima, M. (2003) Molecular machinery for non-vesicular trafficking of ceramide. *Nature* **426**, 803–809

127. Basu, S., Kaufman, B., and Roseman, S. (1973) Enzymatic synthesis of glucocerebroside by a glucosyltransferase from embryonic chicken brain. *J. Biol. Chem.* **248**, 1388–1394

128. Ichikawa, S., Sakiyama, H., Suzuki, G., Hidari, K. I.-P. J., and Hirabayashi, Y. (1996) Expression cloning of a cDNA for human ceramide glucosyltransferase that catalyzes the first glycosylation step of glycosphingolipid synthesis. *Proc. Natl. Acad. Sci.* **93**, 4638–4643

129. Paul, P., Kamisaka, Y., Marks, D. L., and Pagano, R. E. (1996) Purification and characterization of UDP-glucose:ceramide glucosyltransferase from rat liver Golgi membranes. *J. Biol. Chem.* **271**, 2287–2293

130. Eckford, P. D. W., and Sharom, F. J. (2005) The reconstituted P-glycoprotein multidrug transporter is a flippase for glucosylceramide and other simple glycosphingolipids. *Biochem. J.* **389**, 517–526

131. Keenan, T. W., Morré, D. J., and Basu, S. (1974) Ganglioside biosynthesis. Concentration of glycosphingolipid glycosyltransferases in Golgi apparatus from rat liver. *J. Biol. Chem.* **249**, 310–315

132. Roseman, S. (1970) The synthesis of complex carbohydrates by multiglycosyltransferase systems and their potential function in intercellular adhesion. *Chem. Phys. Lipids* **5**, 270–297

133. Basu, S., Basu, M., Chien, J.-L., and Presper, K. A. (1980) *Structure and Function of Gangliosides* (Svennerholm, L., Mandel, P., Dreyfus, H., and Urban, P.-F., eds.), Springer US, Boston, MA

134. Basu, S., Basu, M., Das, K. K., Daussin, F., Schaeper, R. J., Banerjee, P., Khan, F. A., and Suzuki, I. (1988) Solubilized glycosyltransferases and biosynthesis in vitro of glycolipids. *Biochimie* **70**, 1551–1563

135. Wilkening, G., Linke, T., Uhlhorn-Dierks, G., and Sandhoff, K. (2000) Degradation of Membrane-bound Ganglioside GM1: Stimulation by Bis(monoacylglycero)phosphate and the Activator Proteins Sap-B and GM2-AP. *J. Biol. Chem.* **275**, 35814–35819

136. Meier, E. M., Schwarzmann, G., Fürst, W., and Sandhoff, K. (1991) The human GM2 activator protein. A substrate specific cofactor of beta-hexosaminidase A. *J. Biol. Chem.* **266**, 1879–1887

137. Kolodny, E. H., Kanfer, J., Quirk, J. M., and Brady, R. O. (1971) Properties of a particle-bound enzyme from rat intestine that cleaves sialic acid from Tay-Sachs ganglioside. *J. Biol. Chem.* **246**, 1426–1431

138. Riboni, L., Caminiti, A., Bassi, R., and Tettamanti, G. (1995) The Degradative Pathway of Gangliosides GM1 and GM2 in Neuro2a Cells by Sialidase. *J. Neurochem.* **64**, 451–454

139. Sango, K., Yamanaka, S., Hoffmann, A., Okuda, Y., Grinberg, A., Westphal, H., McDonald, M. P., Crawley, J. N., Sandhoff, K., Suzuki, K., and Proia, R. L. (1995) Mouse models of Tay–Sachs and Sandhoff diseases differ in neurologic phenotype and ganglioside metabolism. *Nat. Genet.* **11**, 170–176

140. Miyagi, T., and Tsuiki, S. (1986) Evidence for sialidase hydrolyzing gangliosides GM2 and GM1 in rat liver plasma membrane. *FEBS Lett.* **206**, 223–228

141. Ito, M., and Yamagata, T. (1989) Purification and characterization of glycosphingolipid-

specific endoglycosidases (endoglycoceramidases) from a mutant strain of Rhodococcus sp. Evidence for three molecular species of endoglycoceramidase with different specificities. *J. Biol. Chem.* **264**, 9510–9519

142. Sofer, A., Schwarzmann, G., and Futerman, A. H. (1996) The internalization of a short acyl chain analogue of ganglioside GM1 in polarized neurons. *J. Cell Sci.* **109**, 2111–2119

143. Yohe, H. C., Jacobson, R. I., and Yu, R. K. (1983) Ganglioside-basic protein interaction: Protection of gangliosides against neuraminidase action. *J. Neurosci. Res.* **9**, 401–412

144. Riboni, L., and Tettamanti, G. (1991) Rapid Internalization and Intracellular Metabolic Processing of Exogenous Ganglioside by Cerebellar Granule Cells Differentiated in Culture. *J. Neurochem.* **57**, 1931–1939

145. Kopitz, J., Sinz, K., Brossmer, R., and Cantz, M. (1997) Partial characterization and enrichment of a membrane-bound sialidase specific for gangliosides from human brain tissue. *Eur. J. Biochem.* **248**, 527–534

146. Rodriguez, J. A., Piddini, E., Hasegawa, T., Miyagi, T., and Dotti, C. G. (2001) Plasma membrane ganglioside sialidase regulates axonal growth and regeneration in hippocampal neurons in culture. *J. Neurosci.* **21**, 8387–8395

147. Holthuis, J. C. M., Pomorski, T., Raggers, R. J., Sprong, H., and Van Meer, G. (2001) The organizing potential of sphingolipids in intracellular membrane transport. *Physiol. Rev.* **81**, 1689–1723

148. Hakomori, S. (2002) The glycosynapse. *Proc. Natl. Acad. Sci.* **99**, 225–232

149. Hanada, K., Nishijima, M., Kiso, M., Hasegawa, A., Fujita, S., Ogawa, T., and Akamatsu, Y. (1992) Sphingolipids are essential for the growth of Chinese hamster ovary cells. Restoration of the growth of a mutant defective in sphingoid base biosynthesis by exogenous sphingolipids. *J. Biol. Chem.* **267**, 23527–23533

150. Ichikawa, S., Nakajo, N., Sakiyama, H., and Hirabayashi, Y. (1994) A mouse B16 melanoma mutant deficient in glycolipids. *Proc. Natl. Acad. Sci.* **91**, 2703–2707

151. Yamashita, T., Wada, R., Sasaki, T., Deng, C., Bierfreund, U., Sandhoff, K., and Proia, R. L. (1999) A vital role for glycosphingolipid synthesis during development and differentiation. *Proc. Natl. Acad. Sci.* **96**, 9142–9147

152. Cheng, J., Ohsaki, Y., Tauchi-Sato, K., Fujita, A., and Fujimoto, T. (2006) Cholesterol depletion induces autophagy. *Biochem. Biophys. Res. Commun.* **351**, 246–252

153. Sharma, D. K., Brown, J. C., Choudhury, A., Peterson, T. E., Holicky, E., Marks, D. L., Simari, R., Parton, R. G., and Pagano, R. E. (2004) Selective Stimulation of Caveolar Endocytosis by Glycosphingolipids and Cholesterol. *Mol. Biol. Cell* **15**, 3114–3122

154. Wei, J., Fujita, M., Nakai, M., Waragai, M., Sekigawa, A., Sugama, S., Takenouchi, T., Masliah, E., and Hashimoto, M. (2009) Protective Role of Endogenous Gangliosides for Lysosomal Pathology in a Cellular Model of Synucleinopathies. *Am. J. Pathol.* **174**, 1891–1909

155. Shen, W., Henry, A. G., Paumier, K. L., Li, L., Mou, K., Dunlop, J., Berger, Z., and Hirst, W. D. (2014) Inhibition of glucosylceramide synthase stimulates autophagy flux in neurons. *J. Neurochem.* **129**, 884–894

156. Sakakibara, K., Momoi, T., Uchida, T., and Nagai, Y. (1981) Evidence for association of glycosphingolipid with a colchicine-sensitive microtubule-like cytoskeletal structure of cultured cells. *Nature* **293**, 76–78

157. Gillard, B. K., Heath, J. P., Thurmon, L. T., and Marcus, D. M. (1991) Association of

glycosphingolipids with intermediate filaments of human umbilical vein endothelial cells. *Exp. Cell Res.* **192**, 433–444

158. Gillard, B. K., Thurmon, L. T., and Marcus, D. M. (1992) Association of glycosphingolipids with intermediate filaments of mesenchymal, epithelial, glial, and muscle cells. *Cell Motil. Cytoskeleton* **21**, 255–271

159. Gillard, B. K., Thurmon, L. T., and Marcus, D. M. (1993) Variable subcellular localization of glycosphingolipids. *Glycobiology* **3**, 57–67

160. Kalvodova, L., Kahya, N., Schwille, P., Ehehalt, R., Verkade, P., Drechsel, D., and Simons, K. (2005) Lipids as Modulators of Proteolytic Activity of BACE: Involvement of Cholesterol, Glycosphingolipids, and Anionic Phospholipids in vitro. *J. Biol. Chem.* **280**, 36815–36823

161. David, D., Sundararabu, S., and Gerst, J. E. (1998) Involvement of Long Chain Fatty Acid Elongation in the Trafficking of Secretory Vesicles in Yeast. *J. Cell Biol.* **143**, 1167–1182

162. Brown, D. A., and Rose, J. K. (1992) Sorting of GPI-anchored proteins to glycolipid-enriched membrane subdomains during transport to the apical cell surface. *Cell* **68**, 533–544

163. Brügger, B., Sandhoff, R., Wegehingel, S., Gorgas, K., Malsam, J., Helms, J. B., Lehmann, W. D., Nickel, W., and Wieland, F. T. (2000) Evidence for Segregation of Sphingomyelin and Cholesterol during Formation of COPI-coated Vesicles. *J. Cell Biol.* **151**, 507–518

164. Mukherjee, S., Soe, T. T., and Maxfield, F. R. (1999) Endocytic sorting of lipid analogues differing solely in the chemistry of their hydrophobic tails. *J. Cell Biol.* **144**, 1271–1284

165. Dotti, C. G., Parton, R. G., and Simons, K. (1991) Polarized sorting of glypiated proteins in hippocampal neurons. *Nature* **349**, 158–161

166. Ledesma, M. D., Simons, K., and Dotti, C. G. (1998) Neuronal polarity: Essential role of protein-lipid complexes in axonal sorting. *Proc. Natl. Acad. Sci.* **95**, 3966–3971

167. Ledesma, M. D., Brügger, B., Bünning, C., Wieland, F. T., and Dotti, C. G. (1999) Maturation of the axonal plasma membrane requires upregulation of sphingomyelin synthesis and formation of protein-lipid complexes. *EMBO J.* **18**, 1761–1771

168. Fiedler, K., and Simons, K. (1995) The role of n-glycans in the secretory pathway. *Cell* **81**, 309–312

169. Mellman, I. S. (1996) Endocytosis and Molecular Sorting. *Annu. Rev. Cell Dev. Biol.* **12**, 575–625

170. Ferrari, G., Fabris, M., and Gorio, A. (1983) Gangliosides enhance neurite outgrowth in PC12 cells. *Brain Res.* **284**, 215–221

171. Schnaar, R. L., Gerardy-Schahn, R., and Hildebrandt, H. (2014) Sialic Acids in the Brain: Gangliosides and Polysialic Acid in Nervous System Development, Stability, Disease, and Regeneration. *Physiol. Rev.* **94**, 461–518

172. Marengo, F. D., Wang, S.-Y., Wang, B., and Langer, G. A. (1998) Dependence of Cardiac Cell Ca2+Permeability on Sialic Acid-containing Sarcolemmal Gangliosides. *J. Mol. Cell. Cardiol.* **30**, 127–137

173. Schauer, R. (2009) Sialic acids as regulators of molecular and cellular interactions. *Curr. Opin. Struct. Biol.* **19**, 507–514

174. Tettamanti, G., Bonali, F., Marchesini, S., and Zambotti, V. (1973) A new procedure for the extraction, purification and fractionation of brain gangliosides. *Biochim. Biophys. Acta - Lipids Lipid Metab.* **296**, 160–170

175. Sonnino, S., and Chigorno, V. (2000) Ganglioside molecular species containing C18- and C20-sphingosine in mammalian nervous tissues and neuronal cell cultures. *Biochim. Biophys. Acta - Rev. Biomembr.* **1469**, 63–77

176. Sturgill, E. R., Aoki, K., Lopez, P. H. H., Colacurcio, D., Vajn, K., Lorenzini, I., Majić, S., Yang, W. H., Heffer, M., Tiemeyer, M., Marth, J. D., and Schnaar, R. L. (2012) Biosynthesis of the major brain gangliosides GD1a and GT1b. *Glycobiology* **22**, 1289–1301

177. Susuki, K., Baba, H., Tohyama, K., Kanai, K., Kuwabara, S., Hirata, K., Furukawa, K., Furukawa, K., Rasband, M. N., and Yuki, N. (2007) Gangliosides contribute to stability of paranodal junctions and ion channel clusters in myelinated nerve fibers. *Glia* **55**, 746–757

178. Kittaka, D., Itoh, M. I., Ohmi, Y., Kondo, Y., Fukumoto, S., Urano, T., Tajima, O., Furukawa, K., and Furukawa, K. (2008) Impaired hypoglossal nerve regeneration in mutant mice lacking complex gangliosides: Down-regulation of neurotrophic factors and receptors as possible mechanisms. *Glycobiology* **18**, 509–516

179. Inoue, M., Fujii, Y., Furukawa, K., Okada, M., Okumura, K., Hayakawa, T., Furukawa, K., and Sugiura, Y. (2002) Refractory skin injury in complex knock-out mice expressing only the GM3 ganglioside. *J. Biol. Chem.* **277**, 29881–29888

180. Tajima, O., Egashira, N., Ohmi, Y., Fukue, Y., Mishima, K., Iwasaki, K., Fujiwara, M., Inokuchi, J., Sugiura, Y., Furukawa, K., and Furukawa, K. (2009) Reduced motor and sensory functions and emotional response in GM3-only mice: Emergence from early stage of life and exacerbation with aging. *Behav. Brain Res.* **198**, 74–82

181. Simpson, M. A., Cross, H., Proukakis, C., Priestman, D. A., Neville, D. C. A., Reinkensmeier, G., Wang, H., Wiznitzer, M., Gurtz, K., Verganelaki, A., Pryde, A., Patton, M. A., Dwek, R. A., Butters, T. D., Platt, F. M., and Crosby, A. H. (2004) Infantile-onset symptomatic epilepsy syndrome caused by a homozygous loss-of-function mutation of GM3 synthase. *Nat. Genet.* **36**, 1225–1229

182. van Heyningen, S. (1974) Cholera Toxin: Interaction of Subunits with Ganglioside GM1. *Science (80-.).* **183**, 656–657

183. Fantini, J., and Barrantes, F. J. (2009) Sphingolipid/cholesterol regulation of neurotransmitter receptor conformation and function. *Biochim. Biophys. Acta - Biomembr.* **1788**, 2345–2361

184. Ariga, T., McDonald, M. P., and Yu, R. K. (2008) Role of ganglioside metabolism in the pathogenesis of Alzheimer's disease - a review. *J. Lipid Res.* **49**, 1157–1175

185. Ledeen, R. W., and Wu, G. (2006) Sphingolipids of the nucleus and their role in nuclear signaling. *Biochim. Biophys. Acta - Mol. Cell Biol. Lipids* **1761**, 588–598

186. Svennerholm, L., Boström, K., Fredman, P., Månsson, J.-E., Rosengren, B., and Rynmark, B.-M. (1989) Human brain gangliosides: developmental changes from early fetal stage to advanced age. *Biochim. Biophys. Acta - Lipids Lipid Metab.* **1005**, 109–117

187. Prioni, S., Mauri, L., Loberto, N., Casellato, R., Chigorno, V., Karagogeos, D., Prinetti, A., and Sonnino, S. (2004) Interactions between gangliosides and proteins in the exoplasmic leaflet of neuronal plasma membranes: A study performed with a tritium-labeled GM1 derivative containing a photoactivable group linked to the oligosaccharide chain. *Glycoconj. J.* **21**, 461–470

188. Traka, M., Goutebroze, L., Denisenko, N., Bessa, M., Nifli, A., Havaki, S., Iwakura, Y., Fukamauchi, F., Watanabe, K., Soliven, B., Girault, J. A., and Karagogeos, D. (2003) Association of TAG-1 with Caspr2 is essential for the molecular organization of

juxtaparanodal regions of myelinated fibers. *J. Cell Biol.* **162**, 1161–1172

189. Ichikawa, N., Iwabuchi, K., Kurihara, H., Ishii, K., Kobayashi, T., Sasaki, T., Hattori, N., Mizuno, Y., Hozumi, K., Yamada, Y., and Arikawa-Hirasawa, E. (2009) Binding of laminin-1 to monosialoganglioside GM1 in lipid rafts is crucial for neurite outgrowth. *J. Cell Sci.* **122**, 289–299

190. Ledeen, R. W., Wu, G., Lu, Z.-H., Kozireski-Chuback, D., and Fang, Y. (1998) The role of GM1 and other gangliosides in neuronal differentiation. Overview and new finding. *Ann. N. Y. Acad. Sci.* **845**, 161–175

191. Mocchetti, I. (2005) Exogenous gangliosides, neuronal plasticity and repair, and the neurotrophins. *Cell. Mol. Life Sci.* **62**, 2283–2294

192. Schnaar, R. L. (2010) Brain gangliosides in axon-myelin stability and axon regeneration. *FEBS Lett.* **584**, 1741–1747

193. Cao, Y., Staropoli, J. F., Biswas-Legrand, S., Espinola, J. A., MacDonald, M. E., Lee, J.-M., and Cotman, S. L. (2011) Distinct Early Molecular Responses to Mutations Causing vLINCL and JNCL Presage ATP Synthase Subunit C Accumulation in Cerebellar Cells. *PLoS One* **6**, e17118

194. Dunn, K. W., Kamocka, M. M., and McDonald, J. H. (2011) A practical guide to evaluating colocalization in biological microscopy. *AJP Cell Physiol.* **300**, C723–C742

195. Tettamanti, G., Bassi, R., Viani, P., and Riboni, L. (2003) Salvage pathways in glycosphingolipid metabolism. *Biochimie* **85**, 423–437

196. Mahfoud, R., Manis, A., Binnington, B., Ackerley, C., and Lingwood, C. A. (2010) A Major Fraction of Glycosphingolipids in Model and Cellular Cholesterol-containing Membranes Is Undetectable by Their Binding Proteins. *J. Biol. Chem.* **285**, 36049–36059

197. Fra, A. M., Masserini, M., Palestini, P., Sonnino, S., and Simons, K. (1995) A photo-reactive derivative of ganglioside GM1 specifically cross-links VIP21-caveolin on the cell surface. *FEBS Lett.* **375**, 11–14

198. D'Azzo, A., Hoogeveen, A. T., Reuser, A. J. J., Robinson, D. G., and Galjaard, H. (1982) Molecular defect in combined beta-galactosidase and neuraminidase deficiency in man. *Proc. Natl. Acad. Sci. U. S. A.* **79**, 4535–4539

199. Vinogradova, M. V., Michaud, L., Mezentsev, A. V., Lukong, K. E., El-Alfy, M., Morales, C. R., Potier, M., and Pshezhetsky, A. V. (1998) Molecular mechanism of lysosomal sialidase deficiency in galactosialidosis involves its rapid degradation. *Biochem. J.* **330**, 641–650

200. Emiliani, C., Urbanelli, L., Racanicchi, L., Orlacchio, A., Pelicci, G., Sorbi, S., Bernardi, G., and Orlacchio, A. (2003) Up-regulation of glycohydrolases in Alzheimer's Disease fibroblasts correlates with Ras activation. *J. Biol. Chem.* **278**, 38453–38460

201. Prior, I. A., Harding, A., Yan, J., Sluimer, J., Parton, R. G., and Hancock, J. F. (2001) GTP-dependent segregation of H-ras from lipid rafts is required for biological activity. *Nat. Cell Biol.* **3**, 368–375

202. Cuatrecasas, P. (1973) Gangliosides and membrane receptors for cholera toxin. *Biochemistry* **12**, 3558–3566

203. Staerk, J., Joerg, R. H., Wiegandt, H., and Ziegler, W. (1974) Interaction of Ganglioside GGtet1 and Its Derivatives with Choleragen. *Eur. J. Biochem.* **48**, 103–110

204. Fishman, P. H., Moss, J., and Osborne, J. C. J. (1978) Interaction of choleragen with the oligosaccharide of ganglioside G(M1): Evidence for multiple oligosaccharide binding sites. *Biochemistry* **17**, 711–716

205. Holmgren, J., Lönnroth, I., and Svennerholm, L. (1973) Tissue receptor for cholera exotoxin: postulated structure from studies with GM1 ganglioside and related glycolipids. *Infect. Immun.* **8**, 208–214

206. Kuziemko, G. M., Stroh, M., and Stevens, R. C. (1996) Cholera toxin binding affinity and specificity for gangliosides determined by surface plasmon resonance. *Biochemistry* **35**, 6375–6384

207. Hu, S., Yang, H., Cai, R., Liu, Z., and Yang, X. (2009) Biotin induced fluorescence enhancement in resonance energy transfer and application for bioassay. *Talanta* **80**, 454–458

208. Rusyn, E., Mousallem, T., Persaud-Sawin, D.-A., Miller, S., and Boustany, R.-M. N. (2008) CLN3p impacts galactosylceramide transport, raft morphology, and lipid content. *Pediatr. Res.* **63**, 625–631

209. Kolter, T., and Sandhoff, K. (2006) Sphingolipid metabolism diseases. *Biochim. Biophys. Acta - Biomembr.* **1758**, 2057–2079

210. Van Der Spoel, A. C., Bonten, E. J., and D'Azzo, A. (2000) Processing of lysosomal-galactosidase. The C-terminal precursor fragment is an essential domain of the mature enzyme. *J. Biol. Chem.* **275**, 10035–10040

211. Galjart, N. J., Gillemans, N., Harris, A., van der Horst, G. T. J., Verheijen, F. W., Galjaard, H., and D'Azzo, A. (1988) Expression of cDNA encoding the human "protective protein" associated with lysosomal β-galactosidase and neuraminidase: Homology to yeast proteases. *Cell* **54**, 755–764

212. Van Der Spoel, A. C., Bonten, E. J., and D'Azzo, A. (1998) Transport of human lysosomal neuraminidase to mature lysosomes requires protective protein/cathepsin A. *EMBO J.* **17**, 1588–1597

213. Sohma, O., Mizuguchi, M., Takashima, S., Satake, A., Itoh, K., Sakuraba, H., Suzuki, Y., and Oyanagi, K. (1999) Expression of protective protein in human tissue. *Pediatr. Neurol.* **20**, 210–214

214. Geng, Y.-Q., Guan, J.-T., Xu, X.-H., and Fu, Y.-C. (2010) Senescence-associated beta-galactosidase activity expression in aging hippocampal neurons. *Biochem. Biophys. Res. Commun.* **396**, 866–869

215. Cuervo, A. M., Mann, L., Bonten, E. J., D'Azzo, A., and Dice, J. F. (2003) Cathepsin A regulates chaperone-mediated autophagy through cleavage of the lysosomal receptor. *EMBO J.* **22**, 47–59

216. Chen, C.-S., Bach, G., and Pagano, R. E. (1998) Abnormal transport along the lysosomal pathway in Mucolipidosis, type IV disease. *Proc. Natl. Acad. Sci.* **95**, 6373–6378

217. Bäckman, M. L., Santavuori, P. R., Åberg, L. E., and Aronen, E. T. (2005) Psychiatric symptoms of children and adolescents with juvenile neuronal ceroid lipofuscinosis. *J. Intellect. Disabil. Res.* **49**, 25–32

218. Langiu, M. (2015) Behavior analysis on a mouse model of CLN3 disease, classical juvenile, and potential therapeutic approaches, Dissertation, Goethe University Frankfurt

219. Pitto, M., Giglioni, A., and Tettamanti, G. (1992) Dual subcellular localization of sialidase in cultured granule cells differentiated in culture. *Neurochem. Int.* **21**, 367–374

220. Conzelmann, E., Burg, J., Stephan, G., and Sandhoff, K. (1982) Complexing of Glycolipids and Their Transfer between Membranes by the Activator Protein for Degradation of Lysosomal Ganglioside GM2. *Eur. J. Biochem.* **123**, 455–464

221. Käkelä, R., Somerharju, P., and Tyynelä, J. (2003) Analysis of phospholipid molecular species in brains from patients with infantile and juvenile neuronal-ceroid lipofuscinosis using liquid chromatography-electrospray ionization mass spectrometry. *J. Neurochem.* **84**, 1051–1065

222. Kahma, K., Brotherus, J., Haltia, M., and Renkonen, O. (1976) Low and moderate concentrations of lysobisphosphatidic acid in brain and liver of patients affected by some storage diseases. *Lipids* **11**, 539–544

223. Meikle, P. J., Duplock, S., Blacklock, D., Whitfield, P. D., MacIntosh, G., Hopwood, J. J., and Fuller, M. (2008) Effect of lysosomal storage on bis(monoacylglycero)phosphate. *Biochem. J.* **411**, 71–78

224. Jabs, S., Quitsch, A., Käkelä, R., Koch, B., Tyynelä, J., Brade, H., Glatzel, M., Walkley, S. U., Saftig, P., Vanier, M. T., and Braulke, T. (2008) Accumulation of bis(monoacylglycero)phosphate and gangliosides in mouse models of neuronal ceroid lipofuscinosis. *J. Neurochem.* **106**, 1415–1425

225. Reaves, B. J., Row, P. E., Bright, N. A., Luzio, J. P., and Davidson, H. W. (2000) Loss of cation-independent mannose 6-phosphate receptor expression promotes the accumulation of lysobisphosphatidic acid in multilamellar bodies. *J. Cell Sci.* **113**, 4099–4108

226. Akgoc, Z., Sena-Esteves, M., Martin, D. R., Han, X., D'Azzo, A., and Seyfried, T. N. (2015) Bis(monoacylglycero)phosphate: a secondary storage lipid in the gangliosidoses. *J. Lipid Res.* **56**, 1006–1013

227. Wassall, S. R., Brzustowicz, M. R., Shaikh, S. R., Cherezov, V., Caffrey, M., and Stillwell, W. (2004) Order from disorder, corralling cholesterol with chaotic lipids: The role of polyunsaturated lipids in membrane raft formation. *Chem. Phys. Lipids* **132**, 79–88

228. Ahonen, I. (2014) Investigating Cellular Morphology and the Mevalonate Pathway in a Genetically Accurate Cell Model of Juvenile Batten Disease, Dissertation, Goethe University Frankfurt

229. Puranam, K. L., Qian, W.-H., Nikbakht, K., Venable, M., Obeid, L., Hannun, Y., and Boustany, R.-M. N. (1997) Upregulation of Bcl-2 and elevation of ceramide in Batten disease. *Neuropediatrics* **28**, 37–41

230. Mahfoud, R., Garmy, N., Maresca, M., Yahi, N., Puigserver, A., and Fantini, J. (2002) Identification of a common sphingolipid-binding domain in Alzheimer, prion, and HIV-1 proteins. *J. Biol. Chem.* **277**, 11292–11296

231. Simons, M., Krämer, E. M., Thiele, C., Stoffel, W., and Trotter, J. (2000) Assembly of myelin by association of proteolipid protein with cholesterol- and galactosylceramide-rich membrane domains. *J. Cell Biol.* **151**, 143–153

232. Zheng, W., Kollmeyer, J., Symolon, H., Momin, A., Munter, E., Wang, E., Kelly, S., Allegood, J. C., Liu, Y., Peng, Q., Ramaraju, H., Sullards, M. C., Cabot, M., and Merrill, A. H. J. (2006) Ceramides and other bioactive sphingolipid backbones in health and disease: Lipidomic analysis, metabolism and roles in membrane structure, dynamics, signaling and autophagy. *Biochim. Biophys. Acta - Biomembr.* **1758**, 1864–1884

233. Persaud-Sawin, D.-A., and Boustany, R.-M. N. (2005) Cell death pathways in juvenile Batten disease. *Apoptosis* **10**, 973–985

234. Siskind, L. J., Kolesnick, R. N., and Colombini, M. (2006) Ceramide forms channels in mitochondrial outer membranes at physiologically relevant concentrations. *Mitochondrion* **6**, 118–125

235. Persaud-Sawin, D.-A., VanDongen, A., and Boustany, R.-M. N. (2002) Motifs within the CLN3 protein: modulation of cell growth rates and apoptosis. *Hum. Mol. Genet.* **11**, 2129–2142

236. Rylova, S. N., Amalfitano, A., Persaud-Sawin, D.-A., Guo, W.-X., Chang, J., Jansen, P. J., Proia, A. D., and Boustany, R.-M. N. (2002) The CLN3 gene is a novel molecular target for cancer drug discovery. *Cancer Res.* **62**, 801–808

237. Puranam, K. L., Guo, W.-X., Qian, W.-H., Nikbakht, K., and Boustany, R.-M. N. (1999) CLN3 Defines a Novel Antiapoptotic Pathway Operative in Neurodegeneration and Mediated by Ceramide. *Mol. Genet. Metab.* **66**, 294–308

238. Fishman, P. H., Max, S. R., Tallman, J. F., Brady, R. O., Maclaren, N. K., and Cornblath, M. (1975) Deficient Ganglioside Biosynthesis: a novel human sphingolipidosis. *Science (80-.).* **187**, 68–70

239. Harlalka, G. V., Lehman, A., Chioza, B., Baple, E. L., Maroofian, R., Cross, H., Sreekantan-Nair, A., Priestman, D. A., Al-Turki, S., McEntagart, M. E., Proukakis, C., Royle, L., Kozak, R. P., Bastaki, L., Patton, M. A., Wagner, K., Coblentz, R., Price, J., Mezei, M., Schlade-Bartusiak, K., Platt, F. M., Hurles, M. E., and Crosby, A. H. (2013) Mutations in B4GALNT1 (GM2 synthase) underlie a new disorder of ganglioside biosynthesis. *Brain* **136**, 3618–3624

240. Wu, D., Liu, J., Wu, B., Tu, B., Zhu, W., and Luo, J. (2014) The Batten disease gene CLN3 confers resistance to endoplasmic reticulum stress induced by tunicamycin. *Biochem. Biophys. Res. Commun.* **447**, 115–120

241. Tessitore, A., del Pilar Martin, M., Sano, R., Ma, Y., Mann, L., Ingrassia, A., Laywell, E. D., Steindler, D. A., Hendershot, L. M., and D'Azzo, A. (2004) GM1-Ganglioside-Mediated Activation of the Unfolded Protein Response Causes Neuronal Death in a Neurodegenerative Gangliosidosis. *Mol. Cell* **15**, 753–766

242. Jeyakumar, M., Thomas, R., Elliot-Smith, E., Smith, D. A., Van Der Spoel, A. C., D'Azzo, A., Perry, V. H., Butters, T. D., Dwek, R. A., and Platt, F. M. (2003) Central nervous system inflammation is a hallmark of pathogenesis in mouse models of GM1 and GM2 gangliosidosis. *Brain* **126**, 974–987

243. Palmer, D. N., Barry, L. A., Tyynelä, J., and Cooper, J. D. (2013) NCL disease mechanisms. *Biochim. Biophys. Acta - Mol. Basis Dis.* **1832**, 1882–1893

244. Braak, H., and Braak, E. (1987) Projection neurons of basolateral amygdaloid nuclei develop meganeurites in juvenile and adult human neuronal ceroid lipofuscinosis. *Clin. Neuropathol.* **6**, 116–9

245. Takamura, A., Higaki, K., Kajimaki, K., Otsuka, S., Ninomiya, H., Matsuda, J., Ohno, K., Suzuki, Y., and Nanba, E. (2008) Enhanced autophagy and mitochondrial aberrations in murine GM1-gangliosidosis. *Biochem. Biophys. Res. Commun.* **367**, 616–622

246. Walkley, S. U., Baker, H. J., and Rattazzi, M. C. (1990) Initiation and growth of ectopic neurites and meganeurites during postnatal cortical development in ganglioside storage disease. *Dev. Brain Res.* **51**, 167–178

247. Zhou, X. Y., Morreau, H., Rottier, R. J., Davis, D., Bonten, E. J., Gillemans, N., Wenger, D. A., Grosveld, F. G., Doherty, P., Suzuki, K., Grosveld, G. C., and D'Azzo, A. (1995) Mouse model for the lysosomal disorder galactosialidosis and correction of the phenotype with overexpressing erythroid precursor cells. *Genes Dev.* **9**, 2623–2634

248. Rottier, R. J., Hahn, C. N., Mann, L. W., del Pilar Martin, M., Smeyne, R. J., Suzuki, K., and D'Azzo, A. (1998) Lack of PPCA expression only partially coincides with lysosomal storage in galactosialidosis mice: indirect evidence for spatial requirement of the catalytic rather

than the protective function of PPCA. *Hum. Mol. Genet.* **7**, 1787–1794

249. Manev, H., Favaron, M., Vicini, S., Guidotti, A., and Costa, E. (1990) Glutamate-induced neuronal death in primary cultures of cerebellar granule cells: protection by synthetic derivatives of endogenous sphingolipids. *J. Pharmacol. Exp. Ther.* **252**, 419–427

250. Lin, M.-S., Chen, L.-Y., Wang, S. S. S., Chang, Y., and Chen, W.-Y. (2008) Examining the levels of ganglioside and cholesterol in cell membrane on attenuation the cytotoxicity of beta-amyloid peptide. *Colloids Surfaces B Biointerfaces* **65**, 172–177

251. Schneider, J. S., Sendek, S., Daskalakis, C., and Cambi, F. (2010) GM1 ganglioside in Parkinson's disease: Results of a five year open study. *J. Neurol. Sci.* **292**, 45–51

252. Maglione, V., Marchi, P., Di Pardo, A., Lingrell, S., Horkey, M., Tidmarsh, E., and Sipione, S. (2010) Impaired Ganglioside Metabolism in Huntington's Disease and Neuroprotective Role of GM1. *J. Neurosci.* **30**, 4072–4080

253. Di Pardo, A., Maglione, V., Alpaugh, M., Horkey, M., Atwal, R. S., Sassone, J., Ciammola, A., Steffan, J. S., Fouad, K., Truant, R., and Sipione, S. (2012) Ganglioside GM1 induces phosphorylation of mutant huntingtin and restores normal motor behavior in Huntington disease mice. *Proc. Natl. Acad. Sci.* **109**, 3528–3533

254. Bernardo, A., Harrison, F. E., McCord, M., Zhao, J., Bruchey, A., Davies, S. S., Jackson Roberts, L., Mathews, P. M., Matsuoka, Y., Ariga, T., Yu, R. K., Thompson, R., and McDonald, M. P. (2009) Elimination of GD3 synthase improves memory and reduces amyloid-β plaque load in transgenic mice. *Neurobiol. Aging* **30**, 1777–1791

255. Martinez, Z., Zhu, M., Han, S., and Fink, A. L. (2007) GM1 Specifically Interacts with α-Synuclein and Inhibits Fibrillation. *Biochemistry* **46**, 1868–1877

256. Zappia, M., Crescibene, L., Bosco, D., Arabia, G., Nicoletti, G., Bagala, A., Bastone, L., Napoli, I. D., Caracciolo, M., Bonavita, S., Di Costanzo, A., Gambardella, A., and Quattrone, A. (2002) Anti-GM1 ganglioside antibodies in Parkinson's disease. *Acta Neurol. Scand.* **106**, 54–57

257. Alter, M. (1998) GM1 Ganglioside for Acute Ischemic Stroke: Trial Design Issues. *Ann. N. Y. Acad. Sci.* **845**, 391–401

258. Schengrund, C.-L., and Mummert, C. M. (1998) Exogenous gangliosides. How do they cross the blood-brain barrier and how do they inhibit cell proliferation. *Ann. N. Y. Acad. Sci.* **845**, 278–284

259. Mitchell, M. D., Henare, K., Balakrishnan, B., Lowe, E., Fong, B. Y., and McJarrow, P. (2012) Transfer of gangliosides across the human placenta. *Placenta* **33**, 312–316

260. Riboni, L., Bassi, R., Prinetti, A., and Tettamanti, G. (1996) Salvage of catabolic products in ganglioside metabolism: a study on rat cerebellar granule cells in culture. *FEBS Lett.* **391**, 336–340

261. Valsecchi, M., Chigorno, V., Sonnino, S., and Tettamanti, G. (1992) Rat cerebellar granule cells in culture associate and metabolize differently exogenous GM1 ganglioside molecular species containing a C18 or C20 long chain base. *Chem. Phys. Lipids* **60**, 247–252

262. Riboni, L., Prinetti, A., Pitto, M., and Tettamanti, G. (1990) Patterns of endogenous gangliosides and metabolic processing of exogenous gangliosides in cerebellar granule cells during differentiation in culture. *Neurochem. Res.* **15**, 1175–1183

263. Brown, R. E., and Hyland, K. J. (1992) Spontaneous transfer of ganglioside GM1 from its micelles to lipid vesicles of differing size. *Biochemistry* **31**, 10602–10609

264. Posse de Chaves, E., and Sipione, S. (2010) Sphingolipids and gangliosides of the nervous

system in membrane function and dysfunction. *FEBS Lett.* **584**, 1748–1759

265. Nishio, M., Fukumoto, S., Furukawa, K., Ichimura, A., Miyazaki, H., Kusunoki, S., Urano, T., and Furukawa, K. (2004) Overexpressed GM1 suppresses nerve growth factor (NGF) signals by modulating the intracellular localization of NGF receptors and membrane fluidity in PC12 cells. *J. Biol. Chem.* **279**, 33368–33378

266. Zha, Q., Ruan, Y., Hartmann, T., Beyreuther, K., and Zhang, D. (2004) GM1 ganglioside regulates the proteolysis of amyloid precursor protein. *Mol. Psychiatry* **9**, 946–952

267. Matsuoka, Y., Saito, M., LaFrancois, J., Saito, M., Gaynor, K., Olm, V., Wang, L., Casey, E., Lu, Y., Shiratori, C., Lemere, C., and Duff, K. (2003) Novel therapeutic approach for the treatment of Alzheimer's disease by peripheral administration of agents with an affinity to beta-amyloid. *J. Neurosci.* **23**, 29–33

268. Ragaglia, V., and Sharma, V. M. (2013), Patent US20130190257 A1, http://www.google.com/patents/US20130190257

269. Orlandi, P. A., and Fishman, P. H. (1998) Filipin-dependent inhibition of cholera toxin: Evidence for toxin internalization and activation through caveolae-like domains. *J. Cell Biol.* **141**, 905–915

270. Antes, P., Schwarzmann, G., and Sandhoff, K. (1992) Detection of protein mediated glycosphingolipid clustering by the use of resonance energy transfer between fluorescent labelled lipids. A method established by applying the system ganglioside GM1 and cholera toxin B subunit. *Chem. Phys. Lipids* **62**, 269–280

271. Parton, R. G., Joggerst, B., and Simons, K. (1994) Regulated internalization of caveolae. *J. Cell Biol.* **127**, 1199–1215

272. Puri, V., Watanabe, R., Singh, R. D., Dominguez, M., Brown, J. C., Wheatley, C. L., Marks, D. L., and Pagano, R. E. (2001) Clathrin-dependent and -independent internalization of plasma membrane sphingolipids initiates two Golgi targeting pathways. *J. Cell Biol.* **154**, 535–547

273. Marks, D. L., and Pagano, R. E. (2002) Endocytosis and sorting of glycosphingolipids in sphingolipid storage disease. *Trends Cell Biol.* **12**, 605–613

274. Bosch, M., Marí, M., Herms, A., Fernández, A., Fajardo, A., Kassan, A., Giralt, A., Colell, A., Balgoma, D., Barbero, E., González-Moreno, E., Matias, N., Tebar, F., Balsinde, J., Camps, M., Enrich, C., Gross, S. P., García-Ruiz, C., Pérez-Navarro, E., Fernández-Checa, J. C., and Pol, A. (2011) Caveolin-1 deficiency causes cholesterol-dependent mitochondrial dysfunction and apoptotic susceptibility. *Curr. Biol.* **21**, 681–686

275. Sinha, B., Köster, D., Ruez, R., Gonnord, P., Bastiani, M., Abankwa, D., Stan, R. V., Butler-Browne, G., Vedie, B., Johannes, L., Morone, N., Parton, R. G., Raposo, G., Sens, P., Lamaze, C., and Nassoy, P. (2011) Cells Respond to Mechanical Stress by Rapid Disassembly of Caveolae. *Cell* **144**, 402–413

276. Wernick, N. L. B., Chinnapen, D. J. F., Cho, J. A., and Lencer, W. I. (2010) Cholera Toxin: An Intracellular Journey into the Cytosol by Way of the Endoplasmic Reticulum. *Toxins (Basel).* **2**, 310–325

277. Shogomori, H., and Futerman, A. H. (2001) Cholera toxin is found in detergent-insoluble rafts/domains at the cell surface of hippocampal neurons but is internalized via a raft-independent mechanism. *J. Biol. Chem.* **276**, 9182–9188

278. Torgersen, M. L., Skretting, G., van Deurs, B., and Sandvig, K. (2001) Internalization of cholera toxin by different endocytic mechanisms. *J. Cell Sci.* **114**, 3737–3747

279. Choudhury, A., Dominguez, M., Puri, V., Sharma, D. K., Narita, K., Wheatley, C. L., Marks, D. L., and Pagano, R. E. (2002) Rab proteins mediate Golgi transport of caveola-internalized glycosphingolipids and correct lipid trafficking in Niemann-Pick C cells. *J. Clin. Invest.* **109**, 1541–1550

280. Sugimoto, Y., Ninomiya, H., Ohsaki, Y., Higaki, K., Davies, J. P., Ioannou, Y. A., and Ohno, K. (2001) Accumulation of cholera toxin and GM1 ganglioside in the early endosome of Niemann-Pick C1-deficient cells. *Proc. Natl. Acad. Sci.* **98**, 12391–12396

281. Kok, J. W., Babia, T., and Hoekstra, D. (1991) Sorting of sphingolipids in the endocytic pathway of HT29 cells. *J. Cell Biol.* **114**, 231–239

282. Puri, V., Watanabe, R., Dominguez, M., Sun, X., Wheatley, C. L., Marks, D. L., and Pagano, R. E. (1999) Cholesterol modulates membrane traffic along the endocytic pathway in sphingolipid-storage diseases. *Nat. Cell Biol.* **1**, 386–388

283. Sandvig, K., and van Deurs, B. (2000) Entry of ricin and Shiga toxin into cells: molecular mechanisms and medical perspectives. *EMBO J.* **19**, 5943–5950

284. Steinman, R. M., Mellman, I. S., Muller, W. A., and Cohn, Z. A. (1983) Endocytosis and the recycling of plasma membrane. *J. Cell Biol.* **96**, 1–27

285. Pagano, R. E. (1990) Lipid traffic in eukaryotic cells: mechanisms for intracelluar transport and organelle-specific enrichment of lipids. *Curr. Opin. Cell Biol.* **2**, 652–663

286. Bretscher, M. S., and Munro, S. (1993) Cholesterol and the Golgi apparatus. *Science* **261**, 1280–1281

287. Martina, J. A., Daniotti, J. L., and Maccioni, H. J. F. (1998) Influence of N-glycosylation and N-glycan trimming on the activity and intracellular traffic of GD3 synthase. *J. Biol. Chem.* **273**, 3725–3731

288. De Matteis, M. A., and Luini, A. (2008) Exiting the Golgi complex. *Nat. Rev. Mol. Cell Biol.* **9**, 273–284

289. Yogalingam, G., Bonten, E. J., van de Vlekkert, D., Hu, H., Moshiach, S., Connell, S. A., and D'Azzo, A. (2008) Neuraminidase 1 Is a Negative Regulator of Lysosomal Exocytosis. *Dev. Cell* **15**, 74–86

290. Kima, P. E., Burleigh, B., and Andrews, N. W. (2000) Surface-targeted lysosomal membrane glycoprotein-1 (Lamp-1) enhances lysosome exocytosis and cell invasion by Trypanosoma cruzi. *Cell. Microbiol.* **2**, 477–486

291. Bonten, E. J., Annunziata, I., and D'Azzo, A. (2014) Lysosomal multienzyme complex: Pros and cons of working together. *Cell. Mol. Life Sci.* **71**, 2017–2032

292. Grimmer, S., Iversen, T.-G., van Deurs, B., and Sandvig, K. (2000) Endosome to Golgi transport of ricin is regulated by cholesterol. *Mol. Biol. Cell* **11**, 4205–4216

293. Sezgin, E., Can, F. B., Schneider, F., Clausen, M. P., Galiani, S., Stanly, T. A., Waithe, D., Colaco, A., Honigmann, A., Wuestner, D., Platt, F. M., and Eggeling, C. (2015) A comparative study on fluorescent cholesterol analogs as versatile cellular reporters. *J. Lipid Res.* **58**, 7250–7257

294. Westermarck, T., Åberg, L. E., Santavuori, P. R., Antila, E., Edlund, P., and Atroshi, F. (1997) Evaluation of the possible role of coenzyme Q10 and vitamin E in juvenile neuronal ceroid-lipofuscinosis (JNCL). *Mol. Aspects Med.* **18**, 259–262

295. Uusi-Rauva, K., Kyttälä, A., Van Der Kant, R., Vesa, J., Tanhuanpää, K., Neefjes, J., Olkkonen, V. M., and Jalanko, A. (2012) Neuronal ceroid lipofuscinosis protein CLN3 interacts with

motor proteins and modifies location of late endosomal compartments. *Cell. Mol. Life Sci.* **69**, 2075–2089

296. Hutagalung, A. H., and Novick, P. J. (2011) Role of Rab GTPases in Membrane Traffic and Cell Physiology. *Physiol. Rev.* **91**, 119–149

297. Cogli, L., Progida, C., Bramato, R., and Bucci, C. (2013) Vimentin phosphorylation and assembly are regulated by the small GTPase Rab7a. *Biochim. Biophys. Acta - Mol. Cell Res.* **1833**, 1283–1293

298. Hölttä-Vuori, M., Määttä, J., Ullrich, O., Kuismanen, E., and Ikonen, E. (2000) Mobilization of late-endosomal cholesterol is inhibited by Rab guanine nucleotide dissociation inhibitor. *Curr. Biol.* **10**, 95–98

299. Locatelli-Hoops, S., Remmel, N., Klingenstein, R., Breiden, B., Rossocha, M., Schoeniger, M., Koenigs, C., Saenger, W., and Sandhoff, K. (2006) Saposin A mobilizes lipids from low cholesterol and high bis(monoacylglycerol)phosphate-containing membranes: Patient variant saposin a lacks lipid extraction capacity. *J. Biol. Chem.* **281**, 32451–32460

300. Remmel, N., Locatelli-Hoops, S., Breiden, B., Schwarzmann, G., and Sandhoff, K. (2007) Saposin B mobilizes lipids from cholesterol-poor and bis(monoacylglycero)phosphate-rich membranes at acidic pH. *FEBS J.* **274**, 3405–3420

301. Pane, M. A., Puranam, K. L., and Boustany, R.-M. N. (1999) Expression of cln3 in Human NT2 Neuronal Precursor Cells and Neonatal Rat Brain. *Pediatr. Res.* **46**, 367–367

302. Pontikis, C. C., Cella, C. V., Parihar, N., Lim, M. J., Chakrabarti, S., Mitchison, H. M., Mobley, W. C., Rezaie, P., Pearce, D. a., and Cooper, J. D. (2004) Late onset neurodegeneration in the Cln3−/− mouse model of juvenile neuronal ceroid lipofuscinosis is preceded by low level glial activation. *Brain Res.* **1023**, 231–242

303. Pontikis, C. C., Cotman, S. L., MacDonald, M. E., and Cooper, J. D. (2005) Thalamocortical neuron loss and localized astrocytosis in the Cln3Δex7/8 knock-in mouse model of Batten disease. *Neurobiol. Dis.* **20**, 823–836

304. Galkina, O. V., Putilina, F. E., and Eshchenko, N. D. (2014) Changes in the lipid composition of the brain during early onthogenesis. *Neurochem. J.* **8**, 83–88

305. Sorice, M., Parolini, I., Sansolini, T., Garofalo, T., Dolo, V., Sargiacomo, M., Tai, T., Peschle, C., Torrisi, M. R., and Pavan, A. (1997) Evidence for the existence of ganglioside-enriched plasma membrane domains in human peripheral lymphocytes. *J. Lipid Res.* **38**, 969–980

306. Crawley, A. C., and Walkley, S. U. (2007) Developmental Analysis of CNS Pathology in the Lysosomal Storage Disease α-Mannosidosis. *J. Neuropathol. Exp. Neurol.* **66**, 687–697

307. Fabritius, A.-L., Vesa, J., Minye, H. M., Nakano, I., Kornblum, H. I., and Peltonen, L. (2014) Neuronal ceroid lipofuscinosis genes, CLN2, CLN3 and CLN5 are spatially and temporally co-expressed in a developing mouse brain. *Exp. Mol. Pathol.* **97**, 484–491

308. Irvin, D. K., Zurcher, S. D., Nguyen, T., Weinmaster, G., and Kornblum, H. I. (2001) Expression patterns of Notch1, Notch2, and Notch3 suggest multiple functional roles for the Notch-DSL signaling system during brain development. *J. Comp. Neurol.* **436**, 167–181

309. Seaberg, R. M., and van der Kooy, D. (2002) Adult rodent neurogenic regions: the ventricular subependyma contains neural stem cells, but the dentate gyrus contains restricted progenitors. *J. Neurosci.* **22**, 1784–1793

310. Sidman, R. L., and Rakic, P. (1973) Neuronal migration, with special reference to developing human brain: a review. *Brain Res.* **62**, 1–35

311. Irwin, L. N., and Irwin, C. C. (1982) Developmental changes and regional variation in the ganglioside composition of the rat hippocampus. *Dev. Brain Res.* **4**, 481–485

312. Seyfried, T. N., Yu, R. K., and Miyazawa, N. (1982) Differential Cellular Enrichment of Gangliosides in the Mouse Cerebellum: Analysis Using Neurological Mutants. *J. Neurochem.* **38**, 551–559

313. Niederöst, B., Oertle, T., Fritsche, J., McKinney, R. A., and Bandtlow, C. E. (2002) Nogo-A and myelin-associated glycoprotein mediate neurite growth inhibition by antagonistic regulation of RhoA and Rac1. *J. Neurosci.* **22**, 10368–10376

314. Kovács, A. D., Weimer, J. M., and Pearce, D. A. (2006) Selectively increased sensitivity of cerebellar granule cells to AMPA receptor-mediated excitotoxicity in a mouse model of Batten disease. *Neurobiol. Dis.* **22**, 575–585

315. Nguyen, T., Mehta, N. R., Conant, K., Kim, K.-J., Jones, M., Calabresi, P. A., Melli, G., Hoke, A., Schnaar, R. L., Ming, G.-L., Song, H., Keswani, S. C., and Griffin, J. W. (2009) Axonal Protective Effects of the Myelin-Associated Glycoprotein. *J. Neurosci.* **29**, 630–637

316. Ogawa-Goto, K., Funamoto, N., Ohta, Y., Abe, T., and Nagashima, K. (1992) Myelin gangliosides of human peripheral nervous system: an enrichment of GM1 in the motor nerve myelin isolated from cauda equina. *J. Neurochem.* **59**, 1844–1849

317. Kay, G. W., Verbeek, M. M., Furlong, J. M., Willemsen, M. A. A. P., and Palmer, D. N. (2009) Neuropeptide changes and neuroactive amino acids in CSF from humans and sheep with neuronal ceroid lipofuscinoses (NCLs, Batten disease). *Neurochem. Int.* **55**, 783–788

318. Autti, T., Raininko, R., Santavuori, P. R., Vanhanen, S. L., Poutanen, V. P., and Haltia, M. (1997) MRI of neuronal ceroid lipofuscinosis. II. Postmortem MRI and histopathological study of the brain in 16 cases of neuronal ceroid lipofuscinosis of juvenile or late infantile type. *Neuroradiology* **39**, 371–377

319. Kuronen, M., Hermansson, M., Manninen, O., Zech, I., Talvitie, M., Laitinen, T., Gröhn, O., Somerharju, P., Eckhardt, M., Cooper, J. D., Lehesjoki, A.-E., Lahtinen, U., and Kopra, O. (2012) Galactolipid deficiency in the early pathogenesis of neuronal ceroid lipofuscinosis model Cln8mnd: implications to delayed myelination and oligodendrocyte maturation. *Neuropathol. Appl. Neurobiol.* **38**, 471–486

320. Schmiedt, M. L., Blom, T., Blom, T., Kopra, O., Wong, A., von Schantz-Fant, C., Ikonen, E., Kuronen, M., Jauhiainen, M., Cooper, J. D., and Jalanko, A. (2012) Cln5-deficiency in mice leads to microglial activation, defective myelination and changes in lipid metabolism. *Neurobiol. Dis.* **46**, 19–29

321. Shibata, R., Misonou, H., Campomanes, C. R., Anderson, A. E., Schrader, L. A., Doliveira, L. C., Carroll, K. I., Sweatt, J. D., Rhodes, K. J., and Trimmer, J. S. (2003) A Fundamental Role for KChIPs in Determining the Molecular Properties and Trafficking of Kv4.2 Potassium Channels. *J. Biol. Chem.* **278**, 36445–36454

322. Carlson, R. O., Masco, D., Brooker, G., and Spiegel, S. (1994) Endogenous ganglioside GM1 modulates L-type calcium channel activity in N18 neuroblastoma cells. *J. Neurosci.* **14**, 2272–2281

323. Ledeen, R. W., and Wu, G. (2002) Ganglioside function in calcium homeostasis and signaling. *Neurochem. Res.* **27**, 637–647

324. Wu, G., Xie, X., Lu, Z.-H., and Ledeen, R. W. (2009) Sodium-calcium exchanger complexed with GM1 ganglioside in nuclear membrane transfers calcium from nucleoplasm to endoplasmic reticulum. *Proc. Natl. Acad. Sci. U. S. A.* **106**, 10829–10834

325. Toischer, K., Kögler, H., Tenderich, G., Grebe, C., Seidler, T., Van, P. N., Jung, K., Knöll, R., Körfer, R., and Hasenfuss, G. (2008) Elevated Afterload, Neuroendocrine Stimulation, and Human Heart Failure Increase BNP Levels and Inhibit Preload-Dependent SERCA Upregulation. *Circ. Hear. Fail.* **1**, 265–271

326. Østergaard, J. R., Rasmussen, T. B., and Mølgaard, H. (2011) Cardiac involvement in juvenile neuronal ceroid lipofuscinosis (Batten disease). *Neurology* **76**, 1245–1251

327. Sano, R., Annunziata, I., Patterson, A., Moshiach, S., Gomero, E., Opferman, J., Forte, M., and D'Azzo, A. (2009) GM1-Ganglioside Accumulation at the Mitochondria-Associated ER Membranes Links ER Stress to Ca2+-Dependent Mitochondrial Apoptosis. *Mol. Cell* **36**, 500–511

328. Brailovskaya, I. V., Sokolova, T. V., Kobylyanskii, A. G., and Avrova, N. F. (2014) Effect of ganglioside GM1 on mitochondrial respiration and viability of PC12 cells under oxidative stress. *J. Evol. Biochem. Physiol.* **50**, 174–176

329. Katz, M. L., Gao, C.-L., Tompkins, J. A., Bronson, R. T., and Chin, D. T. (1995) Mitochondrial ATP synthase subunit c stored in hereditary ceroid-lipofuscinosis contains trimethyl-lysine. *Biochem. J.* **310**, 887–892

330. Kolikova, J., Afzalov, R., Surin, A., Lehesjoki, A.-E., and Khiroug, L. (2011) Deficient mitochondrial Ca2+ buffering in the Cln8 mnd mouse model of neuronal ceroid lipofuscinosis. *Cell Calcium* **50**, 491–501

331. Bektas, M., and Spiegel, S. (2003) Glycosphingolipids and cell death. *Glycoconj. J.* **20**, 39–47

332. Rippo, M. R., Malisan, F., Ravagnan, L., Tomassini, B., Condo, I., Costantini, P., Susin, S. A., Rufini, A., Todaro, M., Kroemer, G., and Testi, R. (2000) GD3 ganglioside directly targets mitochondria in a bcl-2-controlled fashion. *FASEB J.* **14**, 2047–2054

333. Svennerholm, L., Fredman, P., Jungbjer, B., Månsson, J.-E., Rynmark, B.-M., Boström, K., Hagberg, B., Norén, L., and Santavuori, P. R. (1987) Large alterations in ganglioside and neutral glycosphingolipid patterns in brains from cases with infantile neuronal ceroid lipofuscinosis/polyunsaturated fatty acid lipidosis. *J. Neurochem.* **49**, 1772–1783

334. Cataldo, A. M., Barnett, J. L., Berman, S. A., Li, J., Quarless, S., Bursztajn, S., Lippa, C., and Nixon, R. A. (1995) Gene expression and cellular content of cathepsin D in Alzheimer's disease brain: Evidence for early up-regulation of the endosomal-lysosomal system. *Neuron* **14**, 671–680

335. Harzer, K., Paton, B. C., Poulos, A., Kustermann-Kuhn, B., Roggendorf, W., Grisar, T., and Popp, M. (1989) Sphingolipid activator protein deficiency in a 16-week-old atypical Gaucher disease patient and his fetal sibling: Biochemical signs of combined sphingolipidoses. *Eur. J. Pediatr.* **149**, 31–39

336. Pitto, M., Raimondo, F., Zoia, C., Brighina, L., Ferrarese, C., and Masserini, M. (2005) Enhanced GM1 ganglioside catabolism in cultured fibroblasts from Alzheimer patients. *Neurobiol. Aging* **26**, 833–838

337. Yamamoto, N., Taniura, H., and Suzuki, K. (2010) Insulin inhibits Aβ fibrillogenesis through a decrease of the GM1 ganglioside-rich microdomain in neuronal membranes. *J. Neurochem.* **113**, 628–636

338. Yamamoto, N., Matsubara, T., Sato, T., and Yanagisawa, K. (2008) Age-dependent high-density clustering of GM1 ganglioside at presynaptic neuritic terminals promotes amyloid β-protein fibrillogenesis. *Biochim. Biophys. Acta - Biomembr.* **1778**, 2717–2726

339. Steen, E., Terry, B. M., Rivera, E. J., Cannon, J. L., Neely, T. R., Tavares, R., Xu, X. J., Wands, J.

R., and de la Monte, S. M. (2005) Impaired insulin and insulin-like growth factor expression and signaling mechanisms in Alzheimer's disease--is this type 3 diabetes? *J. Alzheimers. Dis.* **7**, 63–80

340. Ma, T., Zhao, Y., Kwak, Y.-D., Yang, Z., Thompson, R., Luo, Z., Xu, H., and Liao, F.-F. (2009) Statin's Excitoprotection Is Mediated by sAPP and the Subsequent Attenuation of Calpain-Induced Truncation Events, Likely via Rho-ROCK Signaling. *J. Neurosci.* **29**, 11226–11236

341. Kabayama, K., Sato, T., Saito, K., Loberto, N., Prinetti, A., Sonnino, S., Kinjo, M., Igarashi, Y., and Inokuchi, J. (2007) Dissociation of the insulin receptor and caveolin-1 complex by ganglioside GM3 in the state of insulin resistance. *Proc. Natl. Acad. Sci. U. S. A.* **104**, 13678–13683

342. Kawashima, N., Yoon, S. J., Itoh, K., and Nakayama, K.-I. (2009) Tyrosine kinase activity of epidermal growth factor receptor is regulated by GM3 binding through carbohydrate to carbohydrate interactions. *J. Biol. Chem.* **284**, 6147–6155

343. Yamashita, T., Hashiramoto, A., Haluzik, M., Mizukami, H., Beck, S., Norton, A., Kono, M., Tsuji, S., Daniotti, J. L., Werth, N., Sandhoff, R., Sandhoff, K., and Proia, R. L. (2003) Enhanced insulin sensitivity in mice lacking ganglioside GM3. *Proc. Natl. Acad. Sci.* **100**, 3445–3449

344. Calvo-Ochoa, E., and Arias, C. (2015) Cellular and metabolic alterations in the hippocampus caused by insulin signalling dysfunction and its association with cognitive impairment during aging and Alzheimer's disease: studies in animal models. *Diabetes. Metab. Res. Rev.* **31**, 1–13

345. Lee, B. Y., Han, J. A., Im, J. S., Morrone, A., Johung, K., Goodwin, E. C., Kleijer, W. J., DiMaio, D., and Hwang, E. S. (2006) Senescence-associated β-galactosidase is lysosomal β-galactosidase. *Aging Cell* **5**, 187–195

346. Edelstein, A. D., Tsuchida, M. A., Amodaj, N., Pinkard, H., Vale, R. D., and Stuurman, N. (2014) Advanced methods of microscope control using μManager software. *J. Biol. Methods* **1**, 10

III. LIST OF FIGURES

IV. LIST OF TABLES

V. APPENDIX

Table 3. Chemicals and kits used in this study

CHEMICAL	SUPPLIER
β-galactosidase staining kit	Cell Signaling, Merck Millipore, Darmstadt, Germany
Bovine serum albumin	Sigma-Aldrich® Co., St. Louis, MO, USA
Calcium chloride dihydrate	Carl Roth® GmbH, Karlsruhe, Germany
CellLytic M	Sigma-Aldrich® Co., St. Louis, MO, USA
Digitonin	Carl Roth® GmbH, Karlsruhe, Germany
DMSO	Pierce Biotechnology, Waltham, MA, USA
Dulbecco's Modified Eagle Medium	Gibco™/Life technologies Corp., Carlsbad, CA, USA
ECL reagents (Luminol, p-cumaric acid)	Sigma-Aldrich® Co., St. Louis, MO, USA
Fetal Bovine Serum	Gibco™/Life technologies Corp., Carlsbad, CA, USA
Ganglioside GM_1 salt	Avanti Polar Lipids, Alabaster, AL, USA
Glycine	Sigma-Aldrich® Co., St. Louis, MO, USA
Geneticin G418	Gibco™/Life technologies Corp., Carlsbad, CA, USA
HEPES	Sigma-Aldrich® Co., St. Louis, MO, USA
JetPrime buffer + reagent	Peqlab, VWR, Erlangen, Germany
L-glutamate	Gibco™/Life technologies Corp., Carlsbad, CA, USA
Lysotracker® Red DND-99	Invitrogen™
Magnesium chloride hexahydrate	Carl Roth® GmbH, Karlsruhe, Germany
Methanol	Carl Roth® GmbH, Karlsruhe, Germany
Methyl-β-cyclodextrin	Sigma-Aldrich® Co., St. Louis, MO, USA
Milk powder	Carl Roth® GmbH, Karlsruhe, Germany
Mowiol w/o anti-bleach reagent	Fluka/Sigma-Aldrich® Co., St. Louis, MO, USA
MTT solution	Carl Roth® GmbH, Karlsruhe, Germany
MTT solubilization solution	Carl Roth® GmbH, Karlsruhe, Germany
NuPAGE Antioxidant	Invitrogen™/Life technologies Corp., Carlsbad, CA, USA
NuPAGE LDS Sample Buffer (4X)	Invitrogen™/Life technologies Corp., Carlsbad, CA, USA
NuPAGE MES SDS Running Buffer (20X)	Invitrogen™/Life technologies Corp., Carlsbad, CA, USA
NuPAGE MOPS SDS Running Buffer (20X)	Invitrogen™/Life technologies Corp., Carlsbad, CA, USA
NuPAGE Transfer Buffer (20X)	Invitrogen™/Life technologies Corp., Carlsbad, CA, USA
Paraformaldehyde	Carl Roth® GmbH, Karlsruhe, Germany
PBS	Sigma-Aldrich® Co., St. Louis, MO, USA
Penicillin/Streptomycin	Gibco™/Life technologies Corp., Carlsbad, CA, USA
Potassium-chloride	Sigma-Aldrich® Co., St. Louis, MO, USA
Protease Inhibitor Cocktail	Sigma-Aldrich® Co., St. Louis, MO, USA
SeeBlue® Plus2 Prestained Standard	Invitrogen™/Life technologies Corp., Carlsbad, CA, USA
TCA	Carl Roth® GmbH, Karlsruhe, Germany
Trypsin/EDTA	Gibco™/Life technologies Corp., Carlsbad, CA, USA
Tween-20	Sigma-Aldrich® Co., St. Louis, MO, USA

Table 4. Equipment used in this study

EQUIPMENT	SUPPLIER
Axioskop 2 mot plus wide field microscope	Carl Zeiss AG, Oberkochen, Germany
Axioskop 50	Carl Zeiss AG, Oberkochen, Germany
Axiovert 200 M microscope	Carl Zeiss AG, Oberkochen, Germany
BD FACSaria flow cytometer	BD Biosciences, Erembodegem, Belgium
bottle top filter, 0.22 µm	NeoLab®, Heidelberg, Germany
Centrifuge 5424	Eppendorf, Hamburg, Germany
Centrifuge 5804 R	Eppendorf, Hamburg, Germany
Combitips plus	Eppendorf, Hamburg, Germany
cover-glasses (12 mm, 15 mm)	NeoLab®, Heidelberg, Germany
Cryo Pure tubes, 1.6 ml	Sarstedt AG, Nümbrecht, Germany
DualView	
Incubator	Heraeus, Hanau, Germany
Intas ChemoStar	Intas, Göttingen, Germany
Herasafe™ KSP Class II Biological Safety Cabinet	Thermo Fisher Scientific Inc., Bonn, Germany
Liquid nitrogen tank	Thermo Fisher Scientific Inc., Bonn, Germany
MicroLine CCD camera	FLI, Lima, NY
Moticam 1SP CMOS camera	Motic, Wetzlar, Germany
Nitrocellulose membranes	Thermo Fisher Scientific Inc., Bonn, Germany
NuPAGE 4-12% Bis-Tris Gel, 1.5 mm x 10 wells	Invitrogen™/Life technologies Corp., Carlsbad, CA, USA
NuPAGE 4-12% Bis-Tris Gel, 1.5 mm x 15 wells	Invitrogen™/Life technologies Corp., Carlsbad, CA, USA
Object-slides, 24x60x1 mm	NeoLab®, Heidelberg, Germany
PCR plate, 96-well	NeoLab®, Heidelberg, Germany
petri dish, 10 cm	NeoLab®, Heidelberg, Germany
Plates, 6-, 12-, 24-well	Greiner Bio One GmbH, Frickenhausen, Germany
PVDF membranes	Sigma-Aldrich® Co., St. Louis, MO, USA
Sarstedt cell culture bottles, 25 cm^2, 75 cm^2	Sarstedt AG, Nümbrecht, Germany
TCS SP5 confocal laser scanning microscope	Leica Microsystems, Heidelberg, Germany
Thermostatic waterbath	Thermo Fisher Scientific Inc., Bonn, Germany
Victor X3 plate reader	PerkinElmer, Waltham, MA, USA

Table 5. Software used in this study

SOFTWARE	VERSION	COMPANY/URL
Fiji/ImageJ	V1.47b	http://fiji.sc/Fiji
CellProfiler	2.0.11710	http://www.cellprofiler.org
CytoScape	3.02	http://www.cytoscape.org/
Huygens	14.xx	SVI, Hilversum, the Netherlands
LabImage 1D		Kapelan, Bio-Imaging Solutions, Germany
Mendeley™ citation manager	1.15.2	Mendeley Ltd., London, UK
MicroManager (346)	1.4	https://www.micro-manager.org/
OrginPro	9+2016	OriginLab Corporation, Northampton, MA, USA
WinMDI	2.9	http://www.cyto.purdue.edu/flowcyt/software/Winmdi.htm
Axiovision	4.6	Carl Zeiss AG, Oberkochen, Germany